# Geology of the Tanamá and Helecho Porphyry Copper Deposits and Vicinity, Puerto Rico

U.S. GEOLOGICAL SURVEY PROFESSIONAL PAPER 1327

# Geology of the Tanamá and Helecho Porphyry Copper Deposits and Vicinity, Puerto Rico

*By* DENNIS P. COX

U.S. GEOLOGICAL SURVEY PROFESSIONAL PAPER 1327

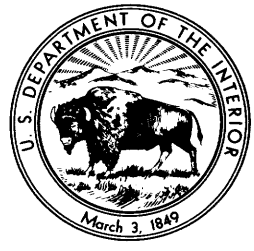


UNITED STATES GOVERNMENT PRINTING OFFICE, WASHINGTON : 1985

**DEPARTMENT OF THE INTERIOR**

**DONALD PAUL HODEL, *Secretary***

**U.S. GEOLOGICAL SURVEY**

**Dallas L. Peck, *Director***

**Library of Congress Cataloging in Publication Data**

Cox, Dennis Purver
Geology of the Tanamá and Helecho porphyry copper deposits and vicinity, Puerto Rico.

(U.S. Geological Survey Professional Paper 1327
Bibliography: p. 58-59
Supt. of Docs. no.: I 19.16:1327
1. Porphyry—Puerto Rico—Tanamá Region. 2. Copper ores—Puerto Rico—Tanamá Region. I. Title. II. Series: United States. Geological Survey. Professional Paper 1327.
QE462.P6C69 553.4'3'0972953 84-600077

For sale by the Superintendent of Documents
U.S. Government Printing Office
Washington, D.C. 20402

# CONTENTS


| | Page |
|---|---|
| Abstract | 1 |
| Introduction | 1 |
| Regional environment | 2 |
| Local geology | 3 |
| Cretaceous basaltic sequence | 3 |
| Utuado batholith | 5 |
| Lower Tertiary felsic volcanic rocks | 6 |
| Tonalite porphyry | 6 |
| Mineralized breccia | 10 |
| Other intrusions of minor extent | 10 |
| Oligocene formations | 11 |
| Faulting | 12 |
| Mineral deposits | 13 |
| History of discovery | 13 |
| Tanamá deposit | 13 |
| Geology | 13 |
| Feldspar-stable alteration and mineralization | 19 |
| Hornblende-dominated assemblages | 20 |
| Chlorite-dominated assemblages | 21 |
| Feldspar-destructive alteration and mineralization | 25 |
| Late-stage zeolite alteration | 27 |
| Veinlets and veinlet stratigraphy | 27 |
| Mineral deposits (continued) | |
| Tanamá deposit (continued) | |
| Thermometry and chemistry of veinlet fluids | 28 |
| Oxygen-isotope thermometry | 28 |
| Types of inclusions and their distribution | 28 |
| Minimum temperature of trapping of inclusions | 29 |
| Pressure corrections | 29 |
| Composition of fluids | 31 |
| Isotopic evidence for sources of hydrothermal fluids | 32 |
| Oxidation and secondary enrichment | 35 |
| Helecho deposit | 35 |
| Geology and structural controls | 35 |
| Mineralization and alteration | 38 |
| Other coppor prospects | 39 |
| Distribution of metallic elements and sulfur | 39 |
| Copper-gold-silver | 43 |
| Sulfur-selenium-chromium-cobalt | 43 |
| Molybdenum | 43 |
| Lead-zinc-manganese-silver | 43 |
| Other elements | 51 |
| Conclusions | 51 |
| References cited | 58 |


# ILLUSTRATIONS


PLATE 1. Geologic map of the Tanamá, Helecho, and Laundry Creek copper deposits and vicinity, Puerto Rico ---------- In pocket

| | Page |
|---|---|
| FIGURE 1. Sketch map of Puerto Rico, showing locations of copper deposits and quadrangles | 2 |
| 2. Photomicrographs showing textures of rocks from the Cretaceous basaltic sequence, Utuado batholith, and Tertiary volcanic sequences | 4 |
| 3. Sketch map showing localization of copper deposits at intersections of aligned clusters of porphyry stocks with axes of elongate porphyry intrusions | 7 |
| 4. Photograph of tonalite porphyry, showing spacing of phenocrysts | 7 |
| 5. Photomicrographs of tonalite porphyry | 8 |
| 6. Plots of chemical variations in amphiboles in tonalite porphyry | 9 |
| 7. Plot of $K_2O$ content versus $SiO_2$ content tonalite porphyry and dacite of Eocene age | 11 |
| 8. Photograph of breccia outcrop, on Río Criminales | 11 |
| 9. Photograph of basal conglomerate of the San Sebastian Formation, weathered to soft, sectile saprolite | 12 |
| 10. Photograph showing surface of low relief in vicinity of Tanamá deposit | 12 |
| 11. Geologic maps of the Tanamá deposit | 14 |
| 12. Cross section of the Tanamá deposit | 17 |
| 13. Interpretive cross section of the Tanamá deposit before faulting | 19 |
| 14. Photographs showing veinlets in tonalite porphyry, Tanamá deposit | 20 |
| 15. Photomicrograph of hornblende in type D veinlet | 21 |
| 16. Photographs showing types C and E veinlets, Tanamá deposit | 23 |

17. Photomicrographs of type D veinlets ---- 23
18. Histograms of $K_2O/Al_2O_3$ and $S/Al_2O_3$ ratios in fresh and altered tonalite porphyry, Tanamá deposit and vicinity ---- 26
19. Photograph and photomicrograph of late-stage veinlets, Tanamá deposit ---- 27
20. Sketch illustrating general appearance and crosscutting relations of veinlets at Tanamá ---- 28
21. Plots of temperatures of final homogenization of fluid inclusions in types C and E quartz veinlets from ore zone in upper part of the Tanamá deposit and from low-grade core zone in lower part ---- 30
22. Histogram of temperatures of melting ice in 55 vapor- and liquid-rich inclusions, Tanamá deposit ---- 31
23. Histogram of temperatures of dissolution of halite and sylvite daughter minerals in inclusions, Tanamá deposit ---- 31
24. Scanning electron micrographs showing daughter minerals in fluid inclusions, Tanamá deposit ---- 33
25. Photomicrographs showing mineral-rich inclusions, Tanamá deposit ---- 34
26. Geologic map of the Helecho deposit ---- 36
27. Diagrams showing lower-hemisphere projections of orientations of veins and mineralized fractures in porphyry and altered volcanic rocks, Helecho deposit ---- 37
28. Photomicrographs showing intergrowths and veinlets of anhydrite ---- 38
29. Geologic sketch map of the Laundry Creek prospect ---- 39
30. Maps comparing outline of greater-than-0.4-weight-percent-Cu ore body with scores on factor 3 for Cu-Au-Ag, Tanamá deposit ---- 46
31. Maps comparing contact of tonalite porphyry with scores on factor 5 for S-Se-Cr-Co, Tanamá deposit ---- 48
32. Map comparing outline of greater-than-0.4-weight-percent-Cu ore body with S values in streambed outcrops and Mo values in drill cores and outcrops, Helecho deposit ---- 50
33. Maps comparing outline of greater-than-0.4-weight-percent-Cu ore body with Mo values in drill cores, Tanamá deposit ---- 52
34. Maps comparing limits of pervasive feldspar-destructive alteration with scores on factor 1 for Pb-Zn-Mn-Ag, Tanamá deposit 54
35. Map comparing outline of greater-than-0.4-weight-percent-Cu ore body with scores on factor 1 for Pb-Zn-Mn-Ag, Helecho deposit ---- 56
36. Schematic cross sections showing deposition and redistribution of silicates and metals in a Tanamá-type deposit ---- 57

# TABLES

Page

TABLE 1. Composition of volcanic and batholithic rocks from the Tanamá area, Puerto Rico ---- 5
2. Partial analyses and structural formulas of amphiboles in weakly altered tonalite porphyry ---- 7
3. Compositions and mineral norms of tonalite porphyry, Tanamá area , Puerto Rico ---- 10
4. Chemical analyses of tonalite porphyry with feldspar-stable alteration, Tanamá and Helecho deposits ---- 19
5. Partial analyses of magnesiohornblende and actinolitic hornblende in feldspar-stable-alteration assemblages, Tanamá deposit ---- 22
6. Partial analyses and structural formulas of fibrous amphibole and chlorite, Tanamá deposit ---- 24
7. Composition of tonalite porphyry with pervasive feldspar-destructive alteration, Tanamá and Helecho deposits ---- 26
8. $\delta^{18}O$ values and equilibrium temperatures for two quartz-magnetite veinlets, Tanamá deposit ---- 29
9. Number of observations of daughter minerals in fluid inclusions within quartz, Tanamá deposit ---- 32
10. Temperatures of dissolution of mineral pairs: halite and iron chloride ---- 32
11. Oxygen- and hydrogen-isotopic ratios of hydrothermal minerals, Tanamá deposit ---- 34
12. Analytical data for selected elements in drill core from the Tanamá deposit ---- 40
13. Analytical data for selected elements in drill core from the Helecho deposit ---- 42
14. Analytical data for selected elements in outcrop samples from the Helecho deposit ---- 44

# GEOLOGY OF THE TANAMÁ AND HELECHO PORPHYRY COPPER DEPOSITS AND VICINITY, PUERTO RICO

By DENNIS P. COX

ABSTRACT

The Tanamá and Helecho copper-deposits are examples of gold-rich porphyry systems in a low-potassium island-arc environment. Discovered in west-central Puerto Rico in 1958, the deposits are localized in tonalite porphyry stocks of late Eocene age that intrude basaltic rocks of Cretaceous age and felsic volcanic rocks of early Eocene age. The mineralized plutons are in elongate clusters of stocks aligned perpendicular to the regional grain of the island. The tonalite porphyry is composed of phenocrysts of calcic plagioclase, hornblende, and quartz in an aplitic-textured groundmass of quartz and sodic feldspar. The amphibole phenocrysts vary in composition; their deuteric-alteration rims and patches have a relatively higher Mg content.

The Tanamá deposit (126 million t, 0.64 weight percent Cu) is in a faulted tonalite porphyry stock. The deposit contains abundant quartz veins and disseminated chalcopyrite and has a secondary-enrichment blanket containing various copper sulfide minerals. Three alteration zones are recognizable: (1) an inner, amphibole-dominated assemblage containing abundant magnetite and of low copper grade; (2) an outer, chlorite-dominated assemblage, locally containing traces of hydrothermal biotite and potassium feldspar and abundant chalcopyrite replacing magnetite; and (3) an upper, sericite-clay-calcite-pyrite zone. Calcic plagioclase is unaltered in the first two zones but totally destroyed in the third. Amphiboles in the first zone approach magnesiohornblende and actinolitic hornblende in composition. Oxygen-isotopic compositions of quartz and magnetite in quartz veins imply equilibrium at 680 to 685 °C. Temperatures of homogenization of vapor bubbles and dissolution of crystalline phases in fluid inclusions within quartz veins mainly range from 200 to 500 °C; some mineral- and vapor-rich inclusions in the interior of the deposit homogenize at above 500 °C. Crystalline phases in inclusions are, in order of abundance: NaCl, Fe chloride, KCl, complex Na-K-Fe-Ca chlorides, hematite, and chalcopyrite. Oxygen-deuterium analyses of amphibole, chlorite, and white micas suggest equilibrium with meteoric or ocean water.

The Helecho copper deposit is similar to the Tanamá deposit and coextensive with a tonalite porphyry stock 1 km to the south. Two porphyry copper prospects, Laundry Creek and Copper Creek, are also located in porphyry stocks to the west of Tanamá. Study of veins and mineralized fractures at Helecho shows a difference in orientation between the porphyry and metavolcanic country rocks. Fractures striking N. 18° W. and N. 2° E. in the Helecho porphyry match mineralized fractures in the Tanamá deposit. N. 30° E.-striking fractures predominate in the volcanic rocks but are rare in the porphyry; these N. 30° E.-striking fractures match the trend of the elongate cluster of stocks of which Helecho and Tanamá are a part.

Factor analysis of analytical data from drill-core samples at Tanamá and Helecho shows three groups of elements (factors) having strong intercorrelation: (a) Cu-Au-Ag—samples scoring high on this factor lie within the ore zone, and their distribution is independent of any alteration zone; (b) S-Se-Cr-Co—samples scoring high on this factor occur in altered volcanic rocks within the pyrite halo surrounding the porphyry systems; and (c) Pb-Zn-Mn-Ag—samples in the sericite-clay-pyrite zone are strongly depleted in these elements. A Pb-Zn-Mn peripheral anomaly has also been recognized from soil geochemical studies. Low concentrations of molybdenum occur erratically in and near the Tanamá deposit; at Helecho, low Mo concentrations are found in a discontinuous zone ranging from 200 to 300 m outward from the deposit.

I conclude that the Tanamá and Helecho deposits were probably formed by introduction of volatile materials — mainly $H_2O$ and $H_2S$ — and metal-chloride complexes from some deep source into a fractured porphyry intrusion. Potassium was also introduced from depth, as indicated by the low initial $K_2O$ content of intrusive rocks and wallrocks. This $K_2O$ was fixed as biotite in an early-formed potassic-alteration zone surrounding a core zone in which hydrothermal amphiboles were dominant. Within this potassic-alteration zone, the copper-gold ore bodies were deposited from chloride solutions. Meteoric or marine water entered the system through fractures and caused widespread nearly complete replacement of amphiboles and biotite by chlorite. This replacement released $K^+$ and $H^+$ and caused extensive plagioclase destruction and sericitization in the upper parts of the system. Also in these upper levels, pyrite replaced magnetite as the temperature and oxygen activity decreased. The copper-gold ore body was not affected by these changes, but Pb, Zn, and Mn were expelled from the upper levels of the deposits during the sericite-pyrite-alteration stage.

## INTRODUCTION

The Tanamá and Helecho copper deposits are situated in west-central Puerto Rico, the easternmost island of the Greater Antilles chain. The area described in this report, which includes these deposits and two associated copper prospects, extends 13 km eastward and 7.5 km southward of the town of Lares and comprises the south third and the north border, respectively, of the Bayaney and Monte Guilarte 7½ minute quadrangles (fig. 1).

The map area (pl. 1) is characterized by gently rolling uplands dissected by streams with very steep valley slopes. The uplands rise gently from 300-m elevation in the north to a drainage divide in the south edge of the map area at approximately 600-m elevation. The area has an annual rainfall of 200 to 250 cm and supports a heavy vegetation cover. The area has been extensively cultivated in the past, and native vegetation has been replaced largely by coffee, banana, and orange groves and intervening areas of pasture.

Copper deposits in this area have been known since 1958. Their discovery by geologists of the Kennecott Copper Corp. was followed by extensive geologic mapping and diamond drilling. Results of this work were summarized in two reports by J. E. Welsh (unpublished data, 1965) and J. C. Wilson (unpub. data, 1966), which were made available to the writer by the Kennecott Copper Corp. and the Puerto Rico Mining Commission. Geologic mapping of the Bayaney quadrangle by Nelson and Tobisch (1968) laid much of the groundwork for the present study, as did later mapping in the Monte Guilarte quadrangle by R. D. Krushensky and A. F. Curet (unpub. data, 1978). Weaver (1958) and Chen (1969) published petrologic studies of the Utuado batholith that underlies part of the area, and Cox and others (1973) published a brief account of porphyry copper mineralization and alteration in Puerto Rico in which the deposits of the map area (pl. 1) were described.

The present study was carried out in cooperation with the Department of Natural Resources of the Commonwealth of Puerto Rico. The main objective of this study was to describe the mineralogic and geochemical characteristics of a porphyry-type deposit in a potassium-deficient geologic environment that differs markedly from that of most porphyry copper deposits in the conterminous United States.

*Acknowledgments.*—The data collection and analysis and the maturation of ideas on genesis leading to this report were, in large part, made possible by the encouragement and generous assistance of a great number of people in the Kennecott Copper Corp. (KCC), the Puerto Rico Department of Natural Resources (DNR), the U.S. Geological Survey (USGS), and other organizations. Gregorio Chavez (KCC) graciously provided lodging and office space during the fieldwork and core logging. I was assisted in the field at various times by Eduardo Questell (DNR), M. P. Foose (USGS), and Alfonso Arias (Government of Colombia). Most of the chemical analyses were performed under the direction of Ileana Pérez González (DNR). Isotopic and mineralogic data were contributed by J. R. O'Neil, L. B. Wiggins, R. L. Oscarson, and P. J. Loferski, all of the U.S. Geological Survey. Helpful contributions and discussions of regional geologic problems came from R. D. Krushensky and A. E. Nelson (USGS). J. R. Atkinson (KCC) provided the history of exploration of the deposit. Interpretation of the data and development of a genetic model for the deposits, though solely my responsibility, were greatly influenced by discussions with T. G. Theodore, J. J. Hemley, P. B. Barton, Jr., G. K. Czamanske, Ivan Barnes, and E. W. Roedder (all USGS).

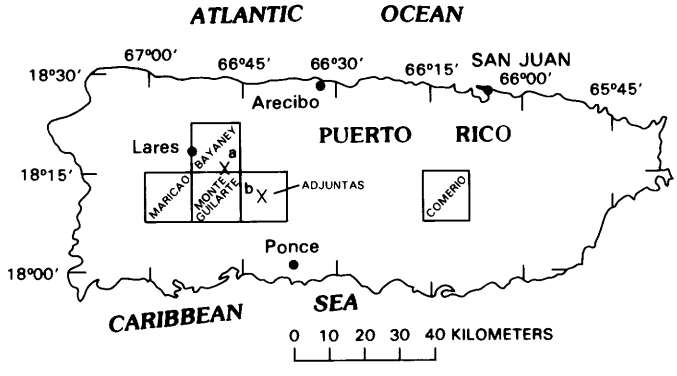


FIGURE 1.—Sketch of Puerto Rico, showing locations of Tanamá-Helecho (a) and Río Viví (b) copper deposits and 7½-minute quadrangles mentioned in text.

## REGIONAL ENVIRONMENT

The relation of porphyry copper mineralization to the geologic development of Puerto Rico and adjacent areas, as described by Barabas (1971, 1982) and Cox and others (1977, p. 701-702), can be summarized as follows:

1. Early sedimentary, volcanic, and tectonic events in southwestern Puerto Rico are recorded in rocks of the Bermeja Complex of Mattson (1958, 1960), which include radiolarian chert containing fossils of Jurassic age, serpentine, and amphibolite with a metamorphic age of 126 Ma, as determined by K-Ar analysis of hornblende.
2. The Bermeja Complex is overlain by volcanic and sedimentary rocks as old as Cenomanian that are part of a thick sequence of basalt, andesite, and breccia, conglomerate, sandstone, and shale derived from volcanic rocks, which were deposited from Albian time to the end of the Cretaceous Period. Volcanism was associated with left-lateral strike-slip displacement along major northwest-striking faults that were active from Cenomanian to Eocene time.
3. This pile of volcanic rocks was intruded by plutons of tonalitic and granodioritic composition beginning in the Aptian and culminating in the Maestrichtian. Two batholiths were emplaced during Maestrichtian time: the San Lorenzo in the eastern part of Puerto Rico and the Utuado in the west-central part.
4. After emplacement of these batholiths, parts of the region were uplifted and eroded, and during the middle to late Eocene Epoch, basaltic to dacitic lava, tuff, and volcaniclastic sediment were deposited in west- central Puerto Rico, mainly along a northwest-trending trough, 100 km long by 10 km wide. This trough may have resulted from rifting.
5. During late Eocene time, small stocks of tonalite were placed along the boundary between the Eocene trough and the Utuado batholith as well as

in other parts of central and northeastern Puerto Rico. These intrusions, which were the latest igneous events in the history of Puerto Rico, were accompanied by hydrothermal alteration and copper mineralization in the Tanamá and Río Viví areas. Batholithic intrusion during the Oligocene in the Virgin Islands, some 100 km to the east, was followed by minor copper and molybdenum mineralization on Virgin Gorda Island.

6. Uplift, erosion, and formation of extensive areas of low relief followed the termination of igneous activity in Puerto Rico. Clastic sediment with thin coal seams (San Sebastian Formation) of middle Oligocene age was overlain by thick marine limestone deposits during the Oligocene and Miocene (Lares Limestone and overlying units).
7. Renewed erosion followed arching and uplift of the island during Pliocene to Holocene time, and the present topography began to develop. A regional saprolite weathering zone was created by intense tropical weathering.

The most important conclusion that has been reached by a study of the regional development of Puerto Rico relative to the occurrence of copper deposits is that formation of the porphyry copper deposits did not accompany the main pulse of volcanic activity during the Maestrichtian but, instead, accompanied a minor terminal igneous event, possibly associated with rifting.

## LOCAL GEOLOGY

### CRETACEOUS BASALTIC SEQUENCE

Thermally metamorphosed basaltic volcanic and volcaniclastic rocks are the oldest in the map area (pl. 1). They are intruded by rocks of the Utuado batholith of Late Cretaceous age and are overlain by Eocene volcaniclastic rocks. These thermally metamorphosed rocks, which were assigned to the Robles Formation by Mattson (1968) and Nelson and Tobisch (1968), are here referred to as the Cretaceous basaltic sequence. Metavolcanic rocks of this unit are dark-greenish-gray hornblende hornfels characterized by abundant relict pyroxene phenocrysts. In most areas, these phenocrysts are completely replaced by amphibole clusters that have a square or short prismatic outline inherited from original pyroxene grains. Over most of the outcrop belt, thermal metamorphism has destroyed primary volcanic textures and structures. Along the south side of this belt, however, where it is crossed by the Río Piedras, Nelson and Tobisch (1968) described volcanic breccia. Along the Río Ángeles, 2 km above its mouth, fresh pyroxenes and lapilli texture can be recognized in the basaltic rocks.

Thin-layered tuffaceous sandstone and shale occur along the divide that forms the boundary between the Municipios of Utuado and Adjuntas. Locally, feldspathic tuff was noted in which the groundmass, now altered to mica, shows structures suggesting collapse pumice. These rocks can be traced discontinuously to the vicinity of the Tanamá deposit, where they are strongly altered to quartz and sericite.

In thin section, the metavolcanic basaltic rocks are seen to be composed mainly of greenish-brown hornblende and minor plagioclase, chlorite, magnetite, and pyrite. The texture is granoblastic, and outlines of original phenocrysts commonly are well preserved (fig. 2*A*). Mafic phenocrysts have been replaced by single hornblende crystals or clusters of parallel amphibole fibers; remnants of clinopyroxene occur rarely in the centers of these clusters. The groundmass has been converted to dense fine-grained hornblende, and hornblende veinlets are common. Plagioclase phenocrysts and small lath-shaped grains commonly are only partly replaced by hornblende. Remnant plagioclase has lamellar twinning and ranges in composition from albite to andesine over short distances. Chlorite is, in most occurrences, a retrograde fracture-controlled mineral, as is pyrite. Magnetite occurs as veinlets and also as clusters of fine grains within mafic phenocrysts. Vesicles are locally well preserved (fig. 2*B*); they may be filled by amphibole grains, chlorite, or quartz.

Analysis of a typical sample of hornblende hornfels (1, table 1) from the east fork of the Río Piedras indicates low silica and high magnesia contents consistent with a basaltic protolith. Cr and Ni contents of 731 and 146 ppm, respectively, are also characteristic of basalt.

Outcrops of unmetamorphosed pyroxene-bearing tuff along the Río Ángeles are included in the Cretaceous basaltic sequence. This tuff contains lapilli 3 to 10 mm in diameter, composed of vesicular glassy material and large clinopyroxene phenocrysts (fig. 2*C*). Vesicles are filled by an isotropic mixture of clay and calcite. Calcite veinlets are common, and some samples are nearly completely replaced by calcite, chlorite, and sericite. Analysis of a sample (2, table 1) from this area shows a typically basaltic composition similar to that of the hornblende hornfels.

Nelson and Tobisch (1968) and Mattson (1968), in the Bayaney and Adjuntas quadrangles, respectively, assigned rocks of the Cretaceous basaltic sequence to the Robles Formation. The Robles is a thick unit of Albian to Santonian age (Mattson, 1971), composed mainly of well-bedded volcanic sandstone and mudstone, whose type locality is in central Puerto Rico (Pease and Briggs, 1960). Krushensky (1978), on the basis of work in the Monte Guilarte quadrangle, pointed

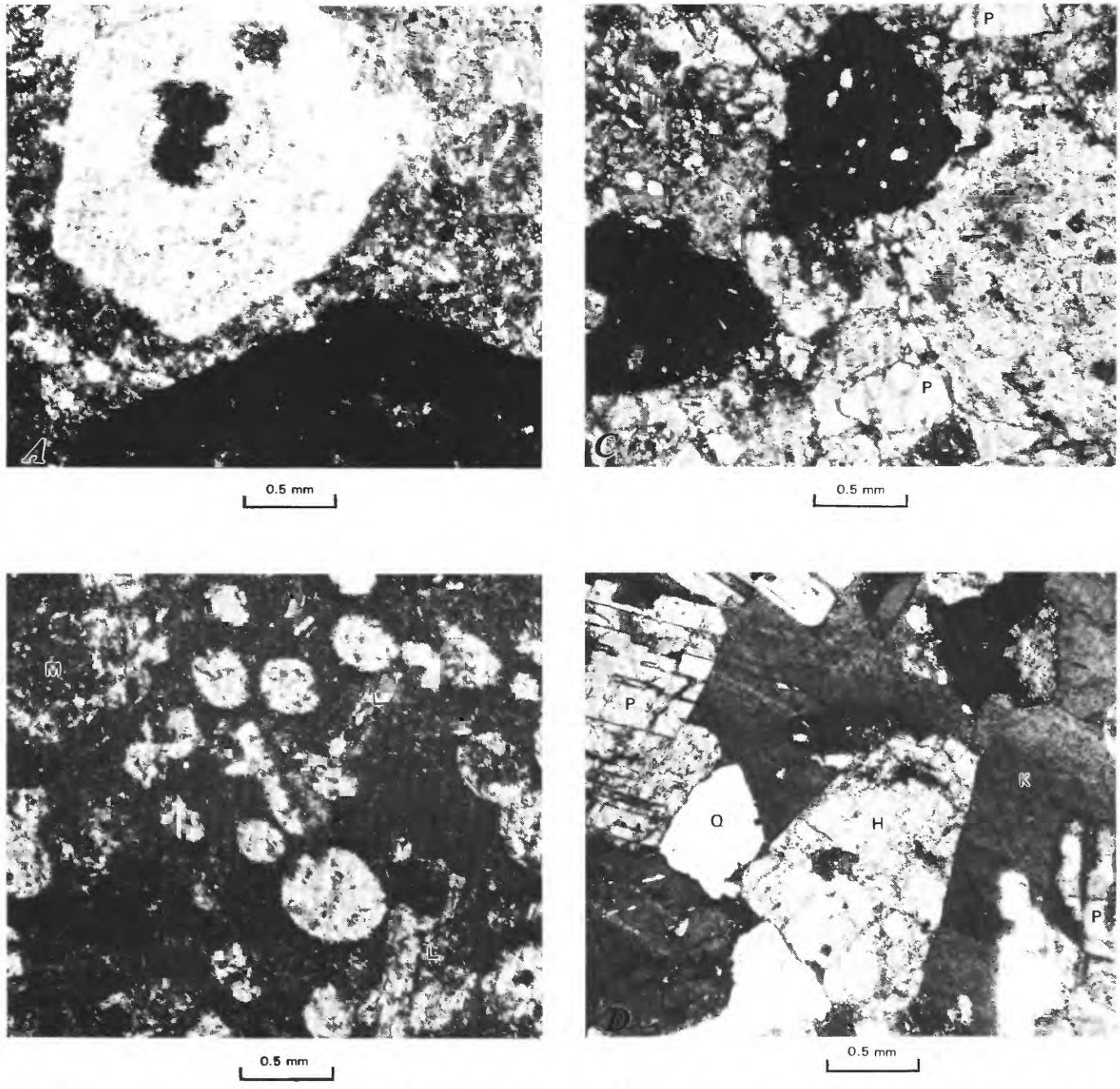


FIGURE 2.—Photomicrographs showing textures of rocks in the Cretaceous basaltic sequence, Utuado batholith, and lower Tertiary volcanic sequences. *A*, Hornfels of the Cretaceous basaltic sequence, showing outlines of original pyroxene phenocrysts replaced by amphibole. Groundmass is fine-grained amphibole and minor albite. Drill hole H67, Helecho deposit. Crossed polarizers. *B*, Hornfels of the Cretaceous basaltic sequence, showing relict ovoid vesicles between large mafic phenocrysts (M) and smaller plagioclase laths (L). Except for clear plagioclase areas, rock is composed mainly of hornblende in varying grain sizes. *C*, Lapilli tuff of the Cretaceous basaltic sequence, showing clinopyroxene phenocrysts (P) and lapilli of vesicular glass. *D*, Potassium-feldspar oikocryst (K) in tonalite of the Utuado batholith exposed in Río Camuy. P, plagioclase; H, hornblende; Q, quartz. Partially crossed polarizers. *E*, Lapilli tuff, Milagros Formation, containing broken plagioclase phenocrysts (P), rock, and pumice fragments. Sample provided by A. E. Nelson. *F*, Welded tuff, Milagros Formation. Clasts are of plagioclase and minor quartz. Sample provided by A. E. Nelson.

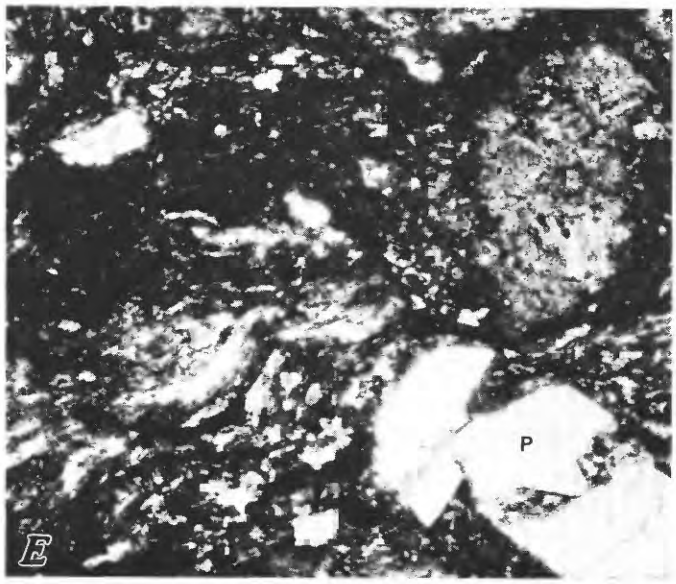


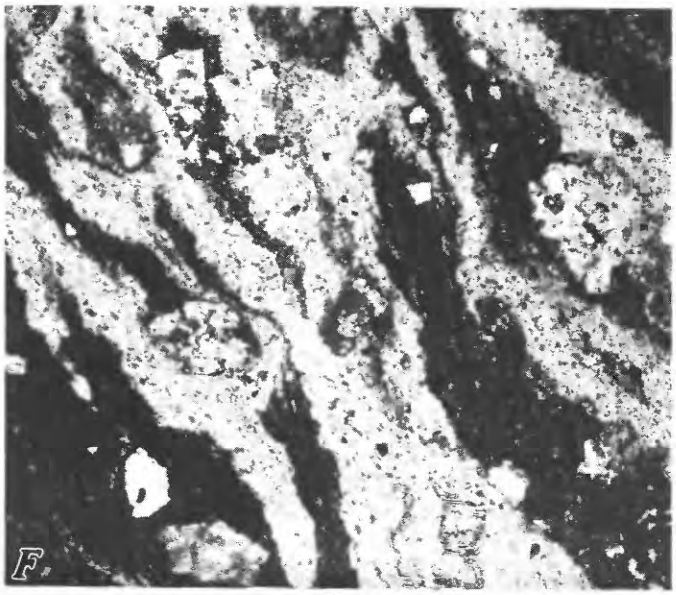


FIGURE 2.—Continued.

out that the rocks of this unit strongly resemble the Maricao Basalt, described by Mattson (1960) and McIntyre and others (1970) from the Maricao quadrangle (fig 1). These workers assigned a Campanian and Maestrichtian age to this unit on the basis of stratigraphic relations. Krushensky (1978), however, showed that basalt of typical Maricao lithology persists into the lower Tertiary section and is interbedded with dacitic lapilli tuff similar to that which overlies basaltic tuff in the Bayaney quadrangle.

TABLE 1. —*Composition of volcanic and batholithic rocks from the Tanamá area, Puerto Rico*

[Chemical analyses in weight percent by rapid rock methods (Shapiro, 1967); X-ray fluorescence spectrographic analyses in parts per million. Analysts: H. Smith and J. Fletcher (samples 1, 2, 5, 6); L. Espos and R. Mays (samples 3, 4)]

| Sample--- | 1 | 2 | 3 | 4 | 5 | 6 |
|---|---|---|---|---|---|---|
| Field No-- | 17-420 | 17-480Q | 17-153 | 71-154 | 31-2 | 31-3A |
| **Chemical analyses** | | | | | | |
| $Fe_2O_3$ --- | 2.7 | 6.0 | 3.07 | 2.82 | 5.6 | 4.5 |
| FeO ----- | 5.6 | 4.9 | 4.16 | 2.99 | .08 | 1.6 |
| MgO ----- | 10.9 | 8.7 | 3.12 | 2.33 | 2.6 | 1.4 |
| CaO ----- | 6.8 | 5.2 | 6.61 | 5.60 | 4.6 | 8.4 |
| $Na_2O$ ---- | 2.4 | 1.5 | 3.31 | 3.31 | 4.6 | 4.5 |
| $K_2O$ ----- | .54 | 1.8 | 1.12 | 1.60 | 1.2 | .87 |
| $H_2O^+$ ---- | 2.2 | 4.4 | 1.50 | 1.17 | 1.6 | 1.2 |
| $H_2O^-$ ---- | .55 | .73 | .25 | .10 | 1.2 | .55 |
| $TiO_2$ ---- | .47 | .96 | .72 | .61 | .41 | .67 |
| $P_2O_5$ ---- | .07 | .19 | .14 | .21 | .15 | .31 |
| MnO ----- | .22 | .33 | .16 | .12 | .24 | .21 |
| $CO_2$ ----- | .07 | 1.7 | .46 | .30 | .03 | 1.3 |
| Total--- | 98.5 | 99.9 | 99.92 | 100.34 | 100.2 | 98.6 |
| **Spectrographic analyses** | | | | | | |
| Co ----- | 25 | 35 | 15 | 10 | 12 | 12 |
| Cr ----- | 730 | 240 | 5 | 5 | 29 | 17 |
| Cu ----- | 200 | 52 | 20 | 70 | 32 | 53 |
| Mo ----- | <1.5 | <1.5 | <2 | <2 | 3 | 7 |
| Ni ----- | 150 | 84 | 5 | 5 | 15 | 4 |
| Pb ----- | <7 | 10 | <7 | <7 | 8 | 9 |
| Zn ----- | 110 | 120 | <100 | <100 | 63 | 68 |

Sample 1. Hornblende hornfels in Cretaceous basalt sequence.
2. Pryoxene lapilli tuff in Cretaceous basalt sequence.
3. Tonalite, Río Camuy; collector, A. H. Barabas.
4. Tonalite, Río Angeles; collector, A. H. Barabas.
5. Dacite breccia of the Milagros Formation and Río Blanco Formation of former usage.
6. Dacite tuff of the Río Blanco Formation of former usage

Except for fairly continuous outcrops in stream bottoms, most of the area mapped (pl. 1) as the Cretaceous basaltic sequence is mantled by saprolite. Saprolite derived from the hornfelsic volcanic rocks is cohesive, gray, and finely speckled; its appearance can best be described as resembling mixed salt and pepper. The saprolite retains as limonite the traces of numerous veinlets originally composed of pyrite, magnetite, or amphibole. Original pyroxene-amphibole phenocrysts have been transformed to limonite, and sparse plagioclase grains to white clays.

### UTUADO BATHOLITH

The Utuado batholith is exposed between the Cretaceous basaltic sequence and the overlying middle Tertiary San Sebastian and Lares Formations. Unweathered exposures of the batholith were studied in

the valleys of the Ríos Camuy and Criminales. Extensive exposures also occur in the canyon of the Río Tanamá, but difficulties of access made their study impractical.

The batholith is composed mainly of tonalite and, less commonly, granodiorite and quartz diorite (nomenclature for plutonic rocks in this report follows that of Streckeisen, 1974). The tonalite typically contains subhedral to euhedral grains of plagioclase, hornblende, and biotite, 1 to 3 mm in diameter, and anhedral interstitial potassium feldspar and quartz. Individual grains of potassium feldspar, which may be as large as 1 cm in diameter (fig. 2*D*), are so choked with plagioclase and hornblende inclusions that the percentage of potassium feldspar in the rock is low (generally 2-10 volume percent). Labradorite ($An_{50-60}$) typically makes up 55 to 60 percent of the rock, quartz 10 to 20 percent, and hornblende and subordinate biotite 20 to 25 percent. Analysis of samples from the Ríos Camuy and Ángeles shows compositions typical of tonalite (samples 3 and 4, respectively, table 1). The tonalite is intruded by porphyroaphanitic tonalite dikes and is commonly cut by numerous veinlets composed of chlorite, epidote, and locally calcite. Weathering of the tonalite creates a granular friable soil and a deeply gullied terrain. The original granitoid texture is easily recognizable, except where feldspar-destructive hydrothermal alteration has been intense.

## LOWER TERTIARY FELSIC VOLCANIC ROCKS

Lower Tertiary rocks lying disconformably on the prebatholith volcanic rocks were assigned to the Matilde and Milagros Formations by Nelson and Tobisch (1967). According to these workers, the Matilde Formation consists chiefly of thin-bedded volcanic sandstone and siltstone and minor andesite flows and lapilli tuff. A middle Eocene age for these beds is based on their contained microfossils (McIntyre and others, 1970).

The overlying Milagros Formation is distinguished from the thin-bedded Matilde Formation by the massiveness of its deposits. The Milagros Formation is composed of massive feldspathic lapilli tuff interstratified with volcanic breccia, andesitic lava flows, and thin-bedded volcanic sandstone and siltstone. The feldspathic tuff contains lapilli of andesite and andesite porphyry containing plagioclase and clinopyroxene phenocrysts, vesicular andesite, and compressed pumice. Quartz phenocrysts are present in some pumice fragments. Figures 2*E* and 2*F* illustrate the various textures in rocks of the Milagros Formation.

The Milagros Formation has not yet yielded fossils in the Bayaney quadrangle. It is assigned a middle Eocene age because it overlies the Matilde Formation (McIntyre and others, 1970). In the Monte Guilarte quadrangle, Krushensky (1978) established that the Milagros Formation is correlative with the upper part of the Anon Formation as described by Mattson (1968) in the Adjuntas quadrangle. Krushensky showed that the simple unconformity between Cretaceous basalt and breccia (Robles or Maricao Formation) and lower Tertiary dacitic tuff (Milagros or upper part of the Anon Formation) exhibited in the Bayaney quadrangle is elsewhere much more difficult to recognize, owing to the appearance of typical Maricao rock types in several places in the lower Tertiary section.

The lower Tertiary volcaniclastic rocks have been altered to sericite, calcite and (or) epidote, chlorite, and pyrite in many places in the Bayaney quadrangle, principally within the Municipio de Mirasol. This alteration may have accompanied intrusion of tonalite plutons, such as at Cerro La Torre. In the Quebrada de los Plátanos, Nelson and Tobisch (1968) noted chalcopyrite in altered intrusive rocks. Weathering of the volcaniclastic rocks generally destroys most of the structural and textural characteristics useful in mapping. Locally, volcanic breccia patterns may be discerned in saprolite.

## TONALITE PORPHYRY

Numerous tonalite porphyry plutons intrude volcanic rocks in both the Cretaceous and lower Tertiary sequences. Some of these plutons are elongate parallel to the contact of the batholith and to the strike of the lower Tertiary beds. Others are more equidimensional and are aligned in two zones, striking N. 30°-40° E. at right angles to the regional tectonic grain—one through the village of Matilde and the other through the Río Coabey (pl. 1, fig. 3). Most of the copper mineralization occurs in plutons that occupy intersections of these transcurrent trends with the axes of elongation of the more nearly concordant plutons (fig. 3).

In hand sample, the tonalite porphyry is medium gray to dark greenish gray and contains closely spaced phenocrysts of plagioclase, chloritized hornblende, and quartz. Phenocrysts range in length from 0.5 to 6 mm, but most are from 2 to 3 mm long (figs. 4, 5*A*). In plutons peripheral to the cluster and in younger dikes cutting ore bodies, phenocrysts are set farther apart than in plutons in the central part of the cluster. Mineral composition of the least altered samples ranges from 14 to 33 percent quartz, 60 to 70 percent plagioclase ($An_{56-66}$), 4 to 15 percent hornblende, and 1 to 2 percent magnetite.

Groundmass texture ranges from very fine grained (0.01-0.02 mm) in the peripheral plutons to fine grained (0.03-0.05 mm) in centrally located porphyries. Groundmass quartz grains may be rounded to give a

microaplitic texture (fig. 5*B*) or may be ragged in outline and choked with inclusions of feldspar, amphibole, and magnetite to give a sieve texture (fig. 5*C*). From study of samples collected from both unmineralized plutons and mineralized porphyry, the distribution of aplitic and sieve groundmass quartz textures appears to be random.

Plagioclase phenocrysts are euhedral, broken, or, more rarely, clustered in aggregates. Oscillatory zoning is common, and anorthite content ranges from 55 to 65 percent. Groundmass plagioclase grains are subhedral and equidimensional and are slightly less calcic in composition.

Hornblende phenocrysts are euhedral and pleochroic, with Z faintly bluish green, Y pale tan, and X pale greenish tan. Basal sections show compositional zoning and patchy changes in color and light absorption. Widespread chloritization of amphiboles makes it difficult to find clean phenocrysts for electron-microprobe analysis. The limited data obtained (table 2) indicate that the amphiboles are calcic and vary widely in composition. Figure 6*A* shows that these variations are achieved mainly by the following mechanism: $Si^{4+}$ substitutes for $Al^{3+}$ in tetrahedral sites, and the charges are balanced by the addition of $Na^{+}$ and $K^{+}$ in A sites and by

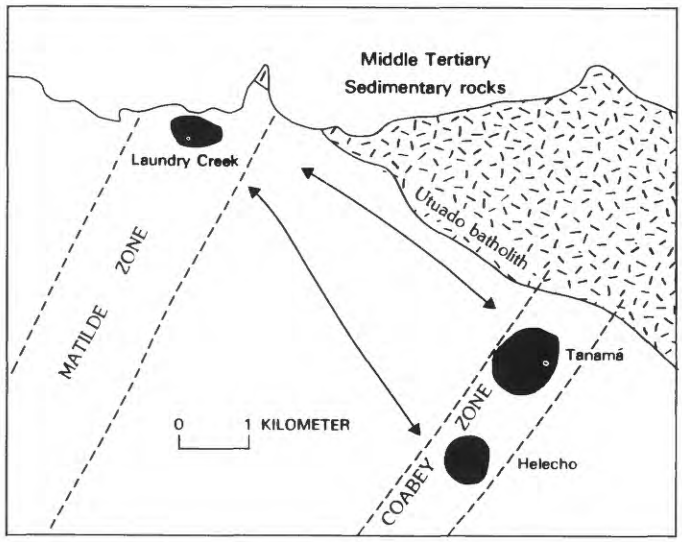


FIGURE 3.—Sketch map of area shown in plate 1, showing localization of copper deposits (black areas) at intersections of two transcurrent zones of porphyry stocks (dashed lines) with axes of elongated semiconcordant porphyry intrusions (arrows).

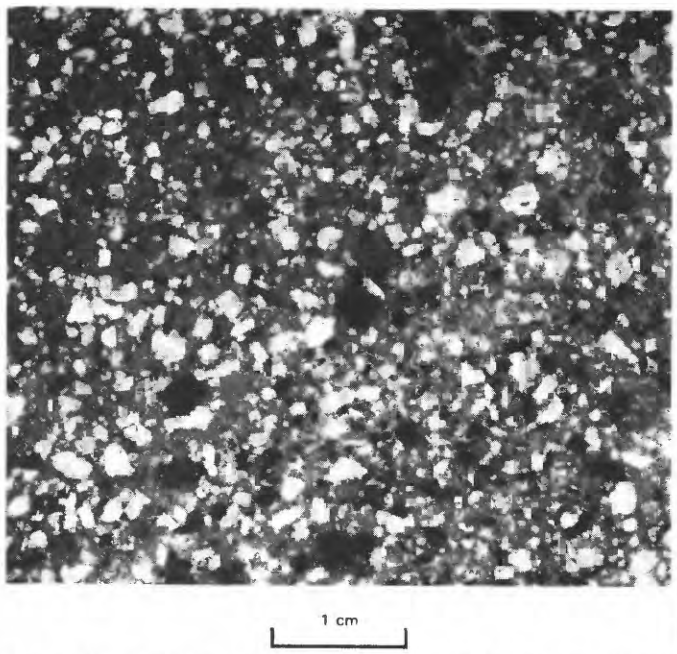


FIGURE 4.—Tonalite porphyry, showing spacing of phenocrysts. From Río Criminales near crossing of Highway 602.

TABLE 2. —*Partial analyses and structural formulas of amphiboles in weakly altered tonalite porphyry*

[Electron-microprobe analyses in weight percent, following the methods of Huebner and others (1976); analyst, L. B. Wiggins, U.S. Geological Survey. Iron was determined as total Fe; $Fe_2O_3$ is the midpoint value calculated using a program supplied by J. J. Papike. Structural formulas in atomic percent, calculated by the methods of Papike and others (1941)]

| Sample--- | 1 | 2 | 3 | 4 | 5 | 6 | 7 | 8 | 9 |
|---|---|---|---|---|---|---|---|---|---|
| Field No-- | 17-258 | | | | | | | 31-1 | 17-421 |
| **Electron-microprobe analyses** | | | | | | | | | |
| $SiO_2$ ----- | 50.2 | 46.1 | 41.9 | 40.8 | 46.3 | 50.4 | 41.9 | 46.3 | 47.3 |
| $Al_2O_3$ ---- | 6.4 | 8.6 | 14.2 | 15.4 | 9.6 | 3.2 | 13.4 | 7.4 | 8.6 |
| $Fe_2O_3$ ---- | 9.8 | 9.9 | 10.2 | 6.7 | 9.3 | 14.0 | 4.1 | 7.6 | 7.9 |
| FeO ------ | 3.7 | 4.7 | 4.5 | 5.0 | 2.4 | 4.7 | 7.6 | 6.6 | 7.0 |
| MgO ------ | 14.9 | 13.1 | 11.3 | 13.1 | 13.9 | 11.2 | 15.1 | 15.8 | 14.7 |
| CaO ------ | 11.1 | 11.3 | 11.7 | 12.5 | 11.5 | 12.8 | 11.3 | 10.4 | 11.1 |
| $Na_2O$ ----- | 1.0 | 1.3 | 1.9 | 2.1 | 1.6 | .1 | 2.5 | 1.2 | 1.4 |
| $K_2O$ ------ | .0 | .0 | .0 | .04 | .0 | .0 | .0 | .0 | .0 |
| $TiO_2$ ----- | 1.0 | 1.4 | 1.7 | 1.7 | 1.6 | .05 | 1.5 | 1.2 | 1.4 |
| $MnO_2$ ----- | .6 | .6 | .5 | .3 | .4 | 2.5 | .2 | 1.2 | 1.4 |
| Total--- | 98.7 | 97.0 | 97.9 | 97.6 | 96.6 | 99.0 | 97.6 | 97.7 | 100.8 |
| **Structural formulas** | | | | | | | | | |
| Si ------ | 7.17 | 6.77 | 6.13 | 5.94 | 6.76 | 7.42 | 6.07 | 6.75 | 6.73 |
| Al ------ | .83 | 1.23 | 1.85 | 2.06 | 1.24 | .56 | 1.93 | 1.25 | 1.27 |
| Al ------ | .24 | .25 | .60 | .59 | .41 | .0 | .35 | .03 | .17 |
| $Fe^{2+}$ ---- | 1.17 | 1.22 | 1.25 | .81 | 1.13 | 1.72 | .49 | .92 | .94 |
| $Fe^{3+}$ ---- | .40 | .52 | .49 | .55 | .27 | .52 | .83 | .72 | .75 |
| Mg ------- | 3.17 | 2.87 | 2.48 | 2.85 | 3.04 | 2.46 | 3.26 | 3.44 | 3.13 |
| Mn ------- | .07 | .08 | .06 | .04 | .05 | .31 | .02 | .08 | .0 |
| Ti ------- | .11 | .16 | .19 | .18 | .18 | .01 | .16 | .13 | .15 |
| XOCT ----- | .15 | .10 | .08 | .02 | .08 | .02 | .11 | .32 | .14 |
| Ca ------- | 1.70 | 1.78 | 1.84 | 1.96 | 1.80 | 2.02 | 1.76 | 1.63 | 1.69 |
| Na ------- | .15 | .12 | .09 | .02 | .12 | .0 | .13 | .05 | .16 |
| Na ------- | .13 | .23 | .47 | .57 | .33 | .03 | .57 | .29 | .21 |
| K -------- | .0 | .0 | .0 | .01 | .0 | .0 | .0 | .0 | .0 |
| Sum A ---- | .14 | .25 | .47 | .57 | .33 | .03 | .57 | .29 | .21 |

Sample 1. Phenocryst 1, outer rim; pale-greenish-tan magnesiohornblende.
2. Phenocryst 1, outer rim, interior to site 1; magnesiohornblende.
3. Phenocryst 1, inner greenish-brown zone; tschermakitic amphibole.
4. Phenocryst 1, inner greenish-brown zone; pargasitic amphibole.
5. Phenocryst 1, inner pale-greenish-tan zone; magnesiohornblende.
6. Phenocryst 2, pale zone; actinolitic hornblende.
7. Phenocryst 2, dark interior; magnesiohastingsitic amphibole.
8. Phenocryst, average of two point of similar composition; magnesiohornblende.
9. Phenocryst, average of three points of similar composition; magnesiohornblende.

the substitution of $Al^{3+}$, $Fe^{3+}$, and $Ti^{4+}$ for $Ca^{2+}$, $Mg^{2+}$, and $Fe^{2+}$ in octahedral sites. Deuteric alteration, as an explanation for these variations, is indicated by the decrease in Ti content in the outer zones of the phenocrysts (fig. 6*B*). These data suggest two trends of alteration: one from magnesiohastingsitic amphibole to actinolitic hornblende by loss of Al, Mg, and Na and gain of Ca and Fe (points 6, 7, figs. 6*B*-6*E*); and the other from pargasitic and tschermakitic amphibole to magnesiohornblende by loss of Al, Ca, and Na and gain of Mg (points 1-5, figs. 6*C-6E*) (amphibole nomenclature follows that of Leake, 1978). The second trend is similar to that which characterizes the hydrothermal amphiboles at Tanamá, as discussed in the subsection below entitled "Hornblende-Dominated Assemblages."

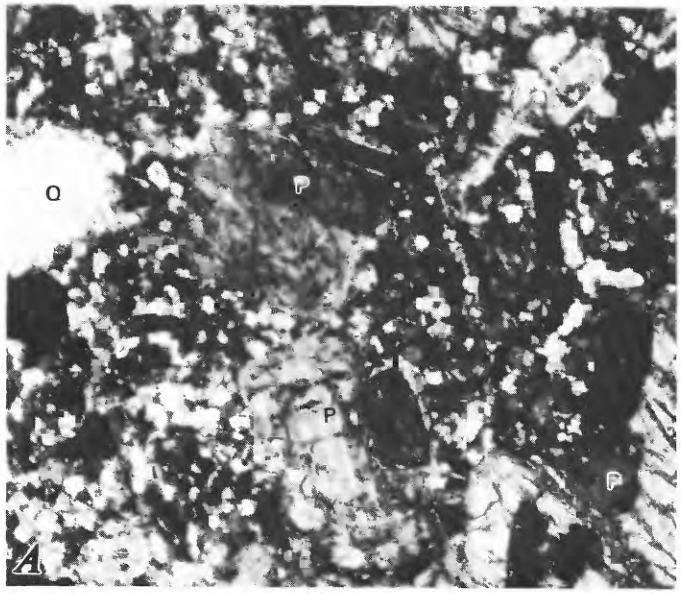


Quartz phenocrysts are strain free, rounded, embayed, and locally clustered in aggregates. They are rimmed by an overgrowth border in which groundmass quartz grains are attached to and in optical continuity with the phenocryst.

Table 3 lists the compositions of weakly altered tonalite porphyry. Varying degrees of propylitic alteration, mainly calcite+chlorite and epidote, are evident from the $CO_2$ content. $K_2O$ content, which ranges from about 0.5 to 1.6 weight percent, does not increase with increasing $SiO_2$ content (fig. 7). The tonalite porphyry from the Tanamá and Río Viví areas (Barabas, 1977) are similar in composition to dacite and tuff of Eocene age (table 1; Barabas, 1977).

K-Ar ages of hornblende in the tonalite plutons at Helecho, La Torrecilla, and other localities in Puerto Rico were reported by Barabas (1971, 1982) and Cox and others (1977). The Helecho sample, a tonalite porphyry

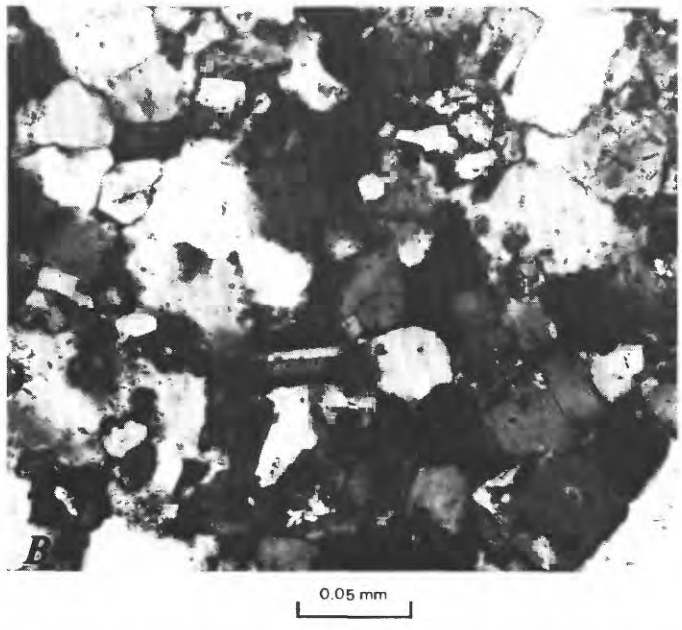


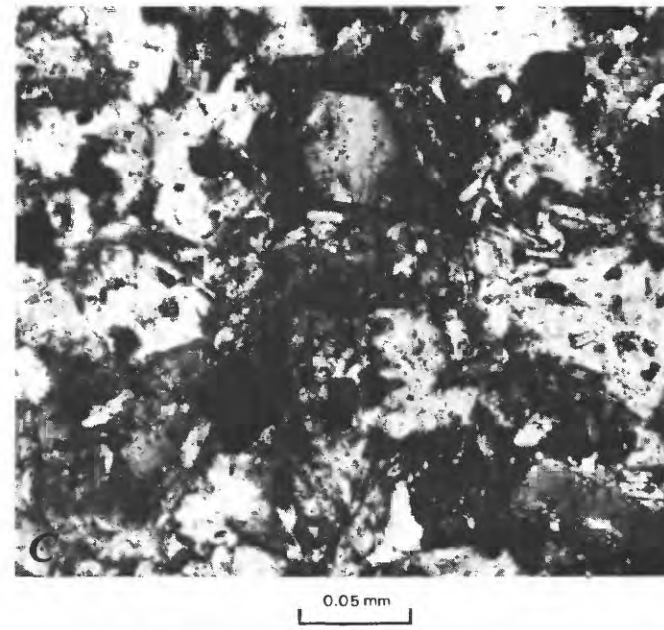


FIGURE 5.—Photomicrographs of tonalite porphyry. *A*, Microaplitic groundmass and plagioclase (P), hornblende, and quartz (Q) phenocrysts. Note overgrowth of quartz phenocryst into groundmass. Sample collected from a small western tributary of Río Criminales near contact with Utuado batholith. Crossed polarizers. *B*, Larger scale view of microaplitic quartz-oligoclase groundmass. Crossed polarizers. *C* Sieve-textured groundmass. Equidimensional quartz grains enclose abundant lath-shaped plagioclase grains. Crossed polarizers.

with an aplitic groundmass from 200 m north of the Helecho ore body, gave an age of 43.2 Ma (Barabas, 1982). The La Torrecilla sample (field No. 31-1) gave ages of 41.8 and 44.3 Ma on two splits of hornblende; these ages fall within the middle of the range of ages of tonalite porphyries over the island (Cox and others, 1977).

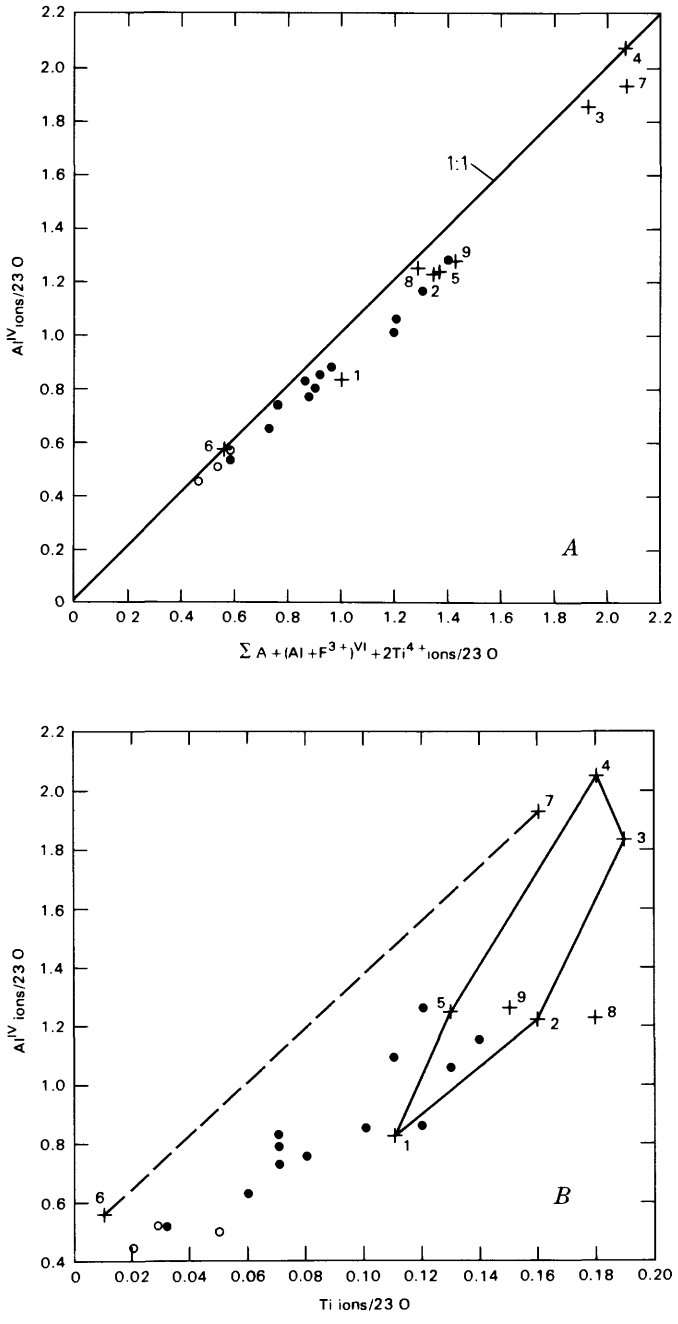


FIGURE 6.—Chemical variations in amphiboles in tonalite porphyry, Tanamá area. +'s, weakly altered rocks (table 2); points within the same phenocrysts are linked by solid and dashed lines. Numbers refer to analyses in table 2. Dots, hornblende from feldspar-stable-alteration assemblage (table 5); circles, fibrous amphiboles (table 6). Aluminum in tetrahedral sites ($Al^{IV}$) is plotted against sum of A-site occupancy plus Al, $Fe^{3+}$, and $Ti^{4+}$ in tetrahedral sites (*A*), Ti (*B*), Mg (*C*), total Fe (*D*), and Ca (*E*) in a unit cell of 23 oxygen atoms.

The tonalite porphyry weathers to a light-gray cohesive soil in which plagioclase phenocrysts, replaced by clay, are conspicuous. The close spacing of these phenocryst traces served to distinguish the porphyry from volcanic rocks in mapping of the saprolite zone. Relict quartz phenocrysts are also visible in soils derived from the porphyry; these phenocrysts commonly have a fine frosted surface under a hand lens.

TABLE 3. —*Compositions and mineral norms of tonalite porphyry, Tanamá area, Puerto Rico*

[Chemical analyses in weight percent by rapid rock methods (Shapiro, 1967); X-ray fluorescence spectrographic analyses in parts per million; mineral norms in percent. Analysts: H. Smith and J. Fletcher (samples 1–4); L. Espos and R. Mays (samples 5, 6)]

| Sample---- | 1 | 2 | 3 | 4 | 5 | 6 |
|---|---|---|---|---|---|---|
| Field No-- | 17-327 | 17-258 | 17-249 | 17-330 | 71-58 | 31-1 |
| | | | Chemical analyses | | | |
| $SiO_2$ ---- | 55.4 | 58.6 | 65.3 | 59.1 | 60.42 | 61.39 |
| $Al_2O_3$ --- | 16.3 | 16.5 | 16.5 | 16.4 | 16.69 | 17.02 |
| $Fe_2O_3$ --- | 3.9 | 2.8 | 2.7 | 2.1 | 2.85 | 2.54 |
| FeO ----- | 3.2 | 3.8 | 2.4 | 3.4 | 3.25 | 2.34 |
| MgO ----- | 3.2 | 3.5 | 1.9 | 3.1 | 3.01 | 2.78 |
| CaO ----- | 6.0 | 5.6 | 4.5 | 5.6 | 5.80 | 6.24 |
| $Na_2O$ ---- | 2.9 | 3.1 | 3.6 | 3.2 | 3.97 | 3.95 |
| $K_2O$ ----- | 1.4 | 1.5 | .65 | 1.1 | .51 | 1.14 |
| $H_2O^+$ ---- | 2.7 | 2.2 | 1.3 | 2.6 | 1.68 | 1.25 |
| $H_2O^-$ ---- | .82 | .91 | .56 | .75 | .27 | .26 |
| $TiO_2$ ---- | .50 | .56 | .34 | .50 | .49 | .49 |
| $P_2O_5$ ---- | .16 | .16 | .17 | .14 | .30 | .11 |
| MnO ----- | .12 | .35 | .07 | .25 | .135 | .139 |
| $CO_2$ ---- | 2.4 | .42 | .08 | 2.0 | .42 | .20 |
| Total-- | 99.0 | 100.0 | 100.1 | 100.2 | 99.80 | 99.85 |
| | | | Spectrographic analyses | | | |
| Co ------ | 20 | 19 | 7 | 13 | 7 | 7 |
| Cr ------ | 27 | 44 | 19 | 21 | 7 | 15 |
| Cu ------ | 368 | 61 | 102 | 20 | 200 | 15 |
| Mo ------ | <1.5 | 3 | <1.5 | <1.5 | <2 | <2 |
| Ni ------ | 12 | 18 | 6 | 8 | 7 | 7 |
| Pb ----- | 10 | 8 | <7 | <7 | <7 | <7 |
| Zn ------ | 76 | 210 | 55 | 204 | <100 | <100 |
| | | | Mineral norms | | | |
| Q ------- | 16.5 | 16.7 | 29.6 | 19.1 | 25.3 | 17.5 |
| C ------- | -- | -- | 2.1 | .1 | -- | -- |
| or ------ | 8.9 | 9.2 | 3.9 | 6.8 | 2.8 | 6.9 |
| ab ------ | 26.4 | 27.2 | 31.0 | 28.5 | 31.6 | 34.1 |
| an ------ | 29.4 | 27.7 | 21.6 | 28.3 | 24.7 | 25.8 |
| wo ------ | .6 | .03 | -- | -- | .2 | 2.1 |
| en ------ | 8.6 | 9.0 | 4.8 | 8.1 | 7.1 | 7.1 |
| fs ------ | 2.2 | 4.6 | 1.8 | 4.4 | 2.9 | 1.7 |
| mt ------ | 6.1 | 4.2 | 4.0 | 3.2 | 3.9 | 3.8 |
| il ------ | 1.0 | 1.1 | .7 | 1.0 | .9 | .9 |
| ap ------ | .4 | .4 | .4 | .3 | .7 | .3 |

Sample 1. Drill hole T146, east of Tanamá ore body.
2. Río Piedras.
3. Río Criminales
4. Drill hole T66, postmineral dike in Tanamá ore body.
5. Río Coabey, north of Helecho ore body.
6. La Torrecilla.

This surface is a result of the previously described overgrowth of phenocrysts into the quartz-rich groundmass of the original porphyry.

## MINERALIZED BRECCIA

Hydrothermally altered breccia crops out in the east fork of the Río Criminales, 400 to 500 m west of Highway 602. The breccia is composed of subangular to subrounded clasts of tonalite porphyry and metavolcanic rocks, ranging in size from small chips to 50 cm in diameter (fig. 8). The matrix is composed of fine to coarse rock fragments and abundant pyrite and white mica. No fragments of tonalite from the Utuado batholith were noted. The metavolcanic rock fragments contain the large equidimensional amphibole clusters after original pyroxene that are common to the Cretaceous basaltic sequence.

Outcrops of tonalite porphyry near the breccia outcrops are strongly fractured, veined, and stained by copper carbonates. Samples from these outcrops and from the breccia contained 1,900 to 3,400 ppm Cu, 20 to 70 ppm Mo, 2 to 5 ppm Ag, and traces of gold.

An attempt was made to trace the extent of the breccia by careful study of saprolite. This effort was only partly successful because of uncertainties in the analysis of vague patterns in the soils. The conclusion of the study was that breccia may underlie an area 600 by 1,500 m along the south contact of a tongue of porphyry intruded along the contact of the Utuado batholith (pl. 1).

The breccia predates or is contemporaneous with the tonalite porphyry. The associated white mica, pyrite, and copper mineralization suggest that the mineralization is hydrothermal in origin and possibly contemporaneous with porphyry copper mineralization at Tanamá.

## OTHER INSTRUSIONS OF MINOR EXTENT

Diorite porphyry dikes cut sericitized metavolcanic rocks and tonalite porphyry at the Helecho deposit and in the Río Criminales near the aforementioned breccia outcrops. The diorite porphyry contains conspicuous plagioclase ($An_{60}$) phenocrysts, 3 to 4 mm in diameter, set 1 to 2 cm apart in a dark-gray to black matrix. Relict phenocrysts of amphibole and pyroxene altered to chlorite, carbonates, and epidote are common. Fresh clinopyroxene phenocrysts were noted at outcrops near Helecho. The groundmass is composed of lath-shaped crystals of plagioclase and altered mafic minerals. Although quartz is very rare in the groundmass, it may occur locally as phenocrysts surrounded by a thin reaction rim of fine-grained amphibole.

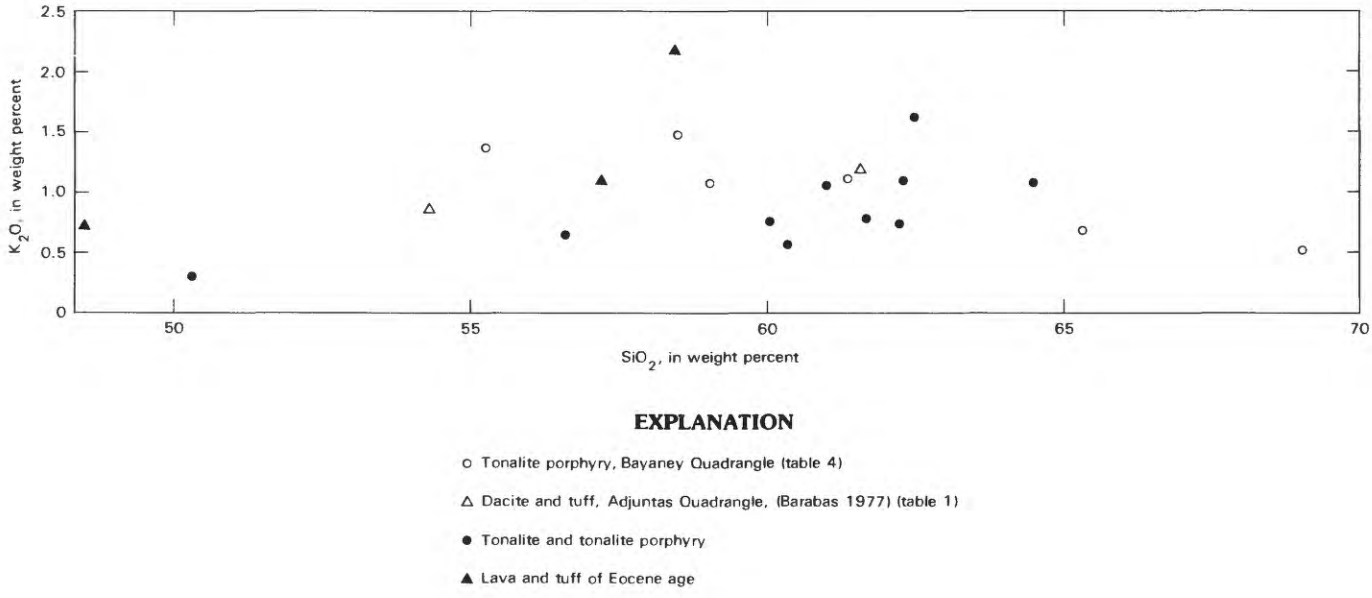


FIGURE 7.—$K_2O$ content versus $SiO_2$ content in tonalite porphyry and dacite of Eocene age, west-central Puerto Rico.

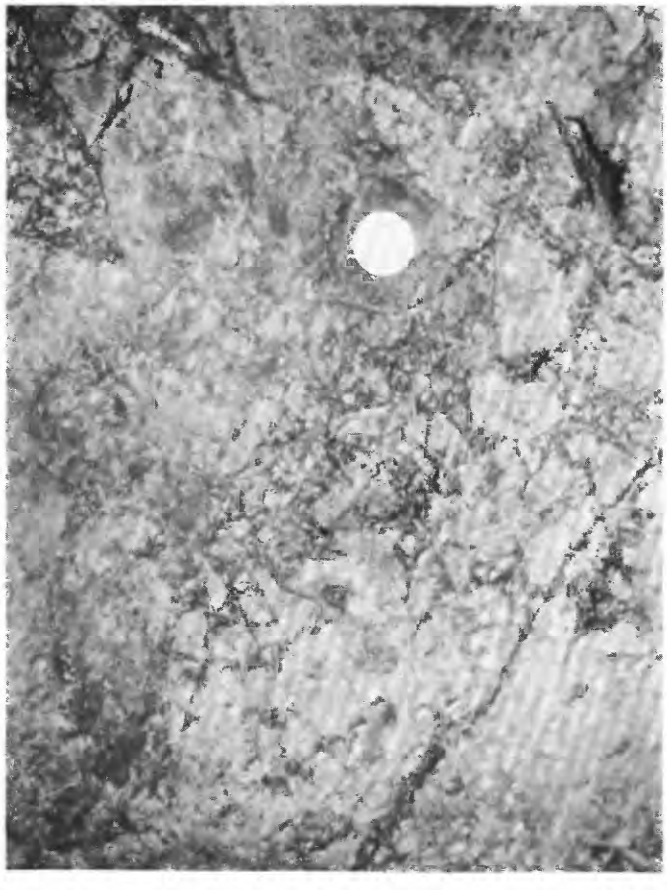

FIGURE 8.—Breccia outcrop on Río Criminales, 200 m west of Highway 602. Fragments are of tonalite porphyry and metavolcanic rock. Coin is 24 mm in diameter.

In the Río Tanamá near its confluence with the Río Coabey, a large mass of basalt porphyry is adjacent to and probably intrudes hydrothermally altered rocks of the Cretaceous basaltic sequence. The basalt porphyry is dull brownish gray and contains conspicuous round to euhedral phenocrysts of clinopyroxene, 3 to 4 mm in diameter, and smaller phenocrysts of plagioclase ($An_{86}$). Equidimensional clusters of serpentine, iddingsite, and carbonate suggest original olivine phenocrysts. The groundmass is composed of calcic plagioclase, clinopyroxene, and magnetite interspersed with abundant iddingsite and carbonates.

### OLIGOCENE FORMATIONS

The San Sebastian Formation of Oligocene age overlies plutonic and metamorphic rocks along the north side of the map area (pl. 1). The formation is composed mainly of yellow to brown clay, siltstone, and sandstone and is intensely weathered in the map area. To the west, in the San Sebastian quadrangle, the formation is better preserved, and many subunits have been recognized (Tobisch and Turner, 1971), including gray and bluish-gray sandstone and siltstone, white clay, conglomerate, and lignite.

In the map area, a conspicuous basal conglomerate is present, composed of chips to boulder-size clasts of quartz, tonalite porphyry, metavolcanic rocks, and tonalite. Preservation of the clastic texture of this unit during weathering allows distinction of the San Sebastian from underlying saprolite (fig. 9). The San Sebastian beds dip 6°-7° N. and lie on a surface of low relief,

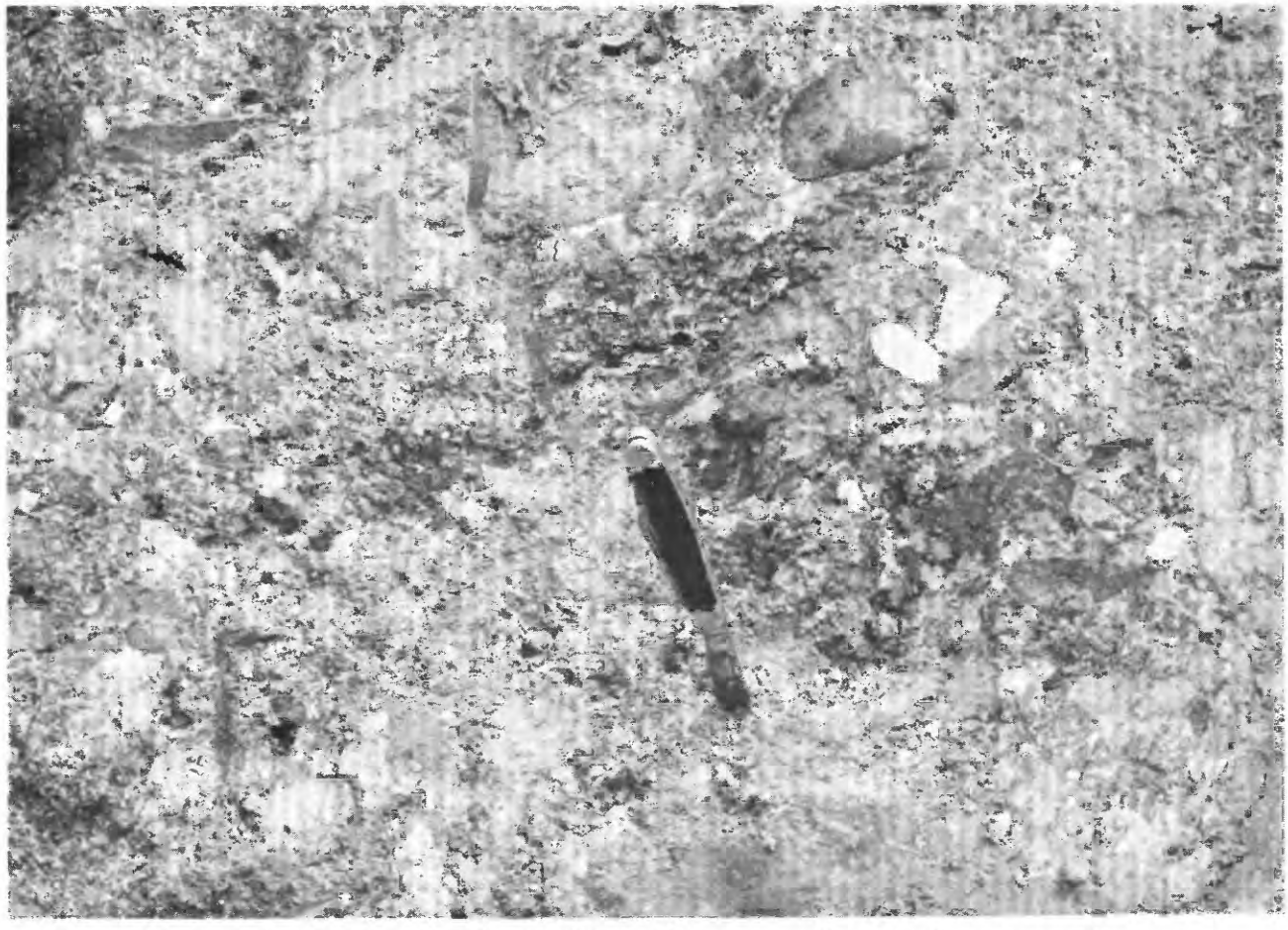

FIGURE 9.—Basal conglomerate of the San Sebastian Formation, weathered to soft, sectile saprolite.

the dissected remnants of which can be recognized as far south as the summit of the 630-m-elevation hill, 1 km north of the Tanamá deposit (pl. 1 and fig. 10).

The San Sebastian Formation is overlain by the Lares Limestone, also of Oligocene age, which forms the strongly karsted terrain north of the map area (pl. 1).

### FAULTING

Three steeply dipping faults offset the contact between the Cretaceous basaltic sequence and the Eocene felsic sequence (pl. 1). One fault, mapped by Nelson and Tobisch (1968), is intruded by Eocene tonalite porphyry near the town of Matilde. A fault trending N. 80° E. was shown by Nelson and Tobisch (1968) in the northwestern part of the map area (pl. 1) and an east-west- trending fault is inferred to cut the Tanamá deposit; the south is downdropped in both localities. R. D. Krushensky and A. F. Curet (unpub. data, 1978) mapped faults cutting Tertiary volcanic rocks in the southwestern part of the map area; one of these faults offsets a porphyry pluton dated as late Eocene (Cox and others, 1977). Widespread fracturing and shearing noted in exposures along stream bottoms

Figure 10.—Surface of low relief sloping northward; view northward from vicinity of Tanamá deposit. The San Sebastian Formation of Oligocene age was deposited on this surface. The San Sebastian is overlain by the Lares Limestone, which forms karst topography in distance.

suggest that faults are abundant in the lower Tertiary and older rocks but are largely obscured by deep weathering. No faults have been mapped in Oligocene and younger rocks in northern Puerto Rico except near the north coast of the island, approximately 14 km northeast of the map area (pl. 1).

## MINERAL DEPOSITS

Two porphyry copper deposits and two porphyry-type prospects are known in the map area (pl. 1). At the largest deposit, Tanamá, 139 million t of ore averaging 0.64 weight percent Cu has been proved by diamond drilling[1]. The Helecho deposit, 1.5 km to the south, contains a slightly smaller amount of ore of about the same grade. The Laundry Creek prospect appeared to be highly attractive on the basis of limited outcrops and geochemical expression but was found on drilling to have too small a tonnage for economic interest. Copper Creek prospect is also a small occurrence showing economic-grade mineralization in only one drill hole.

### HISTORY OF DISCOVERY

The copper deposits in the Tanamá area were discovered by geologists of the Kennecott Copper Corp. The possibility of porphyry copper mineralization in Puerto Rico was recognized by Kennecott Copper Corp. officials in 1956, at about the same time as William R. Bergey discovered the Río Viví deposits (see Bergey, 1966; Cox and others, 1975). Geologists of Kennecott Copper Corp.'s Latin American subsidiary, under the direction of George Ordoñez, reconnoitered the island, and an exploration concession in west-central Puerto Rico was secured in 1958. By late 1958, most of the exploration targets had been delineated by surface mapping and stream-sediment geochemistry, under the direction of Johan Brinck. Diamond drilling began in July 1959 at the Laundry Creek deposit and later that year at Copper Creek and Helecho. The Tanamá deposit was first drilled in late 1960 and in succeeding years received most of the attention because of its large tonnage and amenability to open-pit mining. By 1965, 155 holes, aggregating 44,000 m, had been drilled, and the tonnage of the Tanamá and Helecho deposits had been determined. The Kennecott Copper Corp. and its Puerto Rico subsidiary, Cobre Caribe S.A., applied for a mining lease in September 1965. A long period of negotiations followed between the Puerto Rican Government and the Kennecott Copper Corp. AMAX Inc. and its Puerto Rican subsidiary, the Ponce Mining Co., had, during the same period, drilled out Bergey's discovery at Río Viví (fig. 1). The Ponce Mining Co. also applied for a mining lease and joined with Cobre Caribe S.A.in the negotiations. At the time of this writing (1984), in spite of serious efforts by all parties, agreement has not yet been reached on the terms of a mining lease.

[1]Reserves for Tanamá and Helecho have not been made public by the Kennecott Copper Corp. The source for this reserve estimate is a speech by David H. Ackerman, Vice President of Ponce Mining Co. before the Overseas Press Club in San Juan, Puerto Rico, October 22, 1970.

### TANAMÁ DEPOSIT

The Tanamá deposit is on the west side of the Río Tanamá in the Municipio de Utuado, 3.2 km south of the town of Ángeles (lat 18° 15′ 30″ N., long 66°49′ 29″ W.). The deposit consists of two ore bodies, separated by about 100 m of weakly mineralized rocks. The northern ore body is exposed in a few places, whereas the southern ore body is completely mantled by a thick layer of saprolite. Roadcuts made during the diamond-drilling program in the 1960's largely were collapsed and overgrown with vegetation at the time of the present study 10 years later. Because of the limited information available from the surface, only a geologic sketch map was prepared for this study (fig. 11*A*).

Studies at Tanamá leading to this report were made on drill core provided by the Kennecott Copper Corp. Because time did not permit study of all the available core, samples were selected from two intervals in each drill hole, representing rock from two horizontal sections through the deposit. The first horizontal section, chosen at 430-m elevation, lies just below the secondary-enrichment blanket (fig. 11*B*); the second horizontal section cuts the two ore bodies at 300-m elevation (fig. 11*C*). For all the samples collected from these horizontal sections, the field number also provides the sample location. For example, field No. T56-1 is from drill hole T56 at 430-m elevation (fig. 11*B*) and field No. T56-2 is from the same drill hole at 300-m elevation (fig. 11*C*). In addition, samples were selected from the entire length of 16 drill holes along four vertical sections cutting the two ore bodies. These samples bear labels with prefix 17- (figs. 12, 13). These data were supplemented by information on copper grade from drilling logs prepared by geologists from the Kennecott Copper Corp.

Samples were sectioned and stained for petrographic study. X-ray identification was made of phyllic minerals by Patricia Loferski, and selected samples were polished for microprobe analysis of amphibole. Samples showing intersecting veinlets were polished and studied by fluid-inclusion microthermometry, using a Chaix Meca apparatus. Composite chip samples from each drill hole at two intervals representing the two horizontal sections were analyzed both spectrographically and chemically.

#### GEOLOGY

Three tonalite porphyry bodies enclosed in metavolcanic rocks of the Cretaceous basaltic sequence are hydrothermally altered and mineralized in the Tanamá

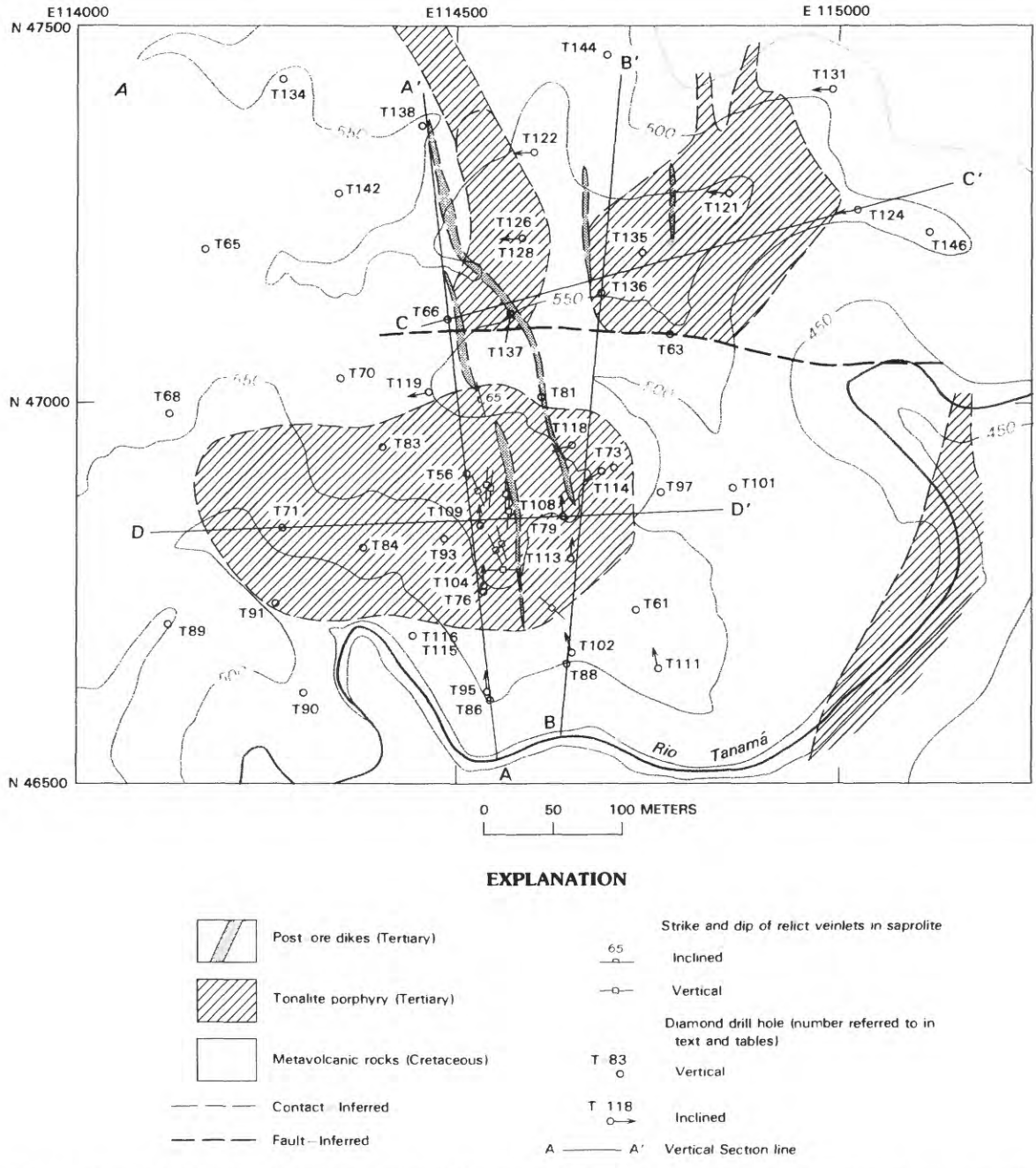


FIGURE 11.—Geologic maps of Tanamá deposit. *A*, Surface geologic sketch map. Contours in meters above sea level; coordinates in meters, Puerto Rico coordinate system. *B*, Horizontal section at 430-m elevation above sea level. For simplicity, postore dikes are shown within ore zone when, in fact, their grade is well below 0.4 weight percent Cu. *C*, Horizontal section at 300-m elevation.

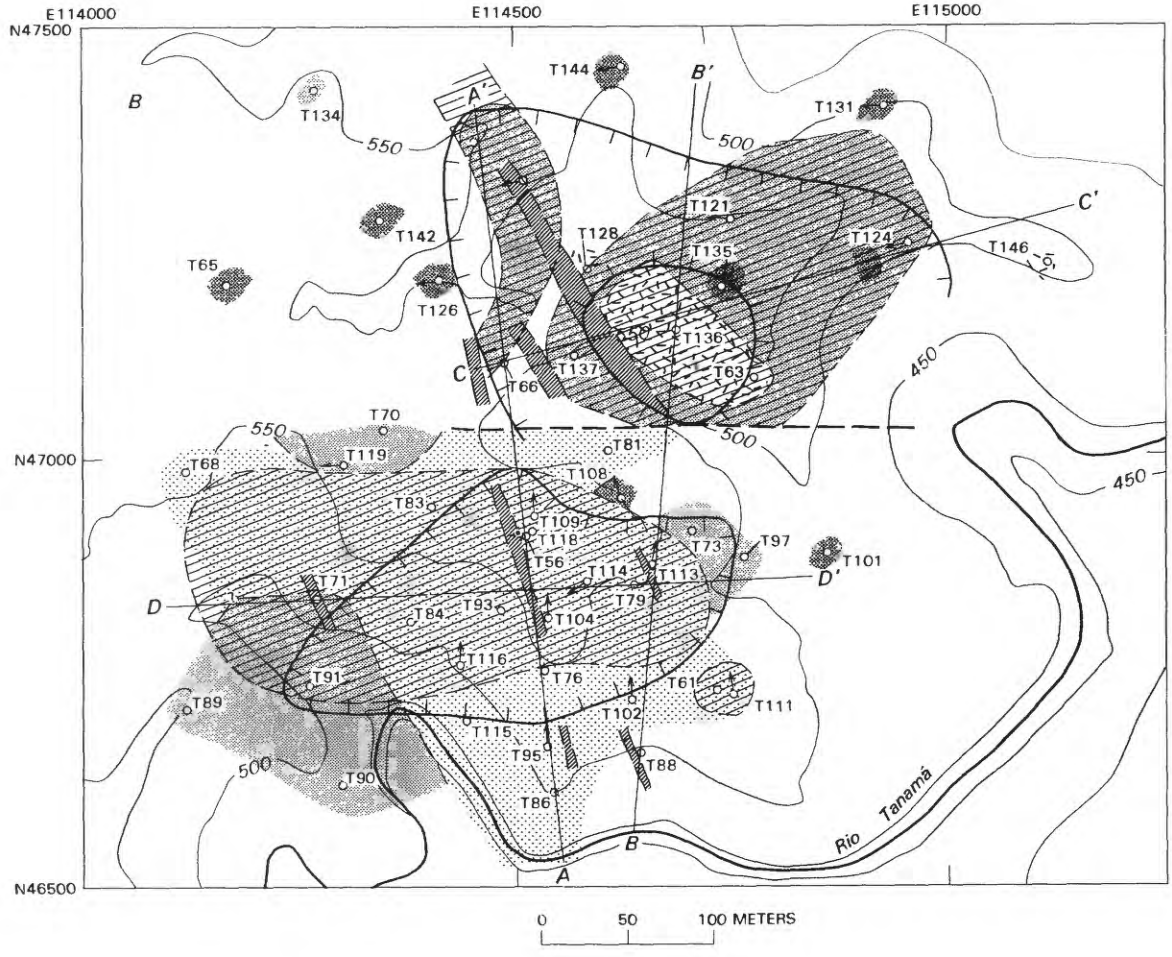


**EXPLANATION**

Hydrothermal alteration assemblages

- Feldspar destructive
- Chlorite
- Chlorite–biotite
- Amphibole

Rock Types

- Post-ore dikes
- Tonalite porphyry
- Metavolcanic rocks
- Contact–Inferred
- Fault–Inferred

Diamond–drill hole

- T83 Vertical
- T118 Inclined
- Limit of greater-than-0.4-weight-percent Cu ore body (hachures on side of higher grade.)

FIGURE 11.——Continued.

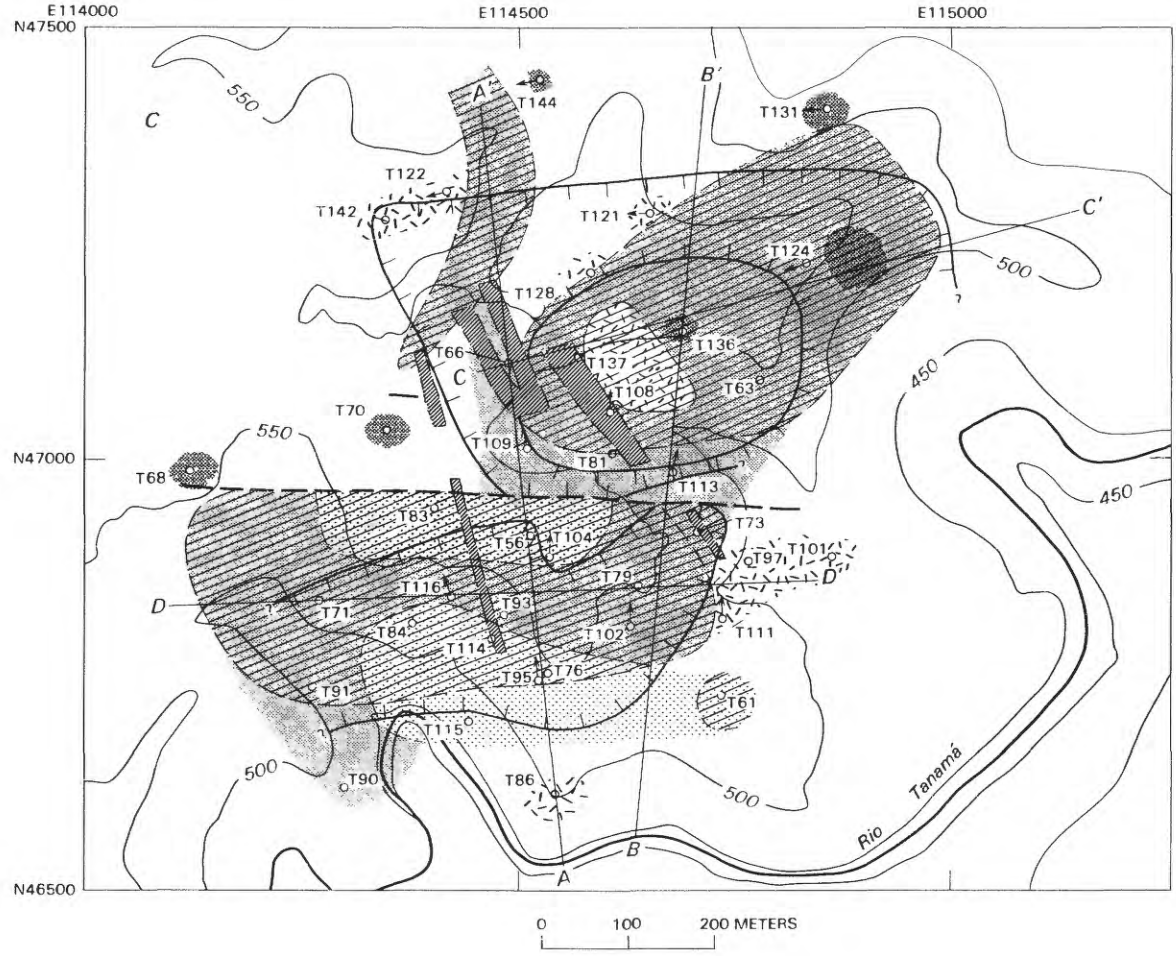


**EXPLANATION**

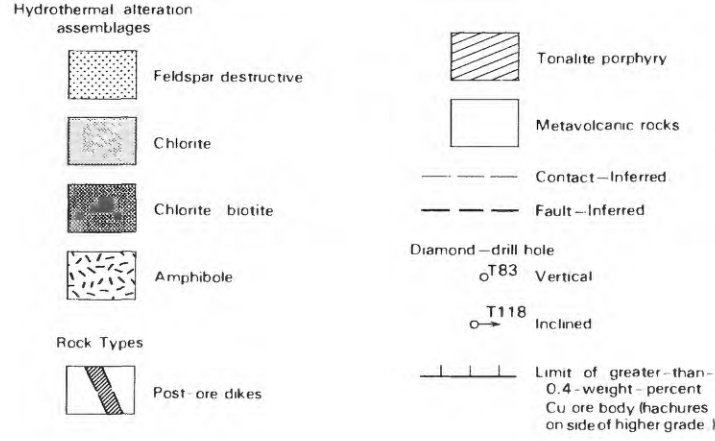


FIGURE 11.—Continued.

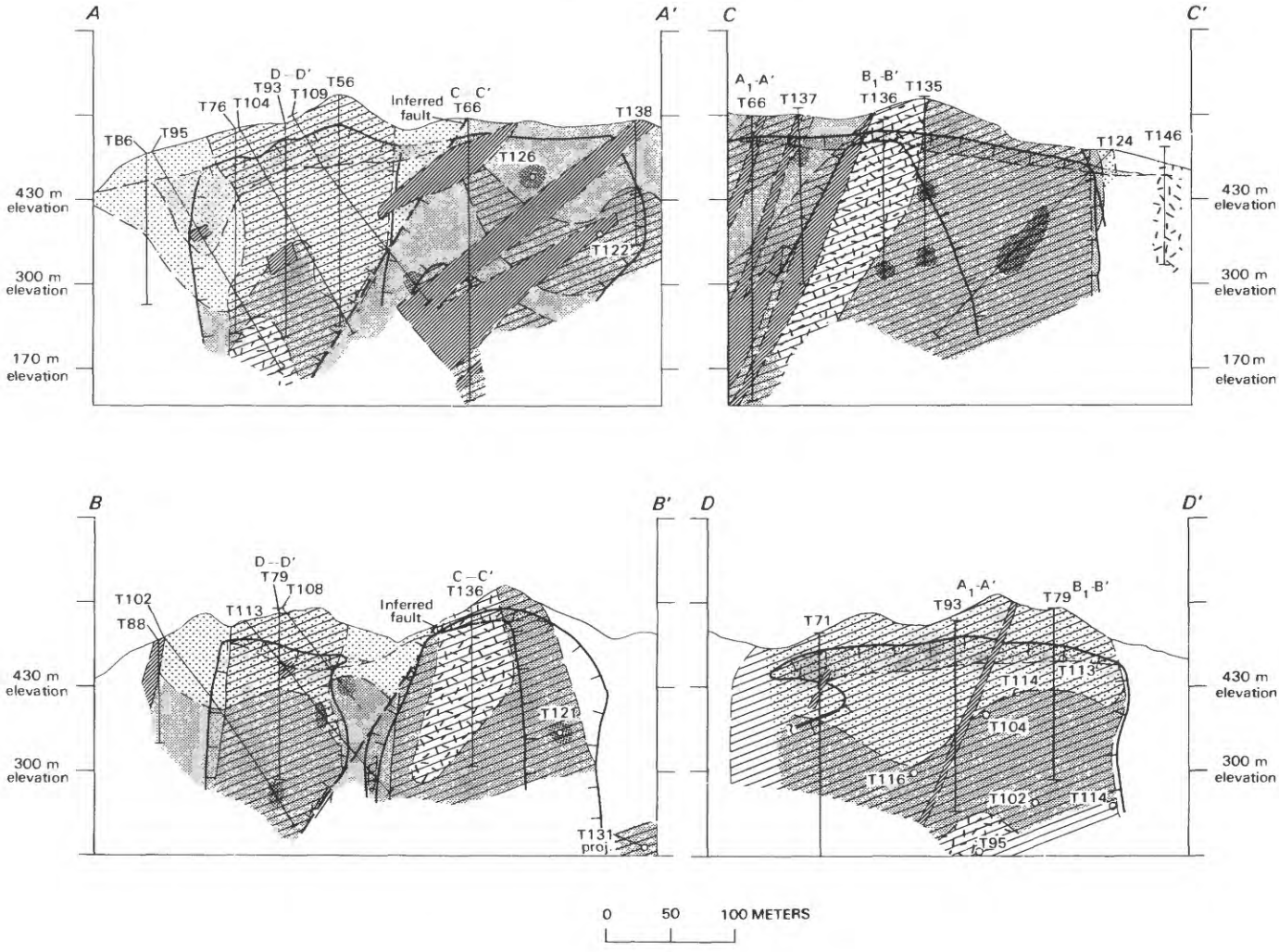


**EXPLANATION**

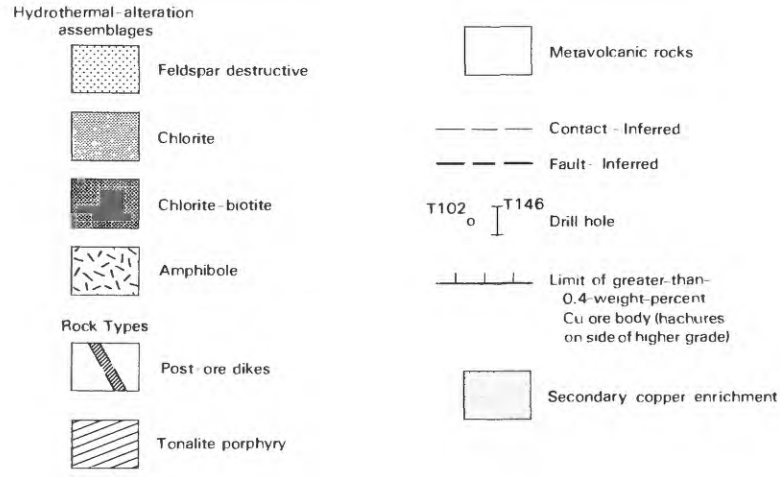


FIGURE 12.—Cross sections of Tanamá deposit (see fig. 11 for locations).

area. These porphyry bodies show no textural or compositional features, other than degree of alteration and mineralization, that distinguish them from tonalite porphyry bodies elsewhere in the map area (pl 1). Contact relations of the porphyry stocks, which were unobservable at the surface, can only be indirectly inferred from drill-core studies. Drill-hole intercepts of mixed porphyry and metavolcanic rocks, tens of meters long, around many porphyry contacts suggest intrusion by magmatic stoping of metavolcanic rocks. Contacts dip steeply to vertically except in the northwestern part of the deposit. There, drill-hole intercepts show that the narrow screen of metavolcanic rocks separating the northwestern and northeastern plutons dips 40°-60° W. (fig. 12*C*); the west contact of the northwestern pluton also dips west.

The plutonic and metavolcanic rocks are intensely fractured, altered, and mineralized and weather to a white to light-tan saprolite containing abundant limonite segregations and relict veinlets. In a few places, the strike of relict veinlets in saprolite can be measured. Most veinlets range in strike from N. 5° E. to N. 25° W.; the preferred orientations are north-south and N. 20° W.

Figure 12 shows drill-hole intercepts of dark-colored tonalite porphyry dikes mapped on the surface by Kennecott Copper Corp. geologists (fig. 11*A*). These dikes, which intrude ore zones but have a very low Cu content, are here referred to as postore porphyry. Postore porphyry, which has a groundmass texture that is microaplitic and fine grained (0.01-0.02 mm), is indistinguishable from the tonalite porphyry bodies that are widespread in the Bayaney quadrangle. Postore porphyry contains clusters of epidote and veinlets of calcite. Chemical analysis of some samples (field Nos. T108-2, T137-2, table 12) showed very high Zn contents, probably derived from sphalerite in calcite veins.

Some of the contacts between the porphyry bodies and metavolcanic rocks are probably faults, although this conclusion was not confirmed by the present study. Maps by Kennecott Copper Corp. geologists, presumably based on studies of fresh bulldozer cuts, show faults separating the northeastern porphyry body from the other two and also bounding the southeast side of the two larger intrusions.

A different structural interpretation is based on the distribution of hydrothermal-alteration zones noted in the present study and on the shape of the north contact of the southern tonalite porphyry cut by drill holes T104 and T109 (cross sec. *A-A'*, fig. 12). An east-west-striking normal fault, dipping 50°-60° S., is inferred to exist, along which the southern porphyry body has been dropped 450 m vertically from its original position above the two northern porphry bodies. This fault is inferred to pass near the collar of drill hole T66 and to be responsible for the overhang in the porphyry contact noted in drill holes T104 and T109 (cross sec. *A-A'*, fig. 12). According to this interpretation, the three exposures of tonalite porphyry as well as the northern and southern ore bodies are believed to be parts of one overall mineralized system (fig. 13).

This normal-fault model explains the marked difference in hydrothermal alteration observed in the northern and southern Tanamá ore bodies. As described below in the next section, feldspar-stable-alteration assemblages containing chlorite, amphibole, magnetite, and chalcopyrite characterize the tonalite porphyry in the northern ore body. The southern ore body contains abundant white mica, clay, pyrite, and chalcopyrite; plagioclase is almost completely destroyed. In the deeper parts of the southern ore body, however, drill holes intercept feldspar-stable-alteration zones similar to those in the northern ore body. According to the normal-fault model, feldspar-destructive alteration in the southern ore body represents the highest level of the hydrothermal system established in and near the porphyry pluton before faulting. Postore porphyry dikes, as mapped by Kennecott Copper Corp. geologists, appear not to be offset by the inferred fault displacement and thus are believed to be younger than the normal-fault movement.

Cross sections drawn in an easterly direction across the northern and southern deposits suggest that both segments of the deposit have been tilted to the east. Evidence for this tilting are: (1) the westerly dip of porphyry contacts in the northwestern part of the deposit, (2) the occurrence of chloritic alteration below amphibole alteration in drill hole T136 and the apparent westward dip of the boundary between these two alteration zones, and (3) the westward dip of postore dikes (see fig. 12).

Figure 13 shows a reconstruction of the Tanamá deposit. The assumed eastward tilt of the area requires a corresponding right-lateral component to the dominantly dip-slip movement on the inferred fault. Therefore, in this reconstruction, cross-section *B-B'* (fig. 11) of the northern ore body is matched with cross-section *A-A'* of the southern ore body to give an oval stock with lateral dimensions of 300 by 700 m, a vertical extent of at least 750 m, and a branching root zone. Copper is distributed in a shell surrounding a low-grade core in the lower part of the stock. The upper limit of this low-grade core, which is not observable in the present faulted configuration, probably was situated about 100 m above the present erosional surface over the northern ore body. In the upper part of the stock the copper ore body is approximately coextensive with the porphyry stock. Three hydrothermal-alteration assemblages are concentrically and vertically distributed in the stock and surrounding volcanic rocks, as discussed in the following subsection.

### Feldspar-Stable Alteration and Mineralization

Two feldspar-stable hydrothermal-mineral assemblages, found in the northern ore body and in the deeper parts of the southern ore body, are: intermediate plagioclase + quartz + hornblende + magnetite ± chalcopyrite and plagioclase + quartz + chlorite + magnetite ± chalcopyrite ± biotite ± actinolite ± epidote ± potassium feldspar. Both assemblages are characterized by the preservation of intermediate plagioclase ($An_{45-60}$) in which igneous oscillatory-zoning patterns are commonly present. The boundary between these zones is indistinct and gradational.

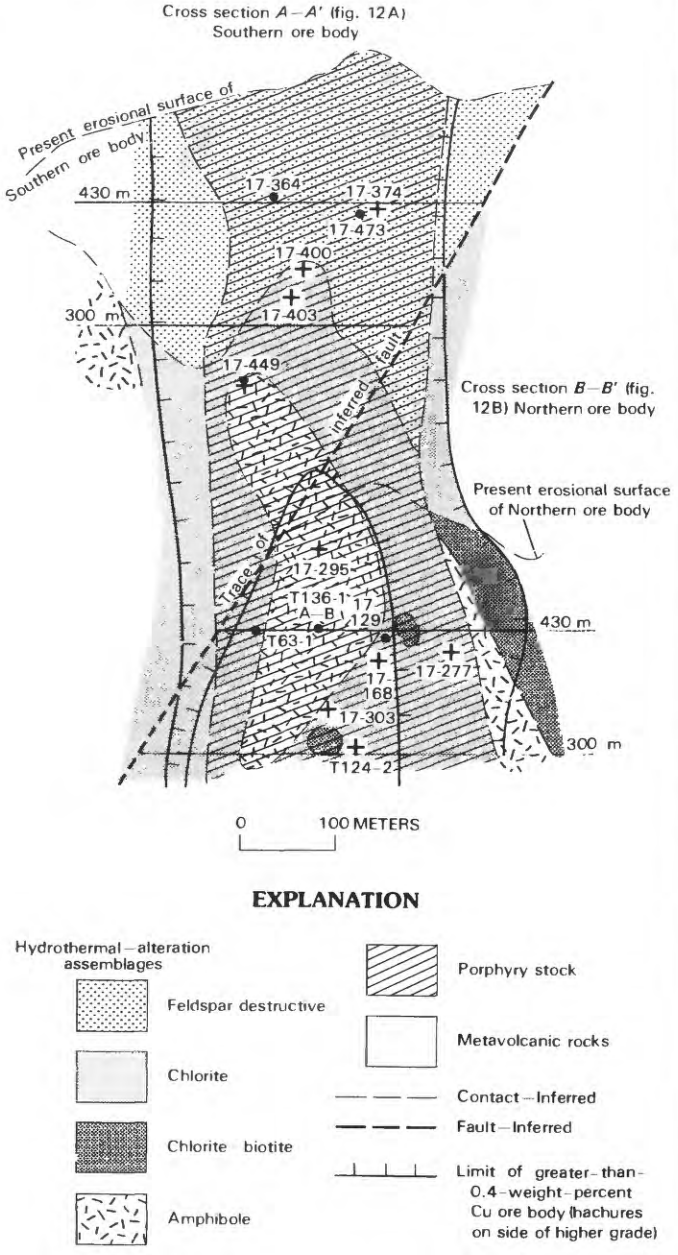


FIGURE 13.—Interpretive cross section of Tanamá deposit before faulting. Samples marked by a "+" show elevation and projected positions of rocks selected for fluid-inclusion study (numbers refer to table 9 and fig. 21); samples marked by dots were analyzed for oxygen- and hydrogen-isotope ratios (numbers refer to table 11).

The presence of abundant veinlets of quartz, quartz-magnetite, and quartz-chalcopyrite without hydrothermal-alteration haloes (fig. 14*A*) distinguishes these assemblages from those of porphyry bodies and metavolcanic rocks elsewhere in the map area (pl. 1). In other respects, the amphibole-dominated assemblage resembles the hornblende-hornfels mineral assemblage common in the Cretaceous basaltic sequence, and the chlorite-dominated assemblage resembles regional-alteration assemblages developed in Eocene porphyry bodies throughout the map area. Both the regional-alteration and ore-zone-alteration assemblages present in Eocene porphyry bodies are mineralogically equivalent to the propylitic-alteration assemblages that surround many porphyry systems in the Andean and North American Cordillera. Evidence supporting a model that explains the close association of propylitic alteration and ore mineralization is presented in the subsection below entitled "Mineralization and Alteration." I propose that the chlorite was derived by replacement of early-formed hydrothermal biotite during subsequent circulation of meteoric fluids.

Chemical analyses of rocks with feldspar-stable alteration (table 4), in comparison with unmineralized tonalite porphyry (table 3), indicate higher $SiO_2$ contents due to introduced quartz as veinlets and lower $Al_2O_3$, CaO, and $Na_2O$ contents due to dilution of these components by the addition of quartz. $K_2O$ content is

TABLE 4.—*Chemical analyses of tonalite porphyry with feldspar-stable alteration, Tanamá and Helecho deposits*

[Chemical analyses in weight percent by single-solution procedure (Shapiro, 1975); analysts, H. Smith and J. Reid. FeO not determined (n.d.) in sample with highest S content. Samples 1 and 2 conteined pyrite veinlets with feldspar-destructive-alteration haloes]

| Sample--- | 1 | 2 | 3 | 4 | 5 | 6 | 7 | 8 |
|---|---|---|---|---|---|---|---|---|
| Field No- | T79-2 | T93-2 | T124-1 | T124-2 | 36 | 85 | T135-1 | 17-294 |
| $SiO_2$ ---- | 68.1 | 68.5 | 68.3 | 66.3 | 62.3 | 64.4 | 65.9 | 64.9 |
| $Al_2O_3$ --- | 14.9 | 11.6 | 14.4 | 14.1 | 15.3 | 14.5 | 15.5 | 15.2 |
| $Fe_2O_3$ --- | 2.0 | 7.2 | 1.8 | 2.8 | 3.9 | 4.7 | 2.7 | 4.7 |
| FeO ----- | 1.0 | n.d. | 1.3 | 3.2 | 3.4 | 3.4 | 2.6 | 3.4 |
| MgO ----- | 2.7 | 2.0 | 2.1 | 2.2 | 2.5 | 2.6 | 2.2 | 1.7 |
| CaO ----- | 1.9 | .56 | 3.8 | 4.2 | 3.7 | 3.5 | 4.1 | 4.7 |
| $Na_2O$ --- | 1.0 | .28 | 2.3 | 2.5 | 2.5 | 3.0 | 2.6 | 3.3 |
| $K_2O$ ---- | 2.6 | 2.4 | .83 | .64 | .89 | .79 | 1.0 | .18 |
| $H_2O^+$ --- | 2.8 | 2.4 | 1.7 | 2.2 | 2.4 | 1.7 | 1.8 | 1.2 |
| $H_2O^-$ --- | .84 | .48 | .48 | .50 | .76 | .57 | .36 | .26 |
| $TiO_2$ --- | .42 | .34 | .36 | .43 | .47 | .47 | .44 | .35 |
| $P_2O_5$ --- | .18 | .21 | .17 | .17 | .18 | .16 | .19 | .16 |
| MnO ----- | .04 | .04 | .06 | .18 | .06 | .04 | .14 | .14 |
| $CO_2$ ---- | .46 | .01 | .08 | .34 | .08 | .04 | .08 | .06 |
| S ------ | 1.3 | 3.7 | 1.3 | .58 | .79 | .51 | .74 | n.d. |
| Total-- | 100.2 | 99.7 | 99.0 | 100.3 | 99.2 | 100.4 | 100.4 | 100.2 |
| Sulfide | 1.1 | 3.3 | 1.1 | .45 | .69 | .38 | .64 | n.d. |

Samples 1,2,3,4, and 7: See figure 12 for location.
Samples 5 and 6 from Helecho deposit, Río Coabey streambed: See figure 33 for location. Sample 8 from Tanamá deposit, drill hole T136, 515m elevation.

doubled by the presence of small veinlets with sericitic alteration haloes (samples T79-2, T93-2, table 4). The sample from drill hole T136 in the barren core of the northern ore body shows a notable depletion in $K_2O$ content relative to unaltered porphyry.

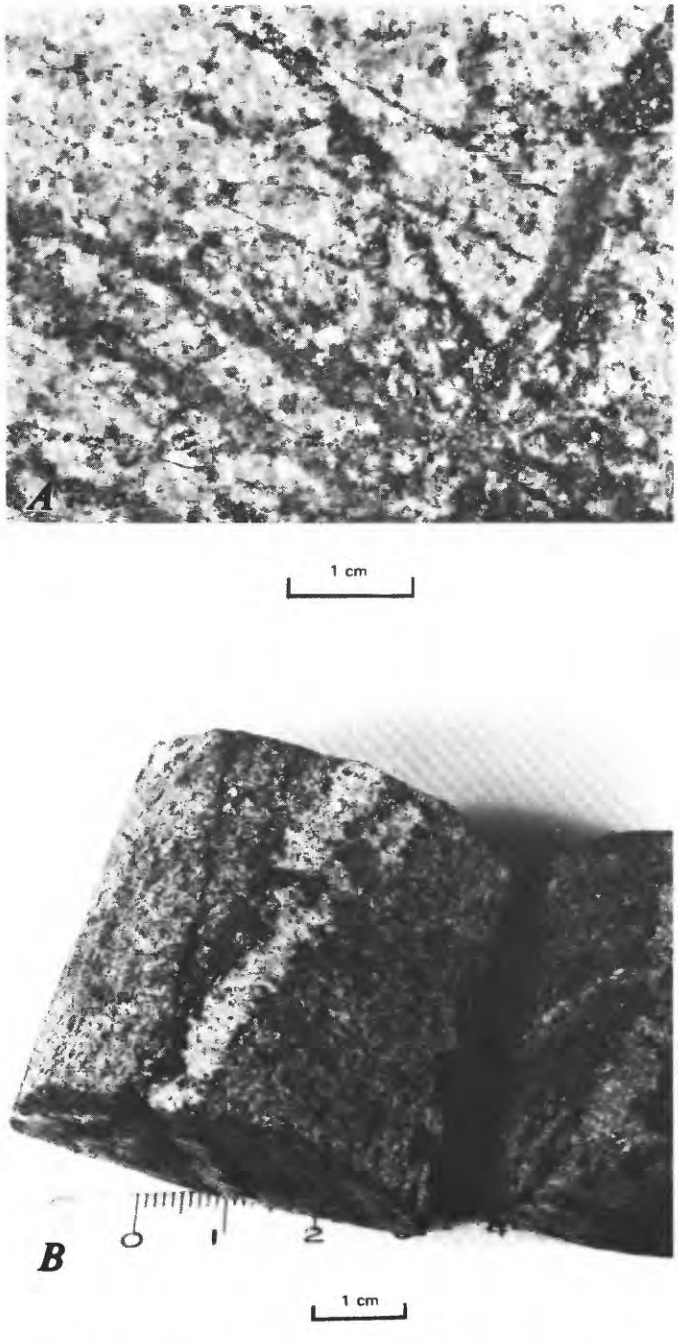


FIGURE 14.—Veinlets in tonalite porphyry, Tanamá deposit. *A*, Closely spaced veinlets of various ages. Chalcopyrite is evenly disseminated throughout rock and crosscutting veins. Drill hole T66, 300-m elevation. *B*, Type C veinlets containing magnetite grains along veinlets walls. Drill hole T135, 195- and 235-m elevation.

### HORNBLENDE-DOMINATED ASSEMBLAGES

Alteration assemblages in which hornblende is the dominant mineral occur in porphyry in the central core of the northern ore body in drill holes T63 and T136. They are also found in porphyry in the deepest parts of the southern ore body in drill hole T95. Metavolcanic wallrocks in which hornblende is the dominant alteration mineral are mainly found in drill-hole intercepts at the 300-m-elevation horizontal section and in two drill holes (T128, T146) at 430-m elevation. The distribution of drill-hole data did not permit mapping of these assemblages in the metavolcanic rocks. As noted above, hornblende-hornfels-facies metamorphism, which is widespread in the map area (pl. 1), produced abundant amphiboles in the basaltic rocks that host the tonalite porphyries. Here, as in other localities, it is difficult to distinguish between a metamorphic and a hydrothermal origin of the hornblende-dominated assemblages in mafic wallrocks of the porphyry deposits.

The most abundant minerals in these assemblages are intermediate plagioclase, quartz, hornblende, and magnetite. Other minerals found in varying amounts, which are believed on petrographic evidence to belong to other assemblages subsequently developed in these rocks, include fibrous cummingtonitic amphibole, chlorite, biotite, epidote, sericite, and calcite. Chalcopyrite is abundant in the hornblende-magnetite assemblage in the lowermost part of the southern ore body cut by drill hole T95, whereas in the northern ore body it is present only in traces.

Quartz occurs in abundant veinlets and as phenocrysts and groundmass grains. Quartz veinlets spatially associated with this alteration assemblage are of two types: thin (2-3 mm wide) veinlets of granular quartz, here designated "type B"; and thicker granular quartz-magnetite veinlets cutting type B veinlets, here designated "type C." Both types of veinlets have parallel and distinct walls and no alteration envelope. Type C veinlets are rich in magnetite, arranged in equant grains along the vein walls (fig. 14*B*).

Hydrothermal hornblende forms pseudomorphs of igneous phenocrysts, clusters of grains replacing phenocrysts, and veinlets. Hornblende in veinlets is accompanied by magnetite but no quartz and only locally by chalcopyrite (fig. 15). These hornblende veinlets cut types B and C quartz veinlets and are here designated "type D". Hydrothermal hornblende is weakly pleochroic, with *X* pale greenish tan, *Y* greenish brown, and *Z* green.Table 5 lists electron-microprobe analyses and structural formulas of these hornblendes, and figure 6 plots the compositional variations. Most amphiboles in hydrothermal assemblages have magnesiohornblendic compositions, and there is some degree of overlap in compositional range with the hornblendes

in phenocrysts in unaltered rocks. The compositional ranges of hydrothermal hornblendes, however, are narrower than those of the igneous amphiboles. Decrease in $Al^{IV}$ is coupled with an increase in Mg and decreases in Ti, Ca, Na, and total Fe, trending toward actinolitic hornblende. The trend toward low-Mg, high-Fe, and Ca-actinolitic compositions noted in weakly altered rocks is absent in the data on hydrothermal amphiboles. Hornblendes from drill hole T95 (fig. 12*A*), cutting the uppermost part of the zone of the hornblende-dominated assemblage, were the only ones with a $K_2O$ content above the analytical-detection limit of about 0.05 weight percent.

Magnetite occurs as abundant rounded grains, disseminated in a porphyry groundmass, in type C quartz veinlets along the vein walls, in type D amphibole veinlets, and in early magnetite veinlets, here designated "type A". Type A veinlets consist of irregular streaks and wispy veinlets of magnetite, generally only a few centimeters long; they are cut by types B and C quartz veinlets. Intergrowth with ilmenite is common in disseminated magnetite grains and in some grains within veinlets.

Chalcopyrite occurs as traces in most of the amphibole-dominated assemblages in the northern (lower) part of the deposit. In the uppermost part of the amphibole-dominated zone cut by drill-hole T95, chalcopyrite is sufficiently abundant that the rock there assays 0.5 weight percent Cu. In general, chalcopyrite is disseminated in the rock and is not controlled by fractures or quartz veins. Locally, chalcopyrite has partly replaced magnetite in disseminated grains and veinlets.

Bornite occurs in traces, everywhere in contact with grains of chalcopyrite. Bornite forms rims and, rarely, crosscutting veins in chalcopyrite grains.

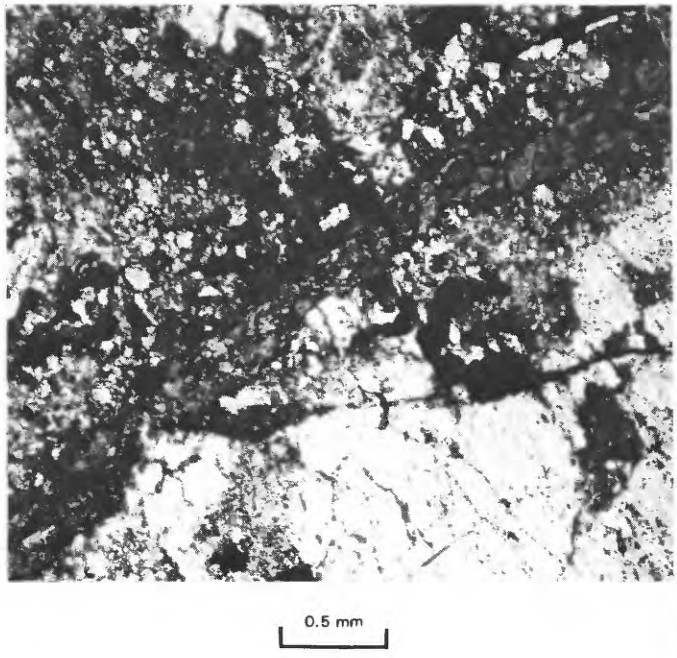


FIGURE 15.—Photomicrograph showing hornblende in type D veinlet, Tanamá deposit. Plane-polarized light. Field No. 17-444, drill hole T95, 225-m elevation.

### CHLORITE-DOMINATED ASSEMBLAGES

Chlorite is the dominant alteration mineral in most of the northern ore body and the deeper half of the southern ore body. The chlorite occurs with abundant quartz veins and with chalcopyrite that is predominantly disseminated rather than fracture controlled. Intergrowth of biotite with chlorite in a few places in altered porphyry suggests that at least part of the chlorite was derived by replacement of early-formed biotite (figs. 17*A*). Altered metavolcanic rocks locally contain abundant biotite as well as chlorite, and biotitic alteration of volcanic rocks is common in drill-hole intercepts at 430-m elevation on the north side of the northern ore body (fig. 11*B*). Other minerals in addition to chlorite, chalcopyrite, and biotite that occur in these assemblages are: quartz, albite, epidote, fibrous amphibole, potassium feldspar, calcite, magnetite, rutile, bornite, pyrite, and molybdenite.

Chalcopyrite is abundant in most parts of the porphyry stock that contain chlorite-dominated alteration assemblages. A major part of the barren core zone penetrated by the lower parts of drillholes T136 and T124, however, exhibits chlorite-dominated alteration assemblages and only traces of chalcopyrite (see fig. 12*C*).

Throughout the ore zone, chalcopyrite is finely disseminated as small equidimensional grains and is less commonly concentrated in veinlets. The same quartz veinlets, types B and C, recognized in the amphibole-dominated alteration assemblages in the interior of the deposit are also recognized in the chlorite-dominated assemblages. Magnetite in type C veins is replaced to varying degrees by chalcopyrite in the chlorite assemblage. In addition to types B and C quartz veins, a third type of quartz veinlet is recognized in porphyry with chlorite alteration. These veinlets, which cut type D veinlets, are here designated "type E". Type E veinlets have no alteration haloes and are distinguished by a thin discontinuous layer of chalcopyrite and minor pyrite running along the center of each vein (fig. 16).

Chlorite occurs in clusters replacing hornblende phenocrysts and replacing hornblende or biotite in veinlets with quartz, chalcopyrite, and magnetite (fig. 17*A*). The

TABLE 5. —*Partial analyses of magnesiohornblende and actinolitic hornblende in feldspar-stable-alteration assemblages, Tanamá deposit*
[Electron-microprobe analyses in weight percent, following the methods of Huebner and others (1976); analyst, L.B. Wiggins, U.S, Geological Survey. Structural formulas in atomic percent, calculated by the methods of Papike and others (1974)]

| Sample---- | 10 | 11 | 12 | 13 | 14 | 15 | 16 | 17 | 18 | 19 | 20 | 21 |
|---|---|---|---|---|---|---|---|---|---|---|---|---|
| Field No.- | T128-2A | | T135-1A | 17-290 | | 17-294 | | 17-304 | | 17-449 | | 17-196 |
| | Electron-microprobe analyses | | | | | | | | | | | |
| $SiO_2$ ---- | 51.4 | 52.7 | 48.0 | 50.7 | 48.3 | 49.5 | 47.2 | 50.6 | 46.6 | 49.3 | 50.9 | 50.0 |
| $Al_2O_3$ --- | 4.8 | 3.7 | 7.3 | 4.5 | 6.9 | 5.2 | 7.4 | 5.3 | 8.2 | 5.9 | 5.6 | 5.0 |
| $Fe_2O_3$ --- | 7.9 | 8.5 | 8.1 | 5.6 | 7.9 | 7.9 | 8.2 | 7.6 | 8.0 | 8.0 | 8.3 | 6.1 |
| FeO ----- | 3.0 | 3.4 | 6.7 | 3.9 | 5.4 | 4.6 | 6.3 | 5.3 | 6.9 | 3.7 | 3.5 | 4.9 |
| MgO ----- | 17.3 | 18.4 | 15.1 | 17.1 | 15.4 | 16.6 | 14.3 | 16.5 | 14.3 | 15.6 | 16.3 | 17.9 |
| CaO ----- | 10.2 | 9.4 | 10.8 | 10.8 | 11.2 | 10.9 | 10.2 | 10.9 | 11.1 | 11.6 | 11.6 | 11.3 |
| $Na_2O$ ---- | .81 | .60 | 1.35 | .83 | 1.50 | .93 | 1.4 | .85 | 1.56 | .96 | 1.01 | .81 |
| $K_2O$ ----- | .0 | .0 | .0 | .0 | .0 | .0 | .0 | .0 | .0 | .10 | .05 | .0 |
| $TiO_2$ ---- | .59 | .27 | 1.27 | .70 | 1.19 | .90 | 1.04 | .68 | 1.15 | 1.08 | .78 | .65 |
| $MnO_2$ ---- | .86 | .79 | .77 | .53 | .48 | .52 | .72 | .73 | .70 | .77 | .14 | .40 |
| Total-- | 96.9 | 97.8 | 99.4 | 94.7 | 98.3 | 97.0 | 96.8 | 98.5 | 98.5 | 97.0 | 98.2 | 97.1 |
| | Structural formulas | | | | | | | | | | | |
| Si ------- | 7.37 | 7.48 | 6.84 | 7.27 | 6.94 | 7.15 | 6.90 | 7.20 | 6.73 | 7.14 | 7.24 | 7.17 |
| Al ------- | .63 | .52 | 1.16 | .73 | 1.06 | .85 | 1.10 | .80 | 1.27 | .86 | .76 | .83 |
| Al ------- | .19 | .09 | .08 | .03 | .10 | .04 | .18 | .08 | .13 | .14 | .19 | .02 |
| $Fe^{2+}$ ----- | .95 | 1.01 | .97 | 1.04 | .95 | .96 | 1.01 | .90 | .96 | .97 | .98 | .73 |
| $Fe^{3+}$ ----- | .32 | .36 | .72 | .42 | .58 | .50 | .69 | .57 | .75 | .41 | .37 | .53 |
| Mg ------- | 3.68 | 3.90 | 3.21 | 3.66 | 3.30 | 3.58 | 3.12 | 3.50 | 3.07 | 3.36 | 3.46 | 3.83 |
| Mn ------- | .10 | .10 | .09 | .06 | .06 | .06 | .09 | .09 | .09 | .09 | .02 | .05 |
| Ti ------- | .06 | .03 | .14 | .07 | .13. | .10 | .11 | .07 | .12 | .12 | .08 | .07 |
| XOCT ----- | .32 | .49 | .20 | .29 | .13 | .24 | .20 | .22 | .13 | .09 | .11 | .22 |
| Ca ------- | 1.56 | 1.43 | 1.66 | 1.66 | 1.72 | 1.69 | 1.60 | 1.66 | 1.72 | 1.80 | 1.77 | 1.73 |
| Na ------- | .12 | .08 | .14 | .05 | .15 | .07 | .20 | .12 | .15 | .11 | .13 | .04 |
| Na ------- | .11 | .08 | .73 | .18 | .27 | .10 | .20 | .12 | .29 | .16 | .15 | .18 |
| K -------- | 0 | 0 | 0 | 0 | 0 | 0 | 0 | 0 | 0 | .02 | .01 | 0 |
| Sum A ---- | .11 | .08 | .23 | .18 | .27 | .19 | .20 | .12. | .29 | .18 | .16 | .18 |

Sample 10. Actinolitic hornblende phenocryst, drill hole T128, 300-m elevation.
11. Actinolitic hornblende phenocryst, drill hole T128, 300-m elevation.
12. Magnesiohornblende phenocryst, drill hole T135, 430-m elevation.
13. Actinolitic hornblende phenocryst, drill hole T136, 374-m elevation.
14. Magnesiohornblende phenocryst, drill hole T136, 374-m elevation.
15. Magnesiohornblende phenocryst, drill hole T136, 515-m elevation.
16. Magnesiohornblende phenocryst, drill hole T136, 515-m elevation.
17. Magnesiohornblende phenocryst, drill hole T135, 345-m elevation.
18. Magnesiohornblende phenocryst, drill hole T135, 345-m elevation.
19. Magnesiohornblende phenocryst in southern ore body, drill hole T95, 240-m elevation.
20. Magnesiohornblende vein in southern ore body, drill hole T95, 240-m elevation.
21. Magnesiohornblende phenocryst from Laundry Creek propsect, drill hole L-28, 335m below surface.

chlorite is faintly pleochroic and has grayish-brown anomalous interference colors. Table 6 lists the compositions of chlorite in the Tanamá deposit.

The morphology of the chlorite grains suggests two origins: The equidimensional block-shaped grains may be derived by replacement of hydrothermal biotite, and the bladelike or needlelike grains may be derived from replacement of amphiboles. Attempts to map the distribution of these morphologies failed because the distinction between them was indefinite in many places.

Chlorite veinlets, which cut types B and C quartz veinlets, occupy the same vein-stratigraphic position as type D veins in the amphibole-dominated assemblage and thus are here given the same designation (see summary, fig. 20). Type D chlorite veins contain magnetite, replaced to varying degrees by chalcopyrite; also present are rutile, epidote, minor quartz, and traces of

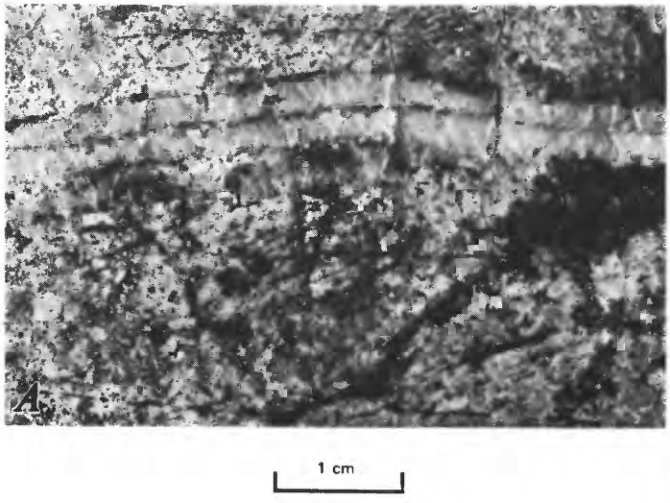


FIGURE 16.—Types C and E veinlets, Tanamá deposit. *A*, Type E veinlet with medial line of fine chalcopyrite grains cutting a type D chlorite veinlet. Drill hole T95, 240-m elevation. *B*, Type E veinlet (vertical) containing a large chalcopyrite grain (bottom) cutting a type C quartz-magnetite veinlet. Zeolite vein (white) cuts type E veinlet. Drill hole T135, 390-m elevation.

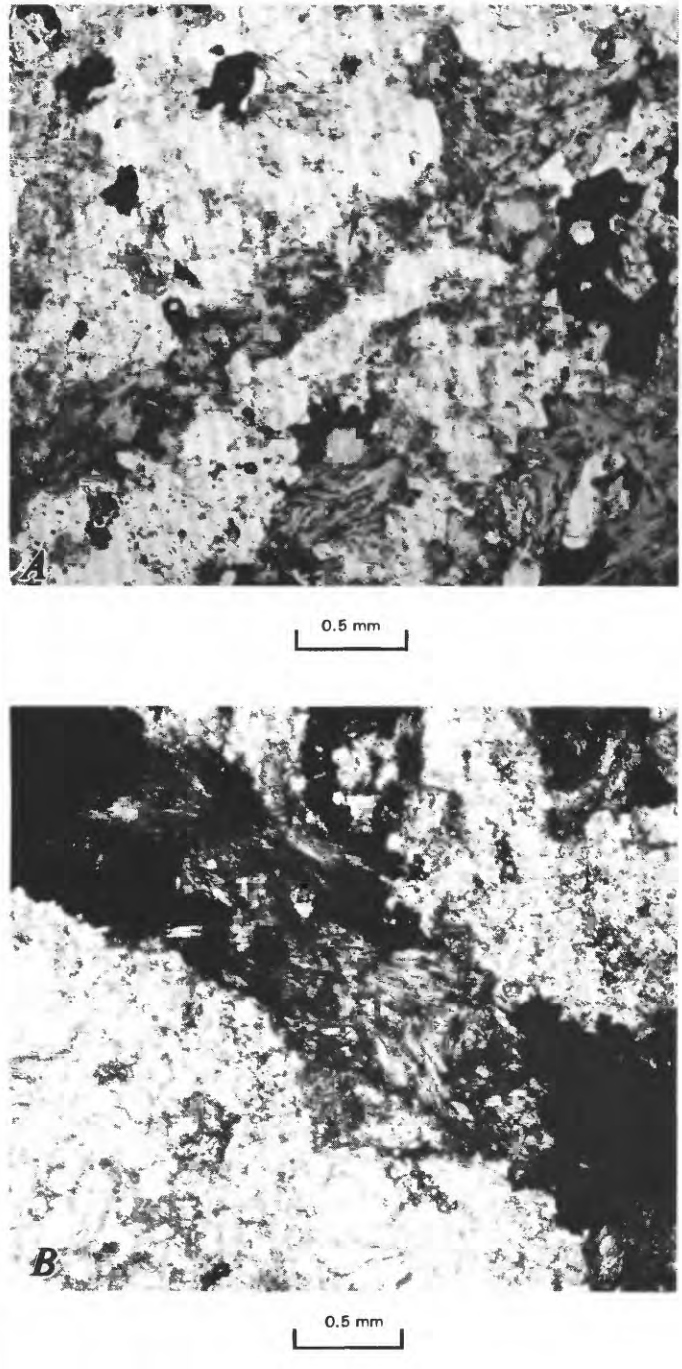


FIGURE 17.—Photomicrographs showing type D veinlets, Tanamá deposit. *A*, Chlorite in type D veinlet. Large opaque grains are chalcopyrite; small nearly opaque grains in chlorite are rutile. Dark shaded areas along chlorite vein are unreplaced remnants of biotite. Plane-polarized light. Field No. 17-128, drill hole T124, 385-m elevation. *B*, Fibrous cummingtonitic amphibole in type D veinlet. Plane-polarized light. Field No. T136-1B, drill hole T136, 430-m elevation.

TABLE 6. —*Partial chemical analyses and structural formulas of fibrous amphibole and chlorite, Tanamá deposit*

[Electron-microprobe analyses in weight percent. Amphibole analyses follow the methods of Huebner and others (1976); analyst, L.B. Wiggins, U.S. Geological Survey. Chlorite analyses by G.K. Czamanske, U.S. Geological Survey. Structural formulas in atomic percent, calculated by the methods of Papike and others (1974)]

| | Amphiboles | | | Chlorites | | | |
|---|---|---|---|---|---|---|---|
| Sample | 22 | 23 | 24 | 25 | 26 | 27 | 28 |
| Field No | T136-1B | 17-286 | 17-294 | 17-128 | | 17-270 | 17-131 |
| **Electron-microprobe analyses** | | | | | | | |
| $SiO_2$ | 52.9 | 53.3 | 53.4 | 27.0 | 28.3 | 27.4 | 28.2 |
| $Al_2O_3$ | 3.4 | 3.0 | 3.7 | 21.2 | 19.0 | 21.6 | 18.7 |
| $Fe_2O_3$ | 10.3 | 11.0 | 11.6 | 16.5 | 17.9 | 13.8 | 18.0 |
| $Fe_3O_4$ | 3.9 | 3.3 | 2.7 | 21.1 | 20.9 | 23.2 | 21.2 |
| MgO | 19.4 | 20.7 | 20.3 | .13 | .26 | .0 | .06 |
| | | | | .0 | .0 | .01 | .0 |
| CaO | 7.3 | 5.0 | 5.1 | .10 | .02 | .02 | .02 |
| $Na_2O$ | .41 | .11 | .33 | .34 | .26 | .12 | .06 |
| $K_2O$ | .0 | .0 | .0 | .37 | .44 | .59 | .32 |
| $TiO_2$ | .28 | .18 | .50 | .05 | .08 | .25 | .17 |
| $MnO_2$ | 1.19 | 1.02 | .98 | .001 | .005 | .01 | .02 |
| Total | 99.1 | 97.6 | 98.6 | 86.8 | 87.2 | 87.0 | 86.8 |
| **Structural formulas** | | | | | | | |
| Si | 7.44 | 7.55 | 7.50 | 5.48 | 5.76 | 5.46 | 5.78 |
| Al | .56 | .44 | .50 | 2.52 | 2.24 | 2.54 | 2.22 |
| Al | .01 | .06 | .11 | 2.50 | 2.25 | 2.50 | 2.22 |
| $Fe^{2+}$ | 1.22 | 1.30 | 1.37 | 2.82 | 3.07 | 2.34 | 3.11 |
| $Fe^{3+}$ | .42 | .35 | .28 | 6.48 | 6.45 | 7.04 | 6.59 |
| | | | | .06 | .08 | .10 | .06 |
| Mg | 4.07 | 4.37 | 4.25 | .05 | .04 | .02 | .01 |
| Mn | .14 | .12 | .12 | .03 | .06 | .0 | .01 |
| Ti | .03 | .02 | .05 | .0 | .0 | .003 | .0 |
| | | | | .03 | .004 | .0 | .01 |
| XOCT | .88 | 1.23 | 1.18 | 11.97 | 11.95 | 12.00 | 12.01 |
| Ca | 1.10 | .76 | .77 | | | | |
| Na | .02 | .02 | .05 | | | | |
| Na | .09 | .02 | .05 | | | | |

Sample 22. Magnesiocummingtonitic amphibole, fibrous vein filling, drill hole T136, 430-m elevation.
23. Magnesiocummingtonitic amphibole, fibrous cluster, drill hole T136, 430-m elevation.
24. Magnesiocummingtonitic amphibole, fibrous cluster, drill hole T136, 515-m elevation (see sample 8, table 4; sample 6, table 5).
25. Chlorite replacing hydrothermal biotite hole T124, 382-m elevation.
26. Chlorite replacing amphibole, drill hole T124, 382-m elevation.
27. Chlorite, drill hole T124, 470-m elevation (average of 2 analyses).
28. Chlorite, drill hole T124, 220-m elevation (average of 2 analyses).

potassium feldspar. In drill hole T124, where patches of secondary biotite are preserved, biotite is replaced by chlorite along the walls of type D chlorite veins (fig. 17*A*).

Biotite occurs in tonalite porphyry as replacement clusters after hornblende phenocrysts and in veinlets with chlorite, chalcopyrite, and quartz. Its distribution is scattered (see figs. 11, 12), and it rarely makes up more than a few tenths of a percent of the rock. Biotite is everywhere intimately intergrown with chlorite, either as interlayers or as cores in chlorite grains. The biotite is pale brown with a weak pleochroism and is intergrown with small grains and needles of rutile. These scattered patches of biotite are interpreted as evidence that an early pervasive biotitic-alteration assemblage was formed in the porphyry column and later replaced by chlorite.

In the Tanamá area, biotite is more abundant in metavolcanic rocks of the Cretaceous basaltic sequence than in the porphyry, but drill-hole data do not permit a mapping of biotite occurrence. Biotite has extensively replaced amphibole in many places near the porphyry contact, giving rise to rocks closely resembling biotite hornfels. Because the original $K_2O$ content of the volcanic rocks is low (table 1), most of the $K_2O$ present in biotite is believed to have been introduced by hydrothermal solutions.

Potassium feldspar is distributed in traces coextensively with biotite. It occurs in type D veinlets with chlorite, epidote, and chalcopyrite and partly replaces plagioclase phenocrysts and groundmass grains. The potassium feldspar has a faint mottled pattern under crossed polarizers that may represent fine perthitic intergrowth with albite. The evidence available at Laundry Creek and at the Piedra Hueca deposit in the Rio Vivi district (Cox and others, 1973) suggests that potassium feldspar may be a stable member of the assemblage quartz + chlorite + potassium feldspar + epidote ± albite ± calcite. At Tanamá, the meager evidence available suggests that the potassium feldspar is a relic of an earlier biotite-potassium feldspar assemblage after chloritization of the biotite. In one locality (drill hole T63, 300-m elev; fig 11*C*), potassium feldspar was found in an aplite veinlet, 2 cm wide, intergrown with quartz in an aplitic to myrmekitic texture.

Fibrous amphibole occurs with chlorite in type D veinlets (fig. 17*B*). Although its occurrence is restricted to the zone of the hornblende-dominant assemblage in the deeper parts of the ore body, its common association and intimate intergrowth with chlorite suggest that the amphibole is a member of the chlorite-dominant assemblage. The fibers have inclined extinction and are pale tan to green with weak pleochroism. Microprobe data (table 6) indicate compositions approaching magnesiocummingtonite. Decrease in $Al^{IV}$ is compensated mainly by increases in Mg and total Fe contents and a large decrease in Ca content relative to hydrothermal hornblende.

Albite is a common constituent of the chlorite-dominated alteration assemblage. It most commonly occurs as rims and crosscutting veinlets within intermediate plagioclase phenocrysts. Where most abundant, the albite forms irregular veinlets and patches of fine equant interlocking grains. Albite veinlets and patches are dusted with fine magnetite.

Other minerals occur in small amounts in the chlorite-dominated assemblage. Magnetite is found in the same textural relations as in the amphibole-dominated assemblages; it is replaced to varying degrees by chalcopyrite and contains varying amounts of ilmenite intergrowths. Epidote forms equant grains and clusters of grains associated with chlorite in altered hornblende phenocrysts and in type D veinlets; it is pale amber to green in thin section. Rutile forms subhedral grains (0.01-0.1 mm diam) with the same distribution pattern as epidote. Rutile may also form nets of needlelike crystals intergrown with chlorite. Calcite occurs as scattered grains, mainly in altered hornblende phenocrysts. Pyrite is rare; it occurs as scattered grains, mainly in types D and E veinlets. Molybdenite is also rare; it occurs in type D veinlets with chlorite and in vuggy quartz veinlets without alteration haloes. The vein-stratigraphic position of these vuggy quartz veinlets has not yet been determined.

### Feldspar-Destructive Alteration and Mineralization

Complete replacement of plagioclase by sericite, clay, and calcite, and of magnetite by pyrite, has occurred throughout the inferred upper part of the tonalite porphyry stock and its metavolcanic wallrocks. This alteration gives rise to the marked contrast between the southern Tanamá ore body and the northern ore body, in which fresh feldspar and magnetite are preserved. The lower limit of pervasive sericite-clay-carbonate alteration is gradational, and veinlets with sericite-clay-carbonate envelopes extend downward hundreds of meters into the deepest parts of the northern ore body, which is characterized mainly by feldspar-stable-alteration assemblages.

Veinlets composed of pyrite, calcite, quartz, and chalcopyrite, here designated "type F", are characteristic of and contemporaneous with feldspar-destructive alteration. They have open, apparently leached-out spaces and sericitic and argillic alteration envelopes several times wider than the veinlets (fig. 19*A*). Calcite and chalcopyrite are locally abundant in type F veinlets. Barite was noted in one sample, sphalerite in another.

Copper-grade distribution can be only weakly correlated with the zone of feldspar-destructive alteration at the 430-m-elevation horizontal section. Part of the greater-than-0.4-weight-percent-Cu ore body lies within this zone, whereas part of the feldspar-destructive zone lies outside the ore body.

Table 7 lists chemical analyses of 10 samples of porphyry containing feldspar-destructive-alteration assemblages. Comparison with fresh rocks or rocks of feldspar-stable-alteration assemblages is difficult because of the large variations in $SiO_2$ content due to the irregular distribution of abundant quartz veinlets. Assuming that aluminum is the least mobile of the major components, the effect of dilution by quartz can be minimized by comparing the $K_2O/Al_2O_3$ ratios in fresh and altered rocks (fig. 18). Rocks with pervasive feldspar-destructive alteration or containing pyrite veinlets with feldspar-destructive-alteration haloes have $K_2O/Al_2O_3$ ratios about 4 times higher than those of fresh rocks or rocks from feldspar-stable-alteration zones. Similarily, a comparison of $S/Al_2O_3$ ratios between feldspar-stable- and feldspar-destructive-alteration assemblages suggests a fourfold increase in sulfur concentration in the latter.

The abundance of pyrite in feldspar-destructive-alteration assemblages accounts for most of the increase in $S/Al_2O_3$ ratio. Pyrite is the dominant mineral in type F veinlets, where it commonly occurs as etched and corroded pyritohedrons.

Quartz occurs as numerous closely spaced veinlets, most of which are probably types B, C, and E veinlets

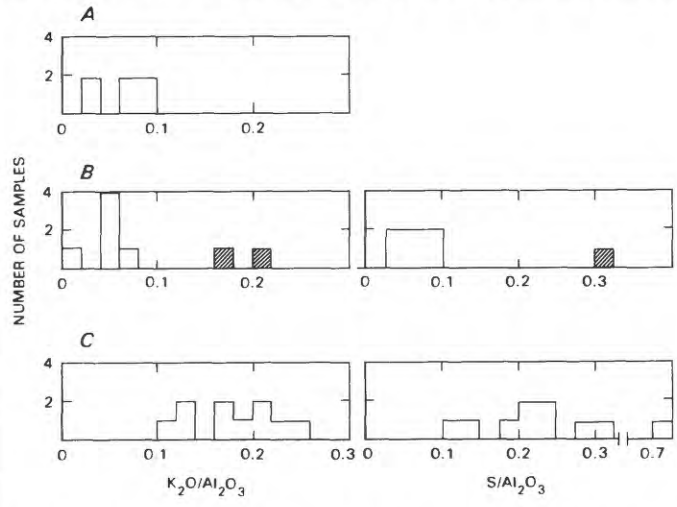


FIGURE 18.—$K_2O/Al_2O_3$ and $S/Al_2O_3$ ratios in fresh and altered tonalite porphyry, Tanamá deposit and vicinity. *A*, Weakly altered porphyry. *B*, Feldspar-stable alteration. *C*, Feldspar-destructive alteration. Hatchured pattern in *B* indicates samples in which pyrite-sericite veinlets are superimposed on feldspar-stable alteration.

TABLE 7. —*Composition of tonalite porphyry with pervasive feldspar-destructive alteration, Tanamá and Helecho deposits*

[Chemical analyses in weight percent by single-solution procedure (Shapiro, 1975); analysts, H. Smith and J. Reid.]

| Sample---- | 1 | 2 | 3 | 4 | 5 | 6 | 7 | 8 | 9 | 10 |
|---|---|---|---|---|---|---|---|---|---|---|
| Field No.-- | T56-1 | T56-2 | T79-1 | T83-1 | T84-1 | T84-2 | T93-1 | T104-1 | T104-2 | -41 |
| $SiO_2$ ------ | 72.3 | 72.0 | 68.9 | 64.2 | 80.9 | 69.9 | 68.9 | 68.8 | 68.0 | 71.6 |
| $Al_2O_3$ ----- | 14.6 | 11.1 | 14.8 | 15.7 | 4.3 | 13.4 | 13.5 | 13.3 | 15.3 | 13.0 |
| Total Fe (as $Fe_2O_3$) -- | 3.2 | 5.8 | 4.4 | 6.8 | 8.9 | 6.0 | 5.6 | 6.7 | 5.2 | 5.1 |
| MgO ------- | 1.5 | 2.1 | 2.4 | 2.7 | 1.4 | .32 | 1.0 | .24 | .89 | 1.9 |
| CaO ------- | .30 | .47 | .35 | .87 | .08 | .28 | .02 | .13 | .03 | .39 |
| $Na_2O$ ------ | .45 | .14 | .14 | .48 | .05 | .14 | .20 | .36 | .18 | .18 |
| $K_2O$ ------- | 2.0 | 2.2 | 3.1 | 1.6 | .57 | 3.3 | 2.9 | 2.2 | 3.5 | 2.2 |
| $H_2O^+$ ------ | 2.5 | 2.0 | 2.5 | 3.5 | .91 | 2.2 | 2.8 | 2.5 | 2.8 | 2.6 |
| $H_2O^-$ ------ | .95 | .41 | 1.1 | 1.7 | .29 | .50 | .54 | .60 | .52 | .71 |
| $TiO_2$ ------ | .42 | .37 | .39 | .51 | .33 | .39 | .34 | .31 | .42 | .36 |
| $P_2O_5$ ------ | .08 | .12 | .19 | .18 | .09 | .12 | .09 | .09 | .09 | .10 |
| MnO ------- | .00 | .02 | .05 | .03 | .04 | .02 | .01 | .02 | .00 | .04 |
| $CO_2$ ------- | .01 | .04 | .01 | .03 | .01 | .03 | .01 | .03 | .03 | .03 |
| S --------- | 1.7 | 2.7 | 1.9 | 3.2 | 3.1 | 3.7 | 3.7 | 4.3 | 3.2 | 2.4 |
| Total---- | 100.0 | 99.5 | 100.2 | 101.5 | 101.0 | 100.3 | 99.6 | 99.6 | 100.2 | 100.6 |
| Sulfide-- | 1.5 | 2.5 | 1.8 | 3.0 | 2.9 | 3.2 | 3.2 | 3.9 | 2.9 | 2.2 |

Samples 1 through 9, see figure 11 for location.
Sample 10 from Helecho deposit, Río Coabey streambed, see figure 32 for location.

inherited from alteration stages preceding feldspar-destructive alteration. Quartz occurs as a minor constituent of type F veinlets.

Chalcopyrite occurs mainly as disseminated equidimensional grains and, locally, in type F veinlets.

Sericite is abundant and ubiquitous in the zone of feldspar-destructive alteration, where it commonly forms fine-grained patches with rectangular outlines of plagioclase phenocrysts. It is the dominant mineral in haloes around type F veinlets (fig. 19*A*).

Chlorite occurs throughout this zone of feldspar-descructive-alteration in clusters with sericite, pyrite, and rutile that mark the sites of original hornblende phenocrysts.

Clay minerals of various species occur throughout the feldspar-destructive-alteration zone. No systematic distribution pattern or consistent mineral-assemblage groupings were discernible from the data available in this study. Minerals identified by X-ray diffraction are, in descending order of abundance: allevardite (a mixed-layer pyrophyllite-montmorillonite), montmorillonite, kaolin, a mixed-layer illite-montmorillonite, and minor pyrophyllite. All these minerals occur together with sericite and chlorite.

Calcite is locally abundant; it occurs as fine-grained patches and in type F veinlets. Epidote is locally present as a relict mineral. Rutile needles form nets in chlorite-sericite clusters. Black sphalerite was noted in type F calcite veins at 300-m elevation in drill holes T124 and T128 in the northern ore body; these veins cut porphyry with predominantly feldspar-stable alteration. Barite was seen in a type F vein in one sample (field No. T91-2) in the southern ore body, as well as in rocks of feldspar-stable-alteration type.

### Late-Stage Zeolite Alteration

The last stage of hydrothermal activity at Tanamá was the introduction of abundant zeolites in thin veinlets without alteration haloes. Leonhardite is the principal zeolite mineral, and stilbite occurs locally. Leonhardite forms bladelike crystals perpendicular to and subparallel to veinlet walls (fig. 19*B*) and may fill small fractures in plagioclase phenocrysts near veinlets. Zeolite veinlets occur in the northern ore body in the chlorite- and amphibole-alteration zones; they have not been detected in zones of feldspar-destructive alteration.

### Veinlets and Veinlet Stratigraphy

Closely spaced crosscutting veinlets of quartz, magnetite, sulfides, and silicates are the most dominant features of the Tanamá deposit. Seven types of veinlets have been briefly described above in the descriptions of the alteration assemblages in which they are found; they are reviewed below in the order of their decreasing age as indicated by their crosscutting relations (fig. 20).

*Type A.*—Indistinct planar arrays of magnetite grains found in the central part of the deposit. Type A veinlets may persist throughout the deposit but are difficult to recognize where chalcopyrite or pyrite has replaced the magnetite grains.

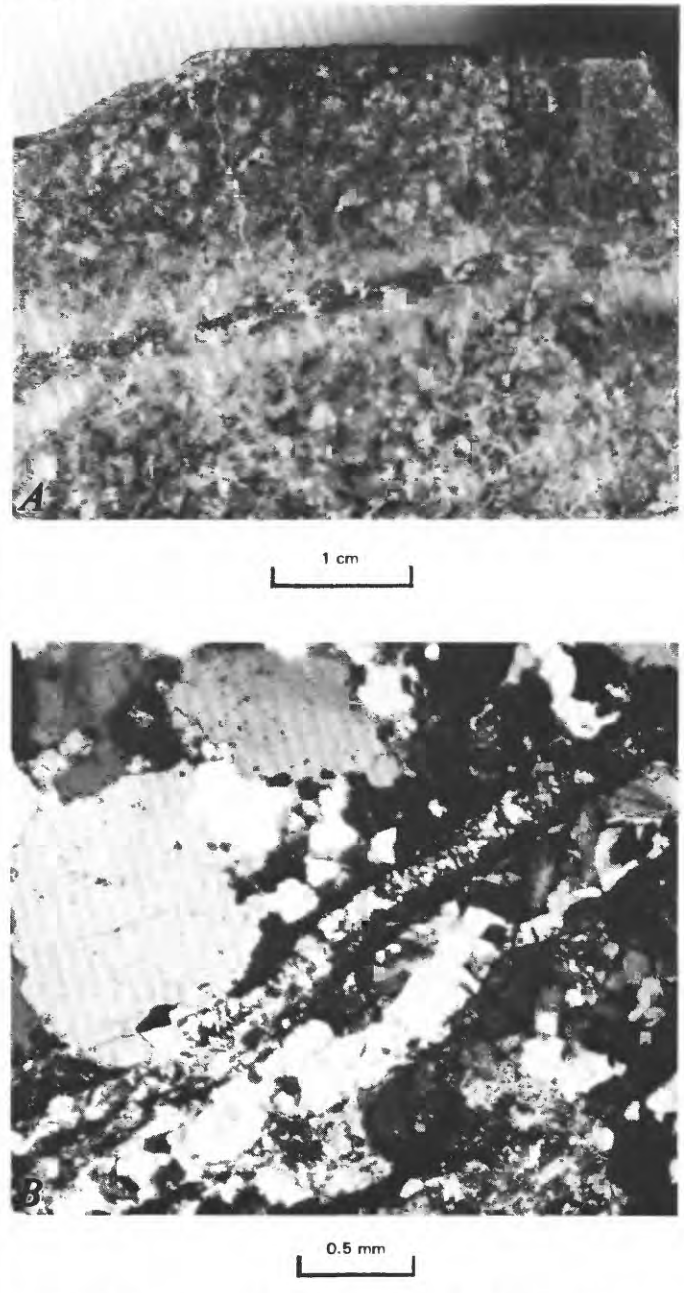


FIGURE 19.—Photograph and photomicrograph of late-stage veinlets, Tanamá deposit. *A*, Type F pyrite veinlet with alteration envelope of sericite and clay. Drill hole T113, 152-m elevation. *B*, Veinlets of leonhardite cutting tonalite porphyry. Crossed polarizers. Drill hole T128, 430-m elevation.

*Type B.*—Thin (1-3 mm thick) sinuous granular quartz veinlets without alteration haloes. Type B veinlets are recognized only in the central core.

*Type C.*—Thick (5-10 mm thick) granular quartz veinlets containing magnetite in equant grains along vein walls in the central core. Magnetite in type C veinlets may be replaced by chalcopyrite in the outer, copper-rich part of the deposit. Type C veinlets, formed during feldspar-stable alteration, persist throughout the deposit and probably are the source of much of the quartz in the pyrite-rich feldspar-destructive-alteration zone.

*Type D.*—Planar arrays of magnetite and amphibole grains in amphibole-dominated assemblages and of chalcopyrite, chlorite, epidote, and minor potassium feldspar grains in chlorite-dominated assemblages occupy the same position in the veinlet stratigraphy. Type D veinlets have no megascopically obvious alteration envelopes. On a microscopic scale, however, biotite may locally be replaced by chlorite, and plagioclase by potassium feldspar, along type D veinlet walls.

*Type E.*—Composed of granular quartz, distinguished by a thin layer of chalcopyrite at their centers. Type E veinlets have no alteration haloes, but because they are found only in porphyry containing chlorite-dominated alteration assemblages, their formation was probably contemporaneous with chlorite or early-stage biotite alteration.

*Type F.*—The only veinlets with obvious alteration haloes in the Tanamá deposit are type F veinlets, composed of pyrite, calcite, and quartz grains with irregular corroded surfaces. Open leached-out spaces are common in these veinlets, and core samples break readily along the veinlet surfaces. Alteration haloes are marked by replacement of plagioclase by sericite, clay minerals, and minor calcite. Where type F veinlets are closely spaced, their alteration haloes merge, and feldspar-destructive alteration becomes pervasive.

*Zeolite.*—The youngest veinlets in the sequence, abundant in porphyry containing feldspar-stable-alteration assemblages. Zeolite veinlets are absent from the feldspar-destructive-alteration zone, probably because calcium and sodium were unavailable from the wallrock to form zeolite minerals.

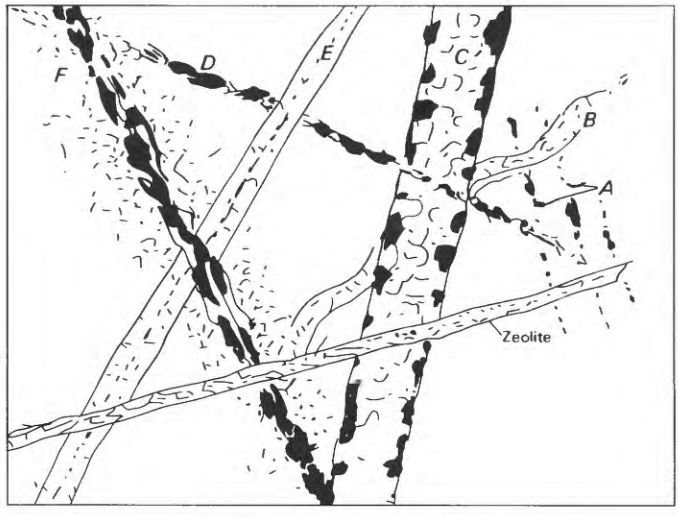


FIGURE 20.—General appearance and crosscutting relations of veinlets at Tanamá deposit. *A*, indistinct magnetite; *B*, thin sinuous quartz; *C*, thick granular quartz containing magnetite; *D*, magnetite-amphibole or chalcopyrite-chlorite; *E*, quartz with thin medial layer of chalcopyrite; *F*, pyrite-calcite-quartz with sericite- or clay-alteration envelopes.

## THERMOMETRY AND CHEMISTRY OF VEINLET FLUIDS

The temperature and chemical composition of the fluids that transported minerals into fractures at Tanamá were investigated by fluid-inclusion studies and oxygen-isotope measurements on quartz-magnetite pairs. The distribution of fluid inclusions of various types was studied in the entire suite of samples, using the petrographic techniques of Nash (1976). In addition, nine samples were selected from various levels in the northern and southern parts of the Tanamá deposit from which types C and E veinlets were sectioned and polished for microthermometry studies, using a Chaix Meca apparatus with an upper temperature limit of between 550 and 600 °C. Veinlets from six samples were slabbed and split with a steel chisel. The fracture surfaces were coated with approximately 20nm of carbon and examined for inclusions with a Cambridge Stereoscan 180 electron microscope. Daughter minerals in the inclusions were analyzed using an Edax energy-dispersive X-ray analyzer. R. L. Oscarson of the U.S. Geological Survey conducted the electron-microscope study.

### OXYGEN-ISOTOPE THERMOMETRY

Quartz and magnetite were separated from two type C veinlets in the low- grade core zone of the northern ore body. The oxygen-isotopic composition of these mineral pairs was determined by J. R. O'Neil of the U.S. Geological Survey. The $\delta^{18}O$ values (table 8), which are similar to those measured in normal igneous rocks, imply equilibrium with igneous rocks at near-magmatic temperatures, 680 to 685 °C.

### TYPES OF INCLUSIONS AND THEIR DISTRIBUTION

Quartz veinlets and phenocrysts contain three distinct types of fluid inclusions: liquid rich, vapor rich, and mineral rich. Liquid-rich inclusions are smooth, rounded to irregular, and amoebalike in form and have a

small vapor bubble making up 5 to 20 percent of the total volume. Vapor-rich inclusions commonly are rounded and characteristically have the form of negative crystals. The vapor bubble makes up more than 50 percent of the total volume, and in some inclusions the liquid phase is nearly invisible; in a few places, small opaque and cubic transparent daughter minerals were seen in vapor-rich inclusions. Mineral-rich inclusions contain a vapor bubble and a liquid crowded with daughter minerals, of which halite predominates. Of the three types, the vapor-rich inclusions are the most abundant in most samples. All three inclusion types occur together in all parts of the low-grade core and ore zone, and no significant difference in inclusion population could be seen under the optical microscope between the deepest levels of the northern ore body and the upper levels of the southern ore body.

The three types of inclusions range in size from less than 1 to 30 μm. Size distribution of the liquid-rich inclusions is skewed toward the smaller diameters, so that most fall within the 5- to 10- μm size range. Vapor- and mineral-rich inclusions are fairly evenly distributed in the 5- to 15- μm size range and average 12 μm in size.

The distribution of fluid inclusions in the metavolcanic wallrocks was not mapped in this study because many of the drill-core samples of metavolcanic rock collected did not contain quartz veinlets. In those samples of wallrock that did contain quartz, however, the abundance and size of inclusions generally correlated positively with copper grade. Fluid inclusions that may have been trapped in type F veinlets with sericitic-alteration haloes were not observed because the samples collected from these veins did not contain sufficient quartz for fluid-inclusion study.

TABLE 8. —*$\delta^{18}O$ values and equilibrium temperatures for two quartz-magnetite veinlets, Tanamá deposit*

[See figure 12 for drill hole location and figure 14 for sample localities. $\delta^{18}O$ values of quartz in permil relative to standard mean ocean water (SMOW). Equilibrium temperatures (T) in degrees Celsius, calculated from the expression of Bottinga and Jaboy (1973): $10^3 \ln\Delta_{Q\text{-}M} = 5.57 \times 10^6 T^{-2}$, where $\Delta_{Q\text{-}M} = (1{,}000 + \delta^{18}O_{quartz})/(1{,}000 + \delta^{18}O_{magnetite})$]

| Field No---------- | 17-295 | 17-303 |
|---|---|---|
| Drill hole and depth---- | T136, 46 m | T135, 226 m |
| $\delta^{18}O$ quartz---------- | 8.09 | 8.29 |
| $\delta^{18}O$ magnetite--------- | 1.99 | 2.11 |
| T ---------- | 685 | 680 |

### MINIMUM TEMPERATURE OF TRAPPING OF INCLUSIONS

Figure 21*A* plots the temperatures of homogenization of vapor and liquid in liquid- and vapor-rich inclusions and the temperatures of final solution of daughter salts in mineral-rich inclusions. These temperatures represent the minimum temperature of hydrothermal fluids at the time of their entrapment in the quartz crystal (Roedder, 1967). Vapor bubbles homogenized at temperatures below the dissolution point of daughter minerals in all inclusions except four in a sample (field No. 17-374) from drill hole T109 in the uppermost part of the deposit, in which halite dissolved in the range 200-350 °C and homogenization occurred above 320 °C.

These temperature data are insufficient to describe the thermal history of fluids in the deposit, mainly because many inclusions could not be homogenized within the temperature range of the microthermometry apparatus. Note, however, that the distribution of temperatures and the abundance of analyzed inclusions with homogenization temperatures in the range 200-500 °C is remarkably uniform in all samples, even though they were selected from a vertical range of more than 550 m in the deposit. Note, also, that no significant difference is discernible between inclusions in type C veinlets and younger, type E veinlets, even though these veinlets appear to be related to different stages of hydrothermal alteration. Nonetheless, a significant difference does exist between the upper and lower levels of the deposit with respect to the abundance of inclusions with very low or very high homogenization temperatures. Veinlets from the ore zone in the upper part of the deposit (southern ore body) contain numerous inclusions homogenizing in the range 100-150 °C (fig. 21*B*), whereas veinlets in the inner, low-grade core zone in the lower part of the deposit (northern ore body) contain abundant inclusions having dissolution temperatures above 500 °C (fig. 21*C*). Liquid-rich inclusions homogenizing between 150 and 250 °C are also present throughout the deposit, including the inner core zone.

### PRESSURE CORRECTIONS

The close association of mineral-rich inclusions with vapor-rich inclusions indicates that solutions were boiling at the time of trapping. Because vapor pressure would equal hydrostatic pressure under boiling conditions, the temperature of homogenization of these inclusions must equal the minimum temperature of trapping.

Most liquid-rich inclusions homogenizing at temperatures below 300 °C were probably not derived from boiling fluids, and so a pressure correction related to

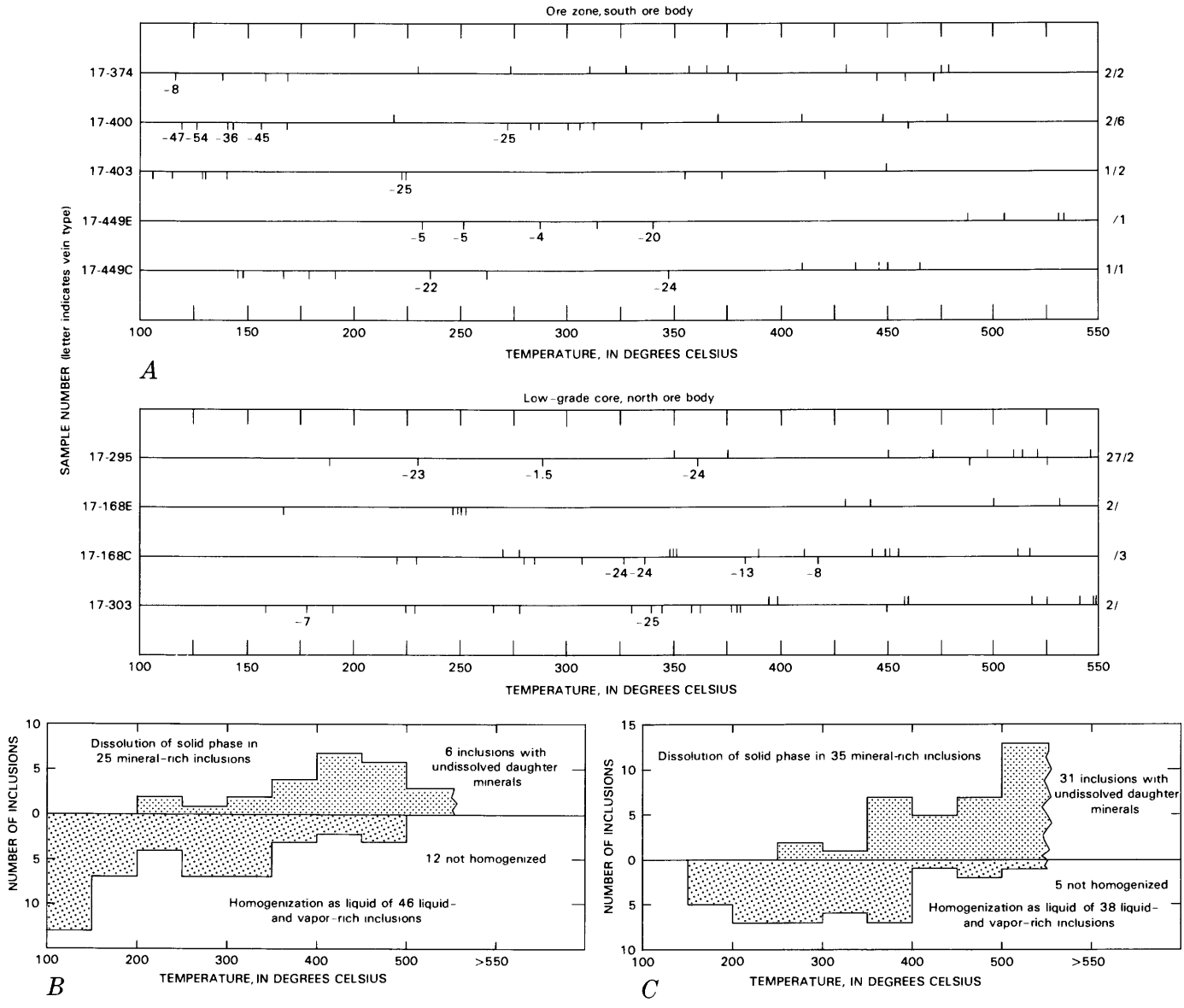


| Field No. | Drill hole | Footage | Elevation (in) meters | Vein type |
|---|---|---|---|---|
| 17-374 | T109 | 530 | 430 | C |
| 17-400 | T79 | 450 | 413 | C |
| 17-403 | T79 | 800 | 308 | Vuggy quartz-molybdenite |
| 17-499 | T95 | 1010 | 240 | C and E |
| 17-295 | T136 | 150 | 500 | C |
| 17-168 | T135 | 650 | 387 | C and E |
| 17-303 | T135 | 740 | 362 | C |

FIGURE 21.—Temperatures of final homogenization of fluid inclusions in types C and E quartz veinlets from ore zone in upper part of Tanamá deposit and from low-grade core zone in lower part. *A*, Temperatures of final dissolution of daughter minerals in mineral-rich inclusions (tickmarks above line) and homogenization temperatures of liquid- and vapor-rich inclusions (tickmarks below line). Small numbers below line indicate temperature of final melting of ice in liquid phase of inclusions. Numbers at far right indicate numbers of inclusions that had not homogenized at 550 °C. See figure 13 for approximate locations of samples. *B*, Summary of data in figure 21*A* for samples from ore zone. *C*, Summary of data in figure 21*A* for samples from low-grade core zone.

their depth of trapping is required. Few data are available at Tanamá from which to estimate the depth of emplacement of the deposit. The south-dipping contact between the Cretaceous basaltic sequence and overlying Tertiary rocks may be a depositional surface representing the base of the volcanic pile that is comagmatic with the Tanamá porphyry. This surface may be projected to a point 1.5 km above Tanamá. Assuming that the pile was about 1.5 km thick at the time of intrusion, then a 3-km depth of formation is reasonable. Also, assuming that the system was open to ground water circulation at this depth, then hydrostatic pressures of between 25 and 30 MPa would have prevailed. These pressures would require temperature corrections of +15 to +40 °C (following Potter and Clynne, 1978); this correction would be largest for the inclusions homogenizing at the lowest temperatures. I conclude that the temperatures of fluids forming liquid-rich inclusions at Tanamá lie mainly within the ranges shown in figure 21*B* and 21*C*, except that fluids trapped at the lowest temperatures were probably above 150 °C in the upper part of the deposit and above 200 °C in the lower part.

### Composition of Fluids

Fluids trapped in inclusions at Tanamá range in salinity from less than 10 to more than 50 weight percent NaCl equivalent. The compositions of fluids apparently were highly complex, as shown by the large number of chemical species found in daughter minerals. Measurements using the freezing-point-depression method of Roedder (1962) (fig. 22), show that about half the population of liquid-rich inclusions contain relatively dilute solutions (less than 10 weight percent NaCl equivalent) and about half contain solutions nearly saturated with respect to NaCl. Most of the vapor-rich inclusions, however, contain nearly saturated solutions, and a few contain small halite daughter minerals. The detection of both vapor- and liquid-rich inclusions that contain solutions with very low freezing points indicates a major proportion of one or more other salts in solution, such as $CaCl_2$, $FeCl_2$, or $MgCl_2$. Vapor-rich inclusions with very low freezing points were found mainly in type C veins preserved in sericitized porphyry in drill holes T109 and T79 in the upper parts of the deposit (field Nos. 17-374, and 17-400) and have homogenization temperatures in the range 110-165 °C. Low-salinity fluids were found in liquid-rich inclusions in all samples, including those from the inner, low-grade core of the deposit.

Temperatures of dissolution of halite in mineral-rich inclusions (fig. 23), which mainly range from 425 to 525 °C, indicate salinities in the range 50-60 weight percent NaCl equivalent. Only two inclusions were found in which dissolution temperatures could be measured for both halite and sylvite. Dissolution temperatures of these mineral pairs (fig. 23) suggest compositions of 25 to 30 weight percent KCl and 40 to 45 weight percent NaCl (see Roedder, 1971). Confidence in these estimates is low, however, because of the unknown effects on dissolution temperatures of the concentrations of other chemical species in the solutions.

Scanning-electron-microscope (SEM) studies of mineral-rich inclusions show that large amounts of sodium, iron, potassium, and calcium, and traces of magnesium and manganese were present in the solutions before entrapment. Table 9 lists the distribution of mineral species as determined by energy-dispersive X-ray analysis of daughter minerals in five type C veins from the low-grade core zone and the inner and outer parts of the ore zone, and in one type F vein from the upper part of

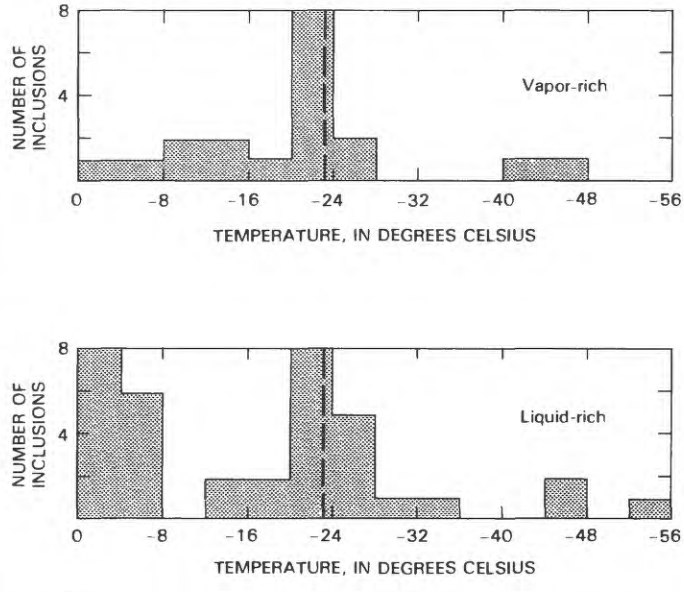


FIGURE 22.—Temperatures of melting ice in 55 vapor- and liquid-rich inclusions, Tanamá deposit. Broken line indicates freezing point of solution saturated with respect to NaCl.

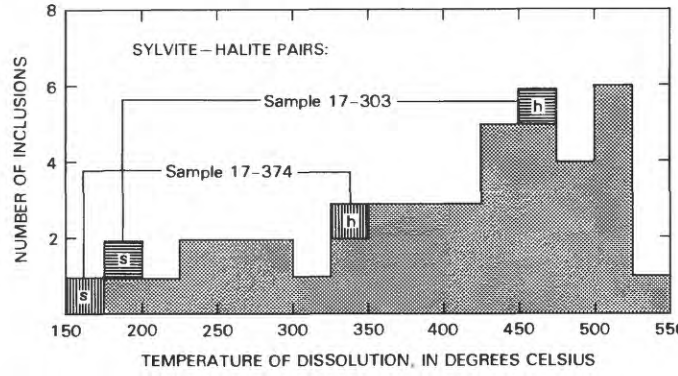


FIGURE 23.—Temperatures of dissolution of halite and sylvite daughter minerals in inclusions, Tanamá deposit. Lined patterns indicate dissolution temperatures of sylvite-halite pairs. See figure 13 for sample localities.

TABLE 9. —*Number of observations of daughter minerals in fluid inclusions within quartz, Tanamá deposit*

[( ), trace amounts; [ ?], suspected, but cannot be detected]

| Sample | 1 | 2 | 3 | 4 | 5 | 6 |
|---|---|---|---|---|---|---|
| Field No. | 17-303 | 17-295 | T124-2 | 17-277 | T91-1 | 17-400 |
| Na-Cl | 4 | 12 | -- | 1 | 1 | -- |
| Fe-Cl-(Mn) | 4 | 7 | 1 | 2 | 1 | 1 |
| K-Cl | -- | 6 | 1 | 2 | 1 | -- |
| Na-K-Fe-Cl-(Mn) | 3 | 1 | -- | 1 | -- | -- |
| K-Fe-Cl-(Mn) | -- | 4 | -- | 2 | -- | -- |
| K-Ca-Fe-Cl | -- | 1 | 1 | 1 | 2 | -- |
| Ca-Fe-Cl-(Mg) | -- | 1 | -- | -- | 6 | -- |
| Ca-Cl-(Mg) | -- | -- | -- | 2 | -- | -- |
| Ca-[$CO_3$?] | -- | -- | 1 | 2 | -- | -- |
| Ca-S[$O_4$?] | -- | -- | 1 | -- | -- | -- |
| Fe-[O?] | 1 | -- | 1 | 2 | 2 | -- |
| Cu-Fe-S | -- | 1 | -- | 4 | 1 | 3 |
| Mineral-rich inclusions (percentage of total inclusions observed) | 35 | 37 | 25 | 36 | 30 | <10 |

Sample 1. Low-grade core, amphibole alteration, drill hole T135, 226-m depth.
2. Low-grade core, amphibole alteration, drill hole T136, 46-m depth.
3. Transition from low-grade core to ore zone, drill hole T124, 274-m depth.
4. Ore zone, chloritic alteration, drill hole T124, 88-m depth.
5. Ore zone, chloritic alteration, drill hole T91, 45-m depth. (Not shown in Fig. 13).
6. Type F vein, feldspar-destructive alteration, drill hole T79, 137-m depth.

the ore zone. In addition to the daughter minerals listed, other minerals, interpreted as preexisting solid phases trapped in inclusions, were found, including plagioclase, biotite, apatite, and zircon.

Of the daughter minerals found in inclusions, halite is the most abundant; it appears as corroded irregular cubes under the SEM and as well-formed cubes under the optical microscope.

The second most abundant mineral gave strong energy peaks for iron and chlorine and traces of manganese on the X-ray analyzer. In the SEM, this iron chloride mineral appears to be hexagonal, with well-developed prism and pinacoid faces (fig. 24*A*) and weakly developed hexagonal-dipyramid faces (fig. 24*B*). A basal cleavage may be present, as suggested by figure 24*C*.

Under the optical microscope, prismatic forms were observed in approximately the same abundance as the iron chloride minerals seen in the SEM (fig. 25*A*). Their optical properties were estimated as follows: Color, pale yellow to greenish yellow; refractive index, high; birefringence, high (0.1); and extinction angle (X-C), 12°. This prismatic mineral is stable at temperatures well above 500 °C, as shown by the temperatures of dissolution determined on the heating stage. The data listed in table 10 indicate that for most samples the prismatic form dissolves at temperatures 50 to 90 °C higher than does the halite in the same inclusion. This relation presumably reflects the common-ion effect, by which the

TABLE 10. —*Temperatures of dissolution of mineral pairs: halite and iron chloride*

[All values in degrees Celsius. See figure 13 for sample localities.]

| Sample | Drill hole and depth | Halite | Iron chloride |
|---|---|---|---|
| 17-303 | T135 | 493 | 560 |
| | 226m | 468 | 588 |
| | | 515 | 525 |
| 17-295 | T136 | 498 | >600 |
| | 46m | 465 | 560 |
| | | 475 | 523 |
| | | 525 | 590 |
| | | 441 | 493 |
| 17-449 | T99 | 532 | 529 |
| | 308m | 498 | 530 |

monovalent sodium dissolves more readily in a solution supersaturated with respect to chloride ion than does the higher valency iron.

A search of the literature revealed no published chemical, optical, or physical properties of mineral or artificial compounds that match the above estimates. The mineral most closely resembles molysite ($FeCl_3$), but its melting point is much higher.

Sylvite, the third most abundant mineral, forms sharply defined cubes; in one inclusion, two separate sylvite cubes were noted. Chalcopyrite, characteristically in small (< 2 μm) octahedra, was observed in many inclusions. Hematite, seen as small plates and rounded forms in the SEM and as red translucent grains under the optical microscope, is also common.

As listed in table 9, at least four other complex mineral species occur as daughter minerals that could be observed in the SEM and under the optical microscope. The chlorides of K ± Na + Fe have irregular forms, of which the grain shown in figure 24*A* is typical. The chlorides of Ca + Fe + K generally have bladed or sheet-like forms with a hexagonal outline, commonly showing sharp wedge-shaped edges such as those shown in figure 24*D*; figure 25*B* shows a daughter mineral believed to be of this group.

Other irregular forms giving energy peaks for Ca + Cl, Ca + S (anhydrite?), and Ca alone (calcite?) were rarely observed. Ca-bearing daughter minerals generally are more common in samples from the outer parts of the ore zone.

## ISOTOPIC EVIDENCE FOR SOURCES OF HYDROTHERMAL FLUIDS

Sheppard and others (1969) showed that the clay minerals in feldspar-destructive-alteration assemblages at


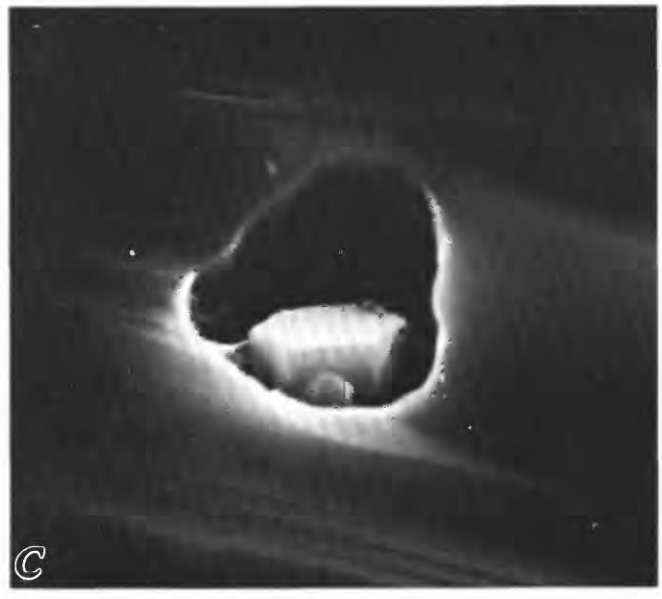


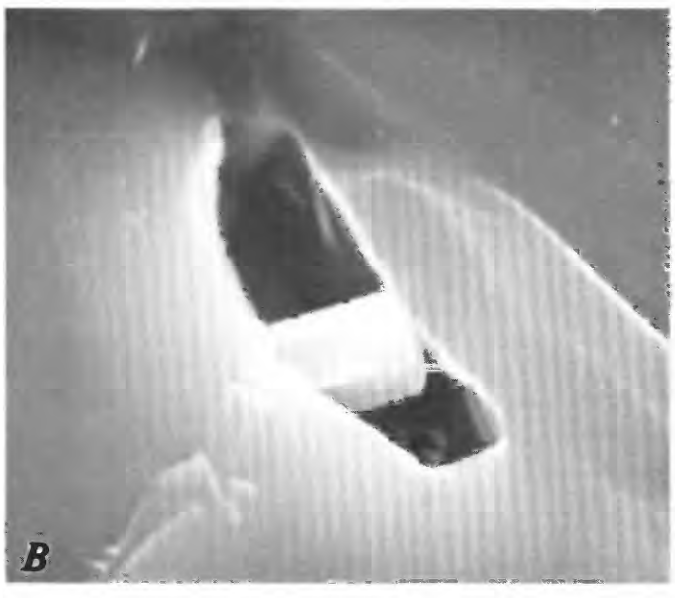



FIGURE 24.—Scanning electron micrographs showing daughter minerals in fluid inclusions, Tanamá deposit. (see Figure 13 for location) *A*, Fluid inclusion in type C vein (field No. 17-303). Hexagonal prism is iron chloride. Irregular mass at upper rear is sodium chloride. Mass at left side is Na-K-Fe chloride. *B*, Fe-Cl mineral, showing prism, pinakoid, and hexagonal-dipyramid faces (field No. 17-303). *C*, Fe-Cl daughter mineral, showing possible basal cleavage (field No. 17-295). *D*, Daughter mineral in fluid inclusion (field No. T91-1). Large wedge-shaped grain in center and smaller grain on edge at left contain K, Ca, Fe, and Cl. Rhombic form at upper left contains Ca, Fe, and Cl. Small grain between previous two contains Na, K, Ca, Fe, and Cl.

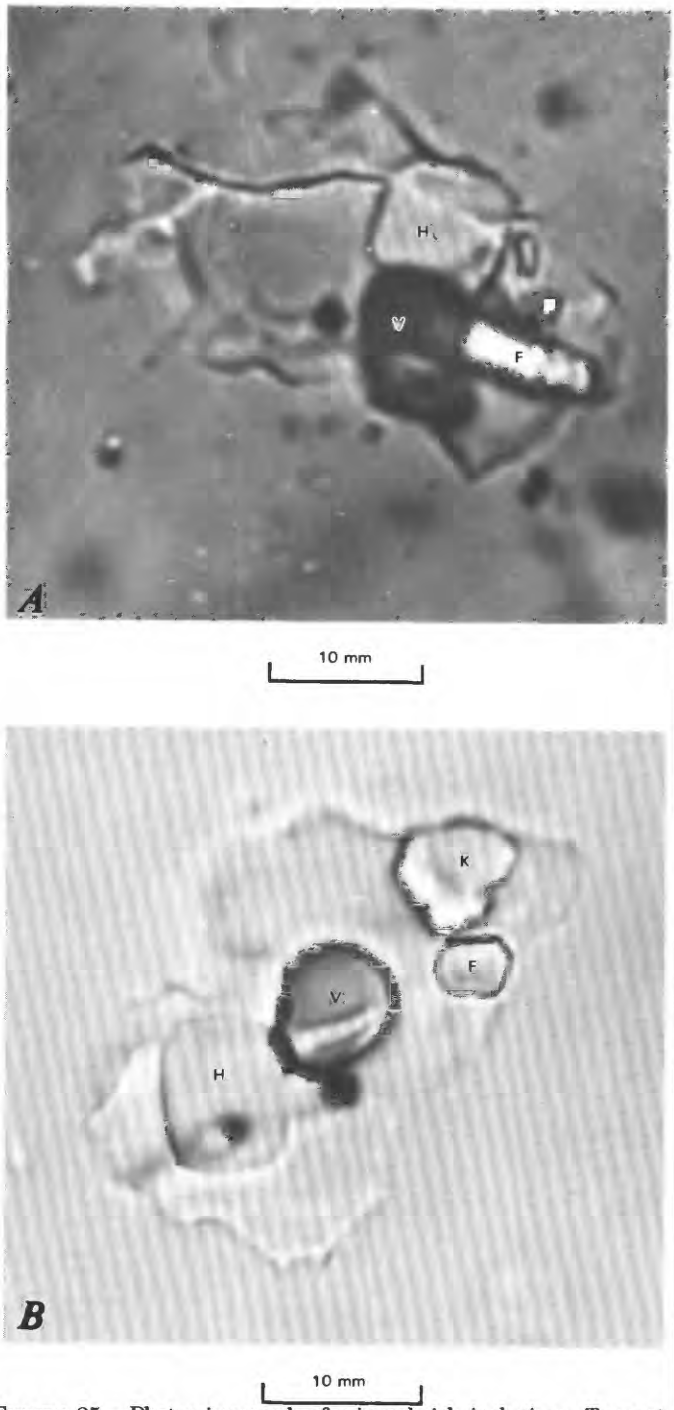


FIGURE 25.—Photomicrograph of mineral-rich inclusions, Tanamá deposit (field No. 17-303, drill hole T135). *A*, Distorted vapor bubble (V), halite crystal (H), and probable iron chloride mineral (F). Three other minerals are present as small grains. On heating, vapor bubble disappeared at 310 °C, and halite melted at 493 °C. Two high-relief small grains disappeared at about 510 °C and iron chloride melted at 560 °C. Small opaque grain at left remained. Crossed polarizers. *B*, Possible complex chloride of K, Fe, or Ca as a corroded hexagonal plate (K); halite (H); opaque grain, possibly chalcopyrite (O); vapor bubble (V); and possible basal section of Fe-Cl mineral (F). Plane-polarized light.

TABLE 11. —*Oxygen- and hydrogen-isotopic ratios of hydrothermal minerals, Tanamá deposit*

[All ratios are in permil; --, not determined. See figure 13 for localities.]

| Field No. | Mineral | $\delta^{18}O$ | $\delta D$ | Source of data or location |
|---|---|---|---|---|
| -- | Kaolinite--- | 17 | -56 | Sheppard and others (1969). |
| -- | ---do------- | 20.6 | -56 | Do. |
| -- | Kaolinite (trace of sericite) | 22.5 | -51 | Do. |
| 17-364 | Sericite | 10.35 | -46 | Southern ore body, drill hole T104, 122-m depth. |
| 17-473 | ---do------- | 11.11 | -40 | Southern ore body, drill hole T56, 172-m depth. |
| T63-1 | Chlorite | 3.97 | -40 | Northern ore body, drill hole T63, 113-m depth. |
| 17-129 | ---do------- | 4.01 | -42 | Northern ore body, drill hole T124, 302-m depth. |
| 17-449 | Amphibole (whole rock) | -- | -42 | Southern ore body, drill hole T99, 308-m depth. |
| T136-1A | ---do------- | -- | -45 | Barren core, drill hole T136, 123-m depth. |
| T136-1B | ---do------- | -- | -43 | Do. |

Tanamá and at other porphyry copper deposits have $\delta^{18}O$ and $\delta D$ values similar to those of clays formed in equilibrium with meteoric water under hydrothermal conditions. Sheppard and others (1971) later extended this model to include sericite in phyllic alteration assemblages.

To investigate the relative importance of waters of meteoric and magmatic origin in the formation of other hydrothermal minerals at Tanamá, J. R. O'Neil (written commun., 1975) determined the $\delta^{18}O$ and $\delta D$ values in two chlorite and two sericite samples and the $\delta D$ values for three whole-rock samples that contain abundant hydrothermal amphibole (table 11). O'Neil concluded that meteoric or marine water was the dominant source of the hydrothermal fluid in all the samples examined. These samples are relatively enriched in deuterium, as would be expected for meteoric waters falling on island areas. The $\delta^{18}O$ values are relatively high because the waters have equilibrated isotopically with igneous rocks at high temperatures. So little hydrogen was initially available in the rocks that the minerals took on the D/H ratio of the original meteoric water.

Of particular interest is the similarity in $\delta D$ values between minerals in the feldspar-destructive (sericite, clay)- and feldspar-stable (chlorite, amphibole)-alteration assemblages. Because of the near-oceanic environment of Tanamá, it should be easy to distinguish between meteoric or ocean water and water of magmatic

origin. Such a distinction cannot be made at Tanamá, however, because all the hydrothermal silicates seem to have equilibrated with waters having δD values of −20 to −26 permil (following Suzuoki and Epstein, 1976), or some 20 to 30 permil heavier than the δD values presumed for waters of magmatic origin.

Studies of some porphyry copper deposits (Sheppard and Gustafson, 1976; Taylor, 1979) have shown that hydrothermal biotite, a mineral common to feldspar-stable alteration in more potassium-rich porphyry systems, has δD values that suggest derivation from magmatic water. For the Butte copper deposits, however, Sheppard and Taylor (1974) found that isotopic exchange may have occurred between water in early-formed biotite of presumed magmatic derivation and hydrothermal fluids of the later main stage mineralization having a meteoric derivation.

At Tanamá, there is no isotopic evidence of a magmatic source for the hydrothermal fluids that contributed to the growth of amphiboles and chlorite in the feldspar-stable-alteration assemblages. Presumably these amphiboles formed within the temperature range 350-680 °C, as indicated by homogenization temperatures of fluid inclusions in quartz and by $\delta^{18}O$ equilibrium temperatures in early quartz-magnetite veins. The presence, deep within the deposit, of fluid inclusions with homogenization temperatures in the range 200-300 °C (fig 21*C*) permits the conclusion that low-temperature fluids of meteoric or marine origin circulated throughout the cooling deposit and exchanged deuterium and hydrogen with water in the early-formed silicates. Thus, as in the Butte deposits, silicates in the entire porphyry column now have isotopic ratios characteristic of meteoric fluids.

### OXIDATION AND SECONDARY ENRICHMENT

Weathering and oxidation have created a zone of leached saprolite, ranging in thickness from 50 to 150 m, over the deposits. Below this zone is a secondary-enrichment blanket, about 50 m thick in the northern ore body and from 60 to 125 m thick in the southern ore body (see fig. 12). Copper grades rarely reach 1 weight percent in the northern ore-body blanket, whereas secondary ore intercepts with average grades of more than 2 weight percent Cu are common in the southern ore body. The greater thickness and higher grade of the southern ore-body blanket reflect the more intense leaching by low-pH waters due to weathering of the pyrite-rich feldspar-destructive alteration zone. Over the central, low-grade core of the northern ore body (in drill hole T136), the blanket is thin and of low grade.

Minerals noted in the northern ore-body blanket are malachite, chrysocolla, and minor chalcocite. In the southern ore-body blanket, R. W. Potter, II (written commun., 1976) suggested a mineral zonation on the basis of his examination of samples from various depths in the blanket in drill holes T76, T108, and T109. Near the top of this blanket, tenorite and hematite as well as badly corroded chalcopyrite and pyrite are noted. Covellite is abundant in the central part of the blanket, and digenite is present; the covellite forms rims around remnants of pyrite and chalcopyrite. Digenite mainly occurs by itself, but where in contact with covellite, the covellite forms partial rims around the digenite. In the lowest part of the blanket, djurleite is the dominant secondary copper mineral; it forms rims around pyrite and chalcopyrite. Digenite is also present, as are possible traces of chalcocite.

## HELECHO DEPOSIT

The Helecho deposit is coextensive with a tonalite porphyry intrusion that crops out along the Río Coabey 1 km south of the Tanamá deposit (pl. 1). The Helecho deposit is named for a prominent spur on the east side of the valley of the Río Coabey that supports a luxuriant growth of treeferns, *helechos* in Spanish. Although most of the deposit is mantled by a thick saprolite layer, the deposit is well exposed in the river and has been penetrated by 31 vertical diamond-drill holes.

A detailed geologic traverse along the Río Coabey was made during 1971 and 1972, extending from its confluence with the Río Tanamá to a short distance south of the Helecho deposit. South of the deposit, the streambed lies above the saprolite-rock contact, and fresh samples are unobtainable. Samples were collected from the least oxidized parts of outcrops at intervals ranging from 10 to 50 m or, in the absence of outcrops, at greater intervals. Samples were also collected from 28 drill holes at various depths below the surface. The sample intercepts were selected so as to lie on a planar surface gently inclined to the north that includes the Río Coabey outcrops. Geologic and geochemical data from both drill-hole and outcrop samples can thus be displayed as a subhorizontal cross section cutting the Helecho deposit and surrounding rocks at the elevation of the Río Coabey (fig. 26). Polished sections and stained thin sections were prepared from a typical specimen from each rock sample, and the rest of the material was crushed and analyzed spectrographically and chemically.

### GEOLOGY AND STRUCTURAL CONTROLS

The tonalite porphyry at Helecho resembles porphyry bodies elsewhere in the map area (pl. 1) and exhibits the same wide ranges in grain size, phenocryst spacing, and groundmass texture already described. Quartz phenocrysts are less common at Helecho than in the other

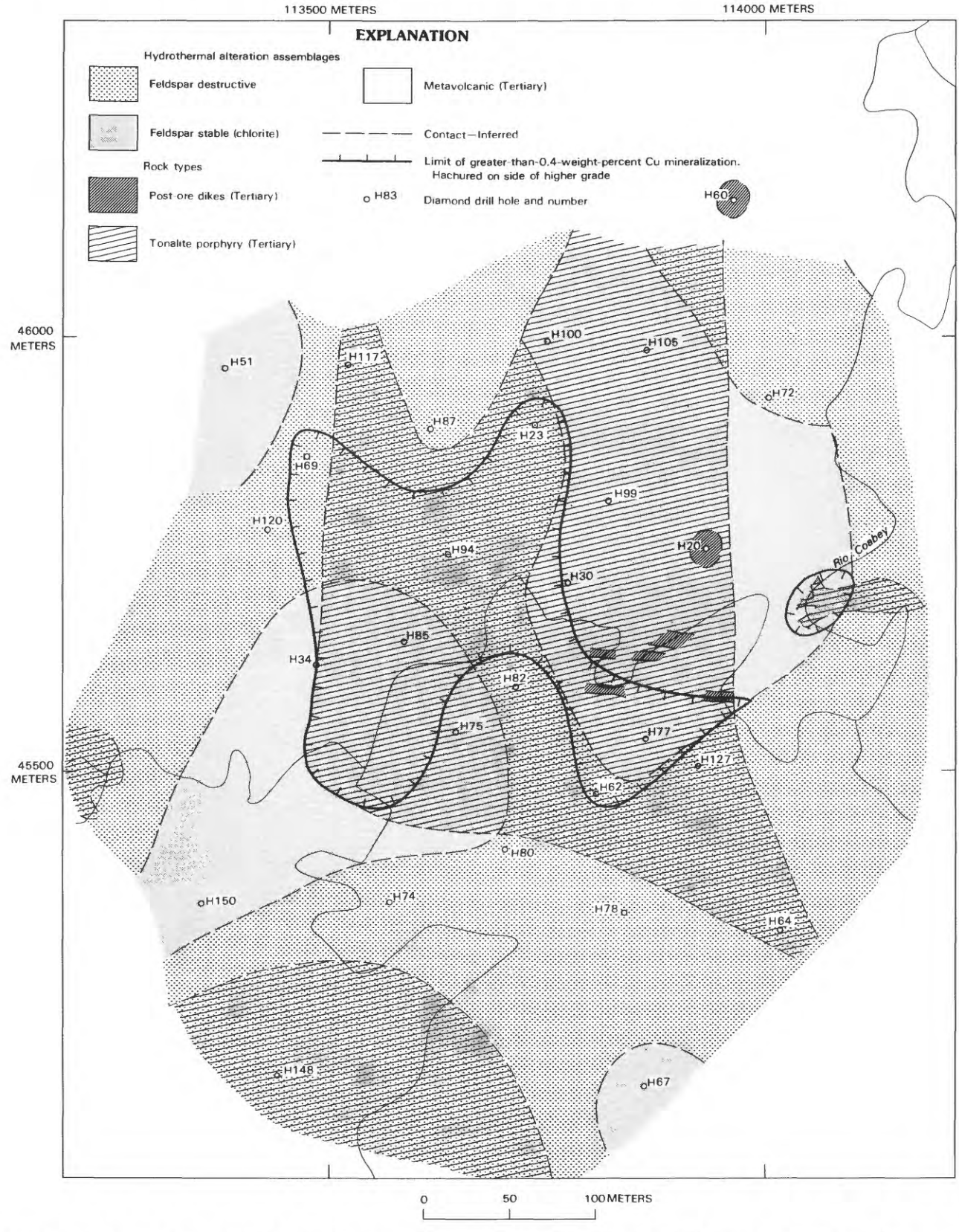


FIGURE 26.—Geologic map of Helecho deposit, showing locations of drill-hole samples in table 13. Coordinates in meters, Puerto Rico coordinate system.

# CORRECTION

## U.S. Geological Survey Professional Paper 1327

Table 1, on page 5, should be replaced by this new version, which includes chemical data for $SiO_2$ and $Al_2O_3$.

Table 1.--Composition of volcanic and batholithic rocks from the Tanama area, Puerto Rico

[Chemical analyses in weight percent by rapid rock methods (Shapiro, 1967); X-ray fluorescence spectorgraphic analyses in parts per million. Analysts: H. Smith and J. Fletcher (samples 1, 2, 5, 6); L. Espos and R. Mays (samples 3, 4)]

| Sample | 1 | 2 | 3 | 4 | 5 | 6 |
|---|---|---|---|---|---|---|
| Field No | 17-420 | 17-480Q | 17-153 | 71-154 | 31-2 | 31-3A |
| | | | Chemical analyses | | | |
| $SiO_2$ | 51.8 | 48.0 | 58.15 | 63.14 | 61.6 | 54.4 |
| $Al_2O_3$ | 14.2 | 15.5 | 17.15 | 16.04 | 16.3 | 18.7 |
| $Fe_2O_3$ | 2.7 | 6.0 | 3.07 | 2.82 | 5.6 | 4.5 |
| FeO | 5.6 | 4.9 | 4.16 | 2.99 | .08 | 1.6 |
| MgO | 10.9 | 8.7 | 3.12 | 2.33 | 2.6 | 1.4 |
| CaO | 6.8 | 5.2 | 6.61 | 5.60 | 4.6 | 8.4 |
| $Na_2O$ | 2.4 | 1.5 | 3.31 | 3.31 | 4.6 | 4.5 |
| $K_2O$ | .54 | 1.8 | 1.12 | 1.60 | 1.2 | .87 |
| $H_2O^+$ | 2.2 | 4.4 | 1.50 | 1.17 | 1.6 | 1.2 |
| $H_2O^-$ | .55 | .73 | .25 | .10 | 1.2 | .55 |
| $TiO_2$ | .47 | .96 | .72 | .61 | .41 | .67 |
| $P_2O_5$ | .07 | .19 | .14 | .21 | .15 | .31 |
| MnO | .22 | .33 | .16 | .12 | .24 | .21 |
| $CO_2$ | .07 | 1.7 | .46 | .30 | .03 | 1.3 |
| Total | 98.5 | 99.9 | 99.92 | 100.34 | 100.2 | 98.6 |
| | | | Spectrographic Analyses | | | |
| Co | 25 | 35 | 15 | 10 | 12 | 12 |
| Cr | 730 | 240 | 5 | 5 | 29 | 17 |
| Cu | 200 | 52 | 20 | 70 | 32 | 53 |
| Mo | <1.5 | <1.5 | <2 | <2 | 3 | 7 |
| Ni | 150 | 84 | 5 | 5 | 15 | 4 |
| Pb | <7 | 10 | <7 | <7 | 8 | 9 |
| Zn | 110 | 120 | <100 | <100 | 63 | 68 |

Sample 1. Hornblende hornfels in Cretaceous basalt sequence.

2. Pryoxene lapilli tuff in Cretaceous basalt sequence.

3. Tonalite, Río Camuy; collector, A. H. Barabas.

4. Tonalite, Río Angeles; collector, A. H. Barabas.

5. Dacite breccia of the Milagros Formation and Río Blanco Formation of former usage.

6. Dacite tuff of the Río Blanco Formation of former usage.

porphyry bodies, and unaltered postmineral dikes contain both hornblende and clinopyroxene phenocrysts. Contact relations with Cretaceous and Tertiary metavolcanic rocks are obscured by absence of outcrops. The metavolcanic rocks are altered to sericite and clay in most places. In a few places on the Río Coabey and in drill holes H67 and H150 (fig. 26), however, feldspar-stable alteration is present. Rocks in these areas contain the conspicuous relict phenocrysts of pyroxene replaced by amphibole that are characteristic of the Cretaceous basaltic sequence.

Abundant outcrops of mineralized porphyry in the Río Coabey permit a study of the pattern of mineralized fractures in and around the Helecho deposit. Figure 27 plots the orientation of poles of mineralized fractures in the Helecho porphyry and in the altered volcanic rocks northeast and southwest of the porphyry pluton. The data from the Helecho porphyry indicate that 95 percent of these fractures are within 20° of vertical and that 90 percent are oriented in two preferred strike directions of about N. 18° W. and N. 2° E.; a smaller number of steeply dipping fractures have strikes clustering around N. 75° W., N. 65° E., and north-south. These orientations, which match closely the strikes of relict veinlets in saprolite measured at Tanamá (fig. 11*A*), indicate that the fracturing of both deposits took place in response to a regional stress rather than to stresses localized around individual plutons. The symmetry of the maxima suggests that the Helecho deposit has not been rotated, as may have been the case for the Tanamá deposit. A weak correlation exists between the maxima in the Helecho diagram and the poles of postore dikes and the proposed fault at Tanamá.

Data from the altered volcanic rocks near Helecho, however, give a distinctly different pattern of poles. The strongest maximum corresponding to a set of N. 30° E.-striking vertical fractures is absent in the Helecho porphyry data. This maximum, which corresponds closely to the N. 30 E. trend of porphyry plutons, may represent a N. 60° W.-oriented tensional stress that existed before crystallization of those plutons and that may have been relieved by intrusion of the porphyry magma. Data from the volcanic rocks show four maxima representing steeply dipping fractures striking N. 50° W., N. 85° E., N. 70° E., and N. 40° E. that do not have corresponding

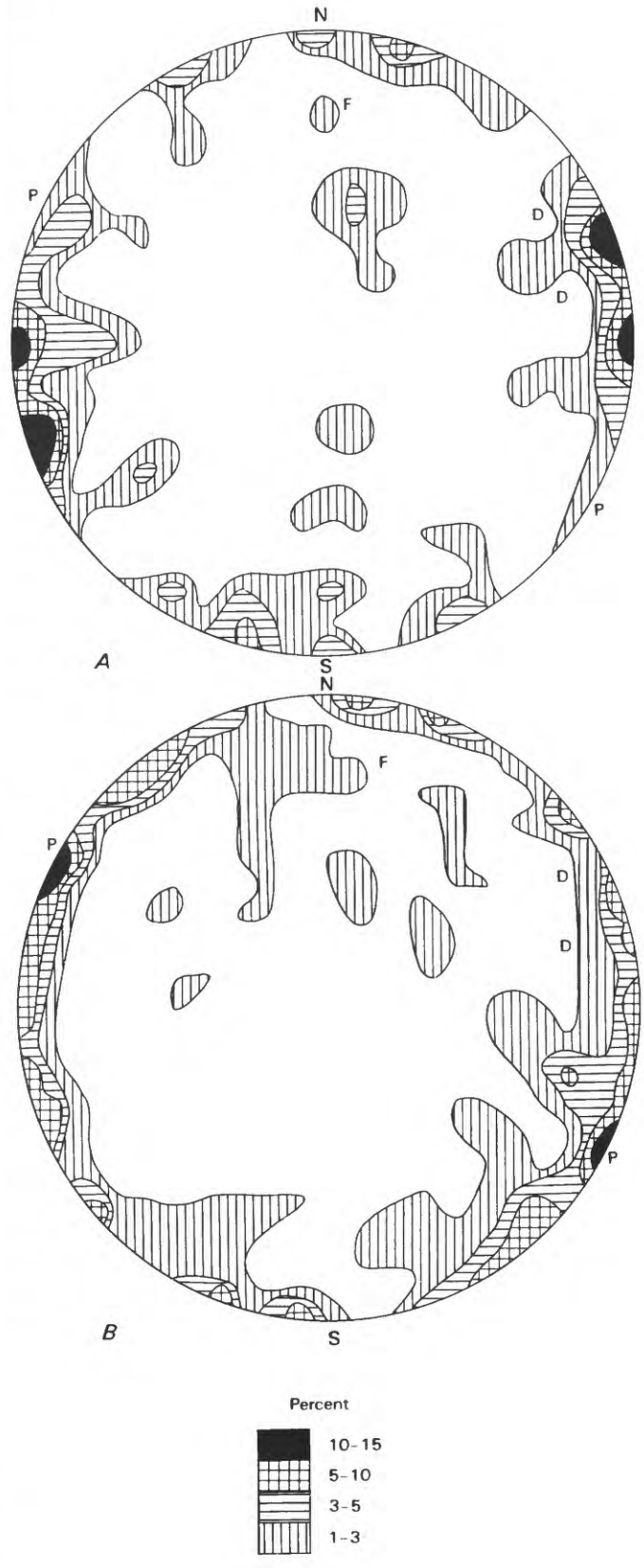


FIGURE 27.—Lower-hemisphere projections showing orientation of veins and mineralized fractures in porphyry and altered volcanic rocks, Helecho deposit. Letters denote trends of quartz diorite plutons (P) and orientations of inferred fault (F) and dikes (D) cutting Tanamá deposit. *A*, Tonalite porphyry, 98 fractures. *B*, Volcanic rocks, 94 fractures.

maxima in the data from the porphyry. The strong maxima representing N. 18° E.- and N. 20° E.-striking fractures in the porphyry, however, have closely corresponding but weaker maxima in the volcanic-rock diagram (fig. 27*B*). The preferred orientation of fractures in volcanic rocks and porphyry intrusive rocks at Helecho suggests a change in the tensional stress field from N. 60° W. to approximately east-west at about the time of intrusion of the tonalite porphyry plutons.

## MINERALIZATION AND ALTERATION

Figure 26 maps the distribution of copper concentrations greater than 0.4 weight percent in the Helecho deposit. Copper ore is generally confined to the porphyry pluton but is not associated with any specific alteration assemblage. Chalcopyrite is associated with magnetite in feldspar-stable-alteration assemblages and with pyrite in the feldspar-destructive-alteration zone. As in the Tanamá deposit, chalcopyrite in the Helecho deposit is more commonly disseminated than veinlet controlled in its distribution.

The feldspar-stable-alteration assemblage at Helecho is nearly identical to the chlorite-dominated-alteration assemblage at Tanamá. Chlorite occurs as clusters of grains replacing ferromagnesian minerals and contains many small crystals of rutile. Epidote is abundant and locally occurs as radiating clusters. Biotite occurs as cores in chlorite grains near the south contact of the porphyry. Potassium feldspar appears as traces in the same locality. The feldspar-destructive alteration at Helecho differs from that at Tanamá in that calcite is abundant and locally exceeds sericite and clay in abundance as the alteration product of plagioclase.

Anhydrite and its alteration product, gypsum, are abundant in the Helecho deposit. The role of anhydrite in the alteration assemblages at Helecho is not clear from the data collected during this study. Some anhydrite is intergrown with chlorite in feldspar-stable assemblages as shown in figure 28*A*. This is the expected association, corresponding to the common observation of anhydrite in potassic alteration assemblages in many deposits. Anhydrite, with pyrite and calcite, also occurs in rocks with feldspar-destructive alteration. Anhydrite veinlets cut quartz veins with sericitie alteration haloes (fig. 28*B*) and thus seem to be late in the paragenesis. J. C. Wilson (unpub. data, 1966) described green fluorite in anhydrite veinlets. Anhydrite and gypsum were noted only as traces at the level of the Río Coabey (in drill holes H23 and H82). Anhydrite becomes abundant deeper in the deposit. Zeolite veins were not noted in the Helecho deposit.

Fluid inclusions are abundant in quartz veins and phenocrysts at Helecho. The abundance and size of mineral-rich inclusions correlate strongly with copper and gold mineralization (J. T. Nash, written commun., 1973). SEM study of one sample indicated the presence of halite, sylvite, prismatic iron chloride, platelike K-Fe and Ca-Fe chlorides, and chalcopyrite. Barabas and

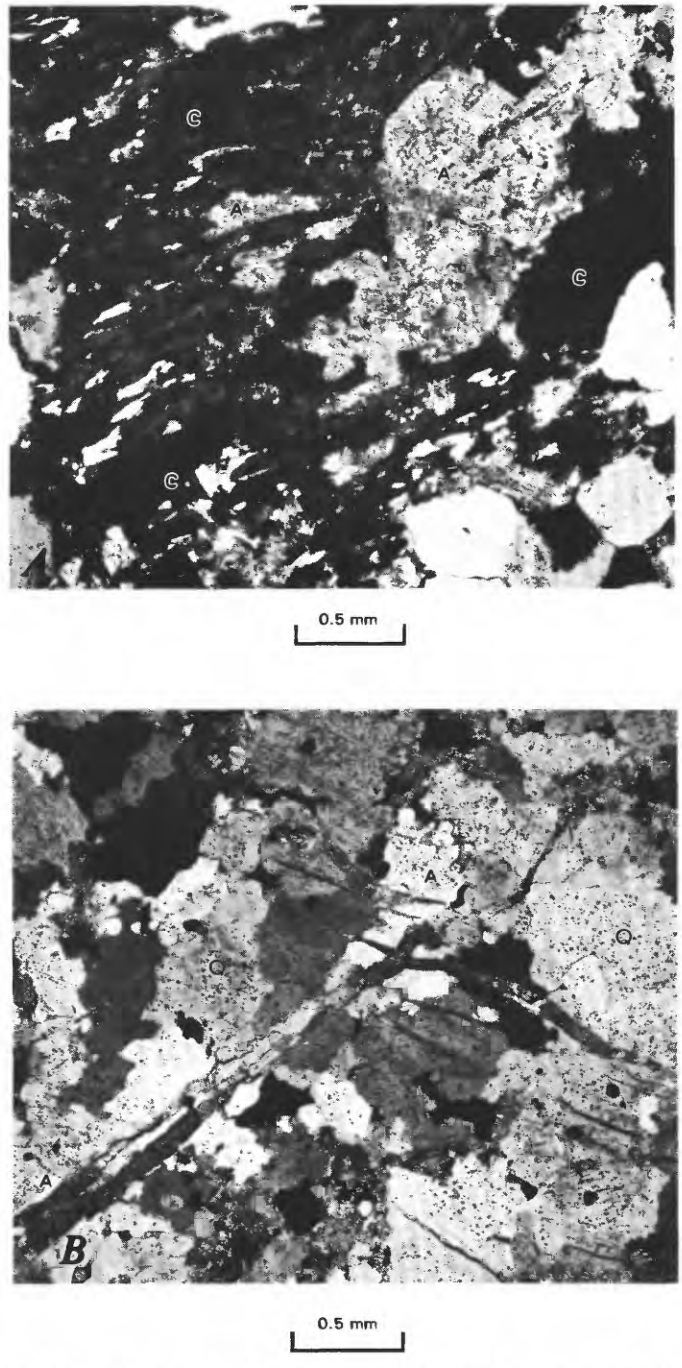


FIGURE 28.—Anhydrite intergrowths and veinlets. *A*, Anhydrite (A) intergrown with Chlorite (C) in feldspar-stable alteration. Crossed polarizers. Helecho deposit, drill hole H30, 165 meters depth. *B*, Anhydrite veinlet (A) cutting quartz vein (Q) in feldspar-destructive alteration. Crossed polarizers. Helecho deposit, drill hole H85, 391 meters depth.

Quinn (1980) recorded homogenization temperatures higher than 400 °C for inclusions in two samples from the Helecho deposit.

### OTHER COPPER PROSPECTS

Two copper prospects, Laundry Creek and Copper Creek, are located in the northeastern and central parts of the map area (pl. 1) Their English names reflect their discovery by Kennecott Copper Corp. geologists on small unnamed tributaries of the Ríos Camuy and Piedras, respectively. Laundry Creek, the earliest discovery in the map area, was recognized by very large stream-sediment copper anomalies and minor copper mineralization in outcrops. Only a small part of the tonalite porphyry pluton at Laundry Creek is mineralized (see pl. 1, fig. 29), whereas at Tanamá and Helecho, ore bodies are approximately coextensive with the intrusive stocks.

The hydrothermal-alteration mineralogy at Laundry Creek was examined petrographically in drill holes L9, L16, L28, and L143 (fig. 29). Sericitic and argillic alteration was found to be interspersed with feldspar-stable alteration in these three drill holes, but no zoning pattern was established. Chlorite is the dominant mineral in the feldspar-stable-alteration assemblage, and biotite is locally abundant as a replacement product of hornblende phenocrysts. Potassium feldspar is locally present and appears to be stable in the assemblage chlorite-potassium feldspar-epidote-albite (see Cox and others, 1973, fig. 3). As at Tanamá, the potassium feldspar may be a stable relict mineral related to an early biotite alteration, now destroyed by propylitization. Late-stage zeolite veins cut the feldspar-stable-alteration part of the deposit.

The Copper Creek prospect comprises sporadic copper mineralization along a southeast-trending tongue of tonalite porphyry. The main outcrop of mineralized rock is in a quarry (crossed hammers, pl. 1). Abundant quartz-magnetite veinlets, resembling the type C veinlets at Tanamá, cut the porphyry, and chrysocolla and malachite coat fractures over a wide area. The use of this colorful rock as road metal in numerous localities in the map area (pl. 1), gives the impression that copper mineralization is more widespread than is actually the case.

Drill hole 40 at Copper Creek was the only one to contain ore-grade copper mineralization. A cursory petrographic study of core from this hole and from drill hole 133 to the southeast showed that feldspar-stable-alteration assemblages rich in chlorite predominate in the porphyry, and those rich in amphibole occur in associated metavolcanic rocks. Anhydrite was noted in drill hole 133 in clusters with chlorite and epidote after hornblende phenocrysts.

### DISTRIBUTION OF METALLIC ELEMENTS AND SULFUR

Samples of ore and wallrock from Tanamá and Helecho were analyzed to investigate the mobility of metals in various hydrothermal environments and the usefulness of certain elements as indicators of undiscovered ore bodies. The data also provided a background for other geochemical exploration studies using soils and stream sediment. At Tanamá, composite chip samples were collected from one or two intervals in each drill hole, representing intercepts with the two horizontal sections shown in figures 11*B* and 11*C*. At Helecho, samples were analyzed from outcrops along the Río Coabey traverse as well as from drill core from intercepts within the subhorizontal section shown in figure 26.

All samples were analyzed spectrographically for 30 elements, following the methods of Grimes and Maranzino (1968), and by atomic absorption spectrophotometry for Au, Cu, Pb, and Zn, using the methods of Thompson and others (1968) and Ward and others (1969). The Tanamá samples and the Helecho

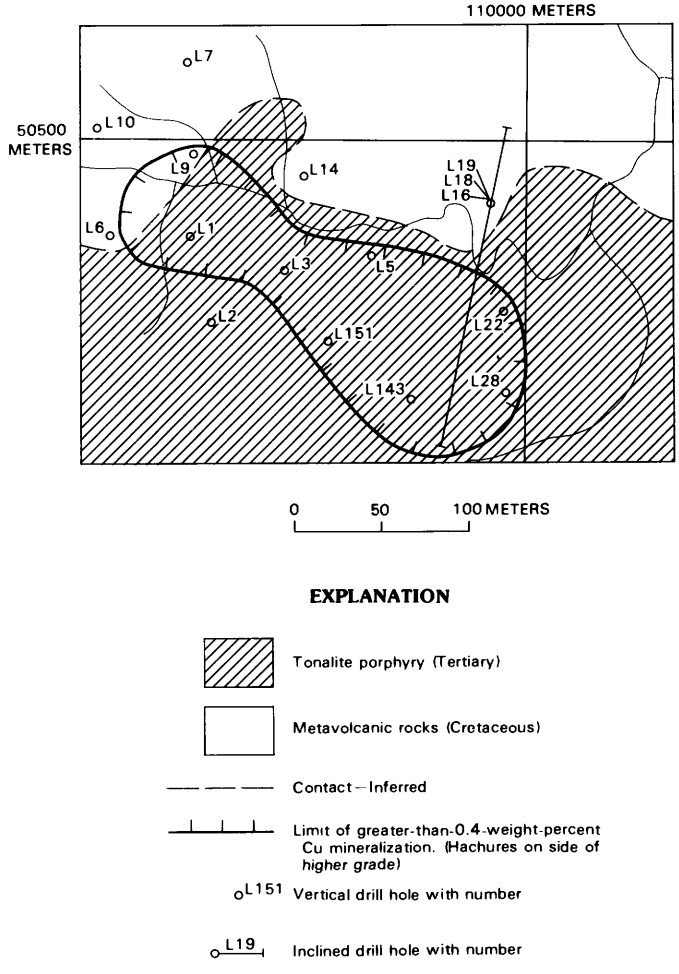


FIGURE 29.—Geologic sketch map of Laundry Creek prospect. Coordinates in meters, Puerto Rico coordinate system.

TABLE 12. —*Analytical data for selected elements in drill core from the Tanamá deposit*

[$K_2O$, $Na_2O$, and S values in weight percent; all others in parts per million. N, not detected at indicated limit; --, not analyzed. Sample numbers suffixed by "-1" and "-2" are from the 430-m and 300-m horizontal sections respectively, (fig. 11). Locations in meters in Puerto Rico coordinate system. Rock types: 1, tonalite porphyry; 2, metavolcanic rock; 3, postmineral dike. Alteration zones: 1, amphibole-dominant feldspar-stable; 2, chlorite-dominant feldspar-stable; 3, biotite-dominant feldspar-stable; 4, feldspar-destructive; 5, unaltered]

| Sample | Location N. | Location E. | Rock type | Alteration zone | Au | Cu | Pb | Zn | $Na_2O$ | $K_2O$ | S | Se | Te | Tl | Mn | Ag | Ba | Co | Cr | Mo | Ni |
|---|---|---|---|---|---|---|---|---|---|---|---|---|---|---|---|---|---|---|---|---|---|
| T56-1 | 46910 | 114513 | 1 | 4 | 0.51 | 4,400 | 6 | 41 | 0.8 | 2.8 | 2.3 | 4 | <0.1 | 0.48 | 100 | 1.0 | 200 | 30 | 50 | 5 | 30 |
| T56-2 | 46910 | 114513 | 1 | 4 | .50 | 4,600 | 6 | 27 | .5 | 2.9 | 5.6 | 5 | .21 | .33 | 300 | 1.5 | 300 | 10 | 70 | 5N | 10 |
| T61-1 | 46722 | 114765 | 1 | 4 | .08 | 100 | 5 | 7 | .8 | 1.5 | 5.4 | 9 | <.1 | .36 | 100 | .5 | 200 | 15 | 150 | 7 | 10 |
| T61-2 | 46722 | 114765 | 1 | 4 | .06 | 370 | 10 | 36 | 1.3 | 3.5 | 4.0 | 4 | .20 | .90 | 700 | .5 | 300 | 7 | 70 | 5N | 10 |
| T63-1 | 47092 | 114778 | 1 | 1 | .75 | 4,700 | 5 | 34 | 2.5 | .5 | 1.0 | 2 | .15 | <.20 | 700 | 2.0 | 150 | 15 | 30 | 5N | 10 |
| T63-2 | 47092 | 114778 | 1 | 3 | .15 | 1,900 | 9 | 49 | 3.0 | .7 | .9 | 1 | .20 | <.2 | 1,500 | 1.0 | 200 | 15 | 30 | <5 | 10 |
| T65-1 | 47202 | 114167 | 2 | 3 | .08 | 230 | 10 | 18 | 1.3 | 1.9 | 5.4 | 4 | .28 | .56 | 700 | .5N | 300 | 20 | 70 | 10 | 30 |
| T66-1 | 47110 | 114489 | 2 | 2 | .68 | 6,700 | 9 | 63 | 3.4 | .6 | 1.0 | 3 | <.1 | <.2 | 1,500 | 2.0 | 150 | 30 | 150 | <5 | 50 |
| T66-2 | 47110 | 114489 | 2 | 2 | .25 | 4,900 | 66 | 430 | .8 | 3.4 | 2.7 | 3 | .98 | .60 | 3,000 | 7.0 | 500 | 10 | 20 | 5 | 10 |
| T68-1 | 46986 | 114118 | 2 | 4 | .04 | 160 | 9 | 11 | .7 | 4.4 | 4.6 | 4 | .12 | .94 | 500 | .5N | 500 | 15 | 70 | 5N | 20 |
| T68-2 | 46986 | 114118 | 2 | 3 | .07 | 340 | 9 | 13 | 1.2 | 2.1 | 4.9 | 4 | .84 | .33 | 700 | .5N | 300 | 15 | 150 | 5 | 20 |
| T70-1 | 47034 | 114350 | 2 | 2 | .07 | 800 | 11 | 15 | 1.9 | .7 | 2.9 | 6 | <.1 | .24 | 700 | .5N | 100 | 15 | 150 | 5N | 30 |
| T70-2A | 47034 | 114350 | 2 | 3 | .04 | 1,100 | 9 | 20 | 1.4 | .8 | 3.9 | 6 | .18 | .25 | 500 | .5 | 100 | 30 | 700 | 5N | 100 |
| T70-2B | 47034 | 114350 | 2 | 3 | .04 | 970 | 11 | 18 | 1.8 | 1.8 | 4.0 | 6 | <.10 | .71 | 200 | .5 | 200 | 20 | 100 | <5 | 30 |
| T71-1 | 46837 | 114272 | 3 | 5 | .06 | 250 | 10 | 27 | 2.8 | .7 | 1.4 | 1 | .27 | .29 | 700 | .5N | 300 | 20 | 500 | 5N | 70 |
| T71-2 | 46837 | 114272 | 1 | 2 | .20 | 4,400 | 6 | 19 | 3.0 | 1.4 | 1.2 | 3 | <.10 | <.20 | 300 | 2.0 | 300 | 20 | 100 | 70 | 20 |
| T73-1 | 46915 | 114704 | 2 | 2 | .30 | 8,400 | 7 | 26 | 1.5 | .9 | 2.3 | 5 | <.10 | <.20 | 300 | 1.0 | 100 | 15 | 20N | 15 | 15 |
| T73-2 | 46915 | 114704 | 2 | 2 | .32 | 7,800 | 9 | 17 | 2.2 | 2.3 | 2.3 | 5 | .14 | .35 | 100 | 1.0 | 300 | 20 | 70 | 30 | 15 |
| T76-1 | 46754 | 114533 | 2 | 4 | .37 | 10,000 | 8 | 40 | .9 | 1.2 | 1.2 | 8 | <.10 | <.20 | 100 | 1.0 | 100 | 15 | 20 | 5N | 15 |
| T79-1 | 46851 | 114639 | 1 | 4 | .18 | 8,700 | 13 | 270 | .6 | 4.2 | 1.1 | 5 | <.10 | .60 | 700 | 2.0 | 500 | 15 | 20 | 5N | 15 |
| T79-2 | 46851 | 114639 | 1 | 2 | .27 | 6,900 | 4 | 26 | 1.3 | 3.2 | 1.5 | 5 | .12 | .76 | 500 | 1.5 | 300 | 10 | 50 | 30 | 10 |
| T81-1 | 47007 | 114609 | 2 | 4 | .05 | 1,700 | 270 | 540 | .5 | 3.5 | .4 | 5 | .34 | .87 | 700 | 1.5 | 300 | 20 | 150 | 30 | 15 |
| T81-2 | 47007 | 114609 | 2 | 2 | .08 | 1,800 | 7 | 21 | 1.1 | 2.3 | 1.5 | 5 | <.10 | .72 | 500 | .7 | 200 | 15 | 200 | 7 | 30 |
| T83-1 | 46943 | 114402 | 1 | 4 | .05 | 1,100 | 5 | 19 | .8 | 2.0 | .4 | 4 | <.10 | .39 | 500 | .5 | 200 | 20 | 30 | 7 | 10 |
| T84-1 | 46811 | 114379 | 1 | 4 | .36 | 12,700 | 8 | 27 | .2 | .7 | 1.8 | 9 | .42 | <.20 | 200 | 1.5 | 150 | 15 | 20 | 5N | 10 |
| T84-2 | 46811 | 114379 | 1 | 4 | .24 | 8,000 | 6 | 13 | .4 | 5.1 | 5.5 | 8 | .79 | .68 | 70 | 2.0 | 300 | 15 | 20 | 5N | 10 |
| T86-1 | 46610 | 114543 | 2 | 4 | .05 | 390 | 14 | 22 | .5 | 2.9 | -- | 6 | .60 | .58 | 100 | .5N | 200 | 20 | 50 | 5N | 15 |
| T86-2 | 46610 | 114543 | 2 | 2 | .43 | 640 | 19 | 100 | 1.9 | 1.0 | 4.5 | 3 | .54 | <.20 | 1,000 | 1.0 | 200 | 10 | 200 | 5N | 20 |
| T88-1 | 46658 | 114642 | 2 | 2 | .05 | 500 | 15 | 29 | 1.1 | 1.0 | 4.5 | 5 | .88 | .28 | 300 | .5N | 100 | 15 | 20N | 5N | 5 |
| T89-1 | 46710 | 114118 | 2 | 2 | .15 | 700 | 15 | 65 | .9 | 1.1 | 3.3 | 7 | 1.30 | .52 | 700 | 1.0 | 100 | 20 | 30 | 5N | 10 |
| T90-1 | 46622 | 114300 | 2 | 2 | .04 | 1,300 | 10 | 34 | 2.8 | 2.2 | 5.6 | 5 | .26 | .25 | 500 | .5N | 200 | 20 | 20N | 5N | 15 |
| T90-2 | 46622 | 114300 | 2 | 2 | <.02 | 43 | 15 | 140 | 3.1 | 2.4 | 3.2 | 4 | 1.40 | .42 | 3,000 | .5N | 100 | 7 | 20N | 5N | 70 |
| T91-1 | 46737 | 114262 | 1 | 2 | .49 | 9,300 | 9 | 38 | 1.6 | 1.3 | 2.2 | 6 | .18 | <.20 | 200 | 1.5 | 200 | 15 | 50 | 20 | 15 |
| T91-2 | 46737 | 114262 | 1 | 2 | .34 | 6,600 | 8 | 52 | 2.4 | 1.9 | 3.8 | 5 | .16 | .30 | 300 | 1.5 | 200 | 15 | 30 | 30 | 15 |
| T93-1 | 46822 | 114485 | 1 | 4 | .19 | 6,600 | 5 | 10 | .4 | 3.7 | 3.8 | 6 | .36 | .42 | 50 | .7 | 300 | 15 | 20 | 10 | 15 |
| T93-2 | 46822 | 114485 | 1 | 2 | .37 | 9,900 | 12 | 63 | .5 | 3.2 | .6 | 8 | .19 | .39 | 500 | 5.0 | 500 | 15 | 20 | <5 | 15 |
| T95-1 | 46668 | 114535 | 2 | 4 | .65 | 660 | 11 | 57 | .7 | 2.0 | 3.2 | 8 | <.10 | .92 | 500 | .5 | 300 | 20 | 70 | 70 | 15 |
| T95-2A | 46747 | 114525 | 1 | 4 | <.02 | 6,700 | 11 | 61 | 1.9 | 1.0 | 1.3 | 4 | <.10 | .24 | 1,000 | .7 | 150 | 15 | 300 | 50 | 50 |
| T95-2B | 46747 | 114525 | 1 | 4 | .18 | 6,300 | 8 | 63 | 1.2 | .2 | .7 | 4 | <.10 | .66 | 700 | 2.0 | 300 | 15 | 50 | 70 | 20 |
| T97-1 | 46882 | 114768 | 2 | 2 | .11 | 2,400 | 10 | 16 | 1.9 | 1.3 | 2.5 | 5 | <.10 | .28 | 200 | .5 | 150 | 15 | 20 | 20 | 10 |

| | | | | | | | | | | | | | | | | | | | | |
|---|---|---|---|---|---|---|---|---|---|---|---|---|---|---|---|---|---|---|---|---|
| T97-2 | 46882 | 114768 | 2 | 1 | .07 | 2,400 | 12 | 18 | .7 | 2.6 | 2.2 | 5 | .11 | .64 | 200 | .5 | 500 | 20 | 30 | 50 | 20 |
| T101-1 | 46888 | 114862 | 2 | 3 | .15 | 1,200 | 6 | 20 | 1.7 | 1.2 | 2.8 | 4 | <.10 | .37 | 200 | .5 | 200 | 20 | 70 | 15 | 20 |
| T101-2 | 46888 | 114862 | 2 | 4 | .13 | 540 | 10 | 31 | 1.3 | .4 | 5.2 | 4 | .24 | <.20 | 1,500 | .7 | 100 | 30 | 1,500 | <5 | 100 |
| T102-1 | 46722 | 114636 | 2 | 4 | .12 | 2,600 | 9 | 22 | .7 | .8 | 6.6 | 12 | <.10 | .34 | 300 | .7 | 100 | 20 | 20N | 10 | 5 |
| T102-2 | 46810 | 114627 | 1 | 2 | .37 | 7,200 | 6 | 61 | 1.6 | 1.3 | 1.1 | 4 | <.10 | .35 | 700 | 1.5 | 150 | 7 | 50 | 7 | 10 |
| T104-1 | 46820 | 114539 | 1 | 4 | .33 | 4,300 | 2 | 9 | .5 | 1.9 | .6 | 8 | .11 | .35 | 50 | 1.0 | 500 | 15 | 30 | 15 | 15 |
| T104-2 | 46890 | 114534 | 1 | 4 | .09 | 3,900 | 3 | 5 | 2.4 | 3.1 | 2.0 | 4 | .14 | .53 | 30 | .5N | 300 | 10 | 20 | 20 | 10 |
| T108-1 | 46955 | 114620 | 2 | 3 | .28 | 3,200 | 10 | 40 | 1.0 | 1.2 | 2.5 | 5 | .28 | .29 | 300 | .7 | 150 | 10 | 70 | 7 | 20 |
| T108-2 | 47055 | 114605 | 3 | 5 | .05 | 270 | 6 | 1,400 | 1.1 | .4 | 3.2 | 0 | <.10 | <.20 | 5,000 | .5N | 300 | 5 | 20 | 5N | 5 |
| T109-2 | 47012 | 114510 | 2 | 2 | .31 | 3,800 | 9 | 54 | .8 | 1.6 | 2.6 | 4 | <.10 | .55 | 700 | .7 | 200 | 20 | 70 | 5N | 15 |
| T111-1 | 46725 | 114750 | 1 | 4 | .07 | 100 | 3 | 5 | .2 | .3 | 3.2 | 9 | <.10 | <.20 | 50 | .5N | 50 | 20 | 30 | 15 | 7 |
| T111-2 | 46815 | 114737 | 2 | 1 | .12 | 800 | 9 | 20 | 1.1 | 1.5 | 2.6 | 4 | <.10 | .52 | 300 | .5N | 150 | 20 | 100 | <5 | 20 |
| T113-1A | 46880 | 114655 | 1 | 4 | .65 | 13,000 | 7 | 39 | .3 | 2.6 | 3.0 | 7 | <.10 | .47 | 200 | 1.5 | 300 | 10 | 30 | 5 | 10 |
| T113-1B | 46880 | 114655 | 1 | 4 | .50 | 12,000 | 9 | 33 | 1.2 | 1.2 | 2.3 | 7 | <.10 | <.20 | 300 | 1.5 | 200 | 15 | 70 | 5N | 15 |
| T113-2A | 46990 | 114677 | 2 | 2 | .27 | 4,700 | 6 | 14 | 1.9 | 1.6 | 1.9 | 3 | <.10 | .34 | 100 | 1.0 | 200 | 15 | 50 | 70 | 15 |
| T113-2B | 46990 | 114677 | 2 | 2 | .43 | 6,000 | 10 | 27 | 1.6 | 1.6 | 3.2 | 4 | <.10 | .43 | 300 | 1.0 | 200 | 15 | 300 | 15 | 30 |
| T114-1 | 46855 | 114580 | 1 | 2 | .38 | 9,100 | 7 | 36 | 1.3 | 1.1 | 2.7 | 5 | <.10 | .24 | 200 | 1.0 | 300 | 15 | 20 | 10 | 10 |
| T114-2 | 46793 | 114468 | 1 | 4 | .28 | 9,700 | 10 | 76 | .3 | 1.7 | 4.4 | 5 | .28 | .34 | 300 | 2.0 | 300 | 15 | 50 | <5 | 15 |
| T115-1 | 46697 | 114442 | 2 | 4 | .19 | 3,400 | 9 | 24 | .7 | 1.0 | 4.3 | 8 | .19 | .27 | 200 | .5 | 200 | 20 | 20N | 5N | 10 |
| T115-2 | 46697 | 114442 | 2 | 4 | .08 | 1,100 | 14 | 25 | .8 | .3 | 7.0 | 6 | .23 | <.20 | 300 | .5 | 50 | 15 | 100 | 5 | 15 |
| T116-1 | 46763 | 114435 | 1 | 4 | .63 | 6,700 | 9 | 24 | .4 | 2.0 | 4.2 | 7 | .31 | <.20 | 200 | 1.0 | 300 | 10 | 30 | 5N | 10 |
| T116-2A | 46842 | 114421 | 1 | 2 | .33 | 9,900 | 3 | 31 | 1.4 | 1.3 | 2.2 | 5 | <.10 | .22 | 200 | 1.0 | 300 | 15 | 100 | 5N | 10 |
| T116-2B | 46842 | 114421 | 1 | 2 | .28 | 8,600 | 5 | 17 | .6 | .8 | 2.5 | 7 | <.10 | .28 | 200 | 1.5 | 500 | 15 | 30 | 7 | 10 |
| T119-1 | 46995 | 114300 | 2 | 2 | .08 | 800 | 8 | 17 | 1.0 | .9 | 6.6 | 5 | .14 | .38 | 200 | .5 | 200 | 20 | 150 | <5 | 20 |
| T121-1 | 47275 | 114750 | 1 | 2 | .67 | 5,800 | 7 | 81 | 2.4 | .8 | 2.1 | 2 | .67 | .33 | 700 | 2.0 | 200 | 15 | 30 | 5 | 10 |
| T121-2 | 47285 | 114650 | 2 | 1 | .36 | 5,700 | 6 | 60 | 3.0 | .9 | 1.8 | 2 | .22 | .33 | 1,500 | 1.5 | 200 | 15 | 70 | 15 | 15 |
| T122-1 | 47320 | 114505 | 1 | 2 | .73 | 4,600 | 18 | 180 | 1.6 | 1.1 | 1.1 | 2 | .57 | .39 | 1,500 | 1.5 | 200 | 10 | 20 | 5 | 10 |
| T122-2 | 47310 | 114415 | 2 | 1 | .27 | 3,700 | 11 | 35 | 1.6 | .7 | .3 | 1 | <.10 | <.20 | 1,500 | .7 | 50 | 15 | 1,500 | 5N | 70 |
| T124-1 | 47245 | 114955 | 1 | 2 | .28 | 8,100 | 10 | 40 | 2.0 | .9 | 2.0 | 2 | <.10 | <.20 | 700 | 3.0 | 200 | 15 | 50 | 5N | 10 |
| T124-2 | 47225 | 114830 | 1 | 2 | .33 | 5,800 | 12 | 66 | 2.4 | .7 | .4 | 2 | .26 | <.20 | 1,500 | 2.0 | 150 | 10 | 20 | 15 | 10 |
| T126-1 | 47208 | 114410 | 2 | 3 | .18 | 3,200 | 80 | 120 | .4 | 1.4 | 5.0 | 6 | <.10 | .30 | 1,500 | 1.0 | 200 | 20 | 300 | 5N | 70 |
| T128-1 | 47220 | 114585 | 1 | 2 | .95 | 4,600 | 6 | 32 | 2.3 | .3 | .4 | 2 | .16 | <.20 | 1,000 | 1.0 | 200 | 10 | 100 | 15 | 15 |
| T128-2 | 47220 | 114585 | 2 | 1 | .31 | 5,400 | 12 | 600 | .9 | .5 | 8.0 | 2 | <.10 | .26 | 2,000 | 3.0 | 200 | 30 | 1,000 | 7 | 70 |
| T131-1 | 47405 | 114925 | 2 | 3 | .10 | 1,300 | 6 | 37 | 1.5 | 1.3 | 8.7 | 7 | .12 | .42 | 300 | .5 | 300 | 30 | 50 | 70 | 30 |
| T131-2 | 47402 | 114850 | 2 | 3 | .20 | 3,200 | 16 | 39 | 1.1 | 2.0 | 3.4 | 3 | <.10 | .45 | 300 | 2.0 | 300 | 30 | 500 | 50 | 50 |
| T134-1 | 47430 | 114270 | 2 | 2 | .05 | 1,100 | 10 | 27 | .8 | .2 | 4.2 | 3 | .20 | <.20 | 1,500 | .5N | 100 | 50 | 700 | 5N | 70 |
| T135-1 | 47200 | 114742 | 1 | 2 | .40 | 3,200 | 11 | 72 | 1.6 | .8 | 1.1 | 1 | 1.00 | .23 | 1,500 | 2.0 | 300 | 10 | 20 | 5N | 10 |
| T136-1 | 47148 | 114688 | 1 | 1 | .50 | 1,700 | 4 | 37 | 1.7 | .4 | .3 | 1 | .10 | <.20 | 1,500 | .7 | 150 | 10 | 20 | 5N | 10 |
| T136-2 | 47148 | 114688 | 1 | 2 | .07 | 290 | 6 | 44 | 1.9 | .3 | -- | 0 | <.10 | <.20 | 1,500 | .5N | 150 | 10 | 20 | 5N | 7 |
| T137-1 | 47122 | 114570 | 1 | 2 | .59 | 15,600 | 4 | 40 | 1.2 | .8 | 1.4 | 4 | <.10 | <.20 | 150 | 1.0 | 150 | 15 | 70 | 70 | 20 |
| T137-2 | 47122 | 114570 | 3 | 5 | .18 | 280 | 6 | 620 | 1.3 | .4 | 6.5 | 0 | .50 | <.20 | 5,000G | .5N | 1,000 | 15 | 70 | 5N | 10 |
| T138-1 | 47370 | 114457 | 1 | 2 | .90 | 6,800 | 21 | 2,300 | 1.1 | .2 | 3.1 | 3 | .70 | <.20 | 5,000G | 1.5 | 200 | 15 | 50 | 5N | 15 |
| T142-1 | 47275 | 114350 | 2 | 3 | .07 | 870 | 7 | 22 | .9 | 1.0 | 2.9 | 3 | <.10 | .36 | 700 | .5 | 200 | 20 | 150 | 10 | 30 |
| T142-2 | 47275 | 114350 | 2 | 1 | .27 | 6,900 | 10 | 44 | 1.2 | .2 | 1.1 | 2 | <.10 | .39 | 500 | 1.0 | 150 | 10 | 30 | 15 | 20 |
| T144-1 | 47450 | 114620 | 1 | 3 | .04 | 1200 | 8 | 27 | 1.1 | .2 | 3.1 | 3 | <.10 | .45 | 700 | .5 | 300 | 20 | 30 | 30 | 10 |
| T144-2 | 47440 | 114520 | 3 | 5 | .04 | 180 | 9 | 34 | .9 | .2 | 4.3 | 2 | <.10 | .59 | 1,000 | .5N | 500 | 20 | 20 | <5 | 10 |
| T146-1 | 47220 | 115220 | 2 | 1 | <.02 | 270 | 4 | 210 | 1.4 | .2 | 1.3 | 0 | 1.40 | <.20 | 5,000G | .5N | 200 | 20 | 30 | 5N | 10 |

outcrop samples were analyzed for K, Na, and S. These analyses were carried out in the laboratory of the Department of Public Works, Commonwealth of Puerto Rico, under the direction of Ileana Perez Gonzalez. For the Tanamá samples, Te and Se were determined by atomic absorption, using $NaBH_4$ reduction and a heated quartz atomizer, and Tl by using a heated graphite atomizer. The Te, Se, and Tl determinations were made by R. Mendes of the U.S. Geological Survey, Reston, Va.

Tables 12 through 14 list most of the analytical data. Spectrographic Au, Cu, Pb, and Zn data are omitted because they duplicate more precise spectrophotometric data presented for these elements; spectrographic data for B, Ca, Fe, Mg, Sc, Sr, Ti, V, Y, and Zr are omitted because they failed to show any significant variation between samples. Elements analyzed for spectrographically but not found at their corresponding limits of detectability are as follows:

| *Element* | *Limit of detectability (ppm)* |
|---|---|
| As | 200 |
| Be | 1 |
| Bi | 10 |
| Cd | 20 |
| Nb | 10 |
| Sb | 100 |
| Sn | 10 |
| W | 50 |

Statistical relations between elements and between samples were analyzed by W. D. Menzie II of the U.S. Geological Survey. Samples of postmineral porphyry were omitted from this statistical analysis because its purpose was to examine the dispersion of elements during mineralization. Samples collected from outcrops at

TABLE 13. —*Analytical data for selected elements in drill core from the Helecho deposit*

[All values in parts per million; N, not detected at indicated limit. See figure 26 for sample localities. Locations in meters in Puerto Rico coordinate system. Rock types: 1, tonalite porphyry; 2, metavolcanic rock; 3, postmineral dike. Alteration zones: 1, amphibole-dominant feldspar-stable; 2, chlorite-dominant feldspar-stable; 3, biotite-dominant feldspar-stable; 4, feldspar-destructive; 5, unaltered]

| Sample | Location | | Rock type | Alteration zone | Au | Cu | Pb | Zn | Mn | Ag | Ba | Co | Cr | Mo | Ni |
|---|---|---|---|---|---|---|---|---|---|---|---|---|---|---|---|
| | N. | E. | | | | | | | | | | | | | |
| H 20 | 45750 | 113937 | 1 | 2 | 0.18 | 130 | 14 | 41 | 1,500 | 1N | 300 | 15 | 50 | 5N | 10 |
| H 23 | 45895 | 113740 | 1 | 4 | .16 | 4,800 | 87 | 140 | 1,500 | 5 | 300 | 15 | 150 | 20 | 30 |
| H 30 | 45714 | 113780 | 1 | 2 | .17 | 2,100 | 4 | 69 | 700 | 1 | 200 | 15 | 50 | 5N | 15 |
| H 34A | 45621 | 113490 | 2 | 3 | .18 | 3,100 | 7 | 54 | 500 | 1 | 300 | 15 | 300 | 5N | 50 |
| H 34B | 45621 | 113490 | 1 | 2 | .23 | 3,200 | 3 | 35 | 200 | 1 | 300 | 15 | 30 | 5N | 30 |
| H 51A | 45966 | 113390 | 2 | 1 | .07 | 150 | 13 | 30 | 500 | 1N | 1,500 | 20 | 200 | 5N | 70 |
| H 51B | 45966 | 113390 | 2 | 1 | .10 | 170 | 23 | 50 | 300 | 1 | 700 | 20 | 200 | 5N | 70 |
| H 60 | 46150 | 113956 | 3 | 5 | .03 | 54 | 15 | 52 | 1,500 | 1N | 300 | 15 | 100 | 5N | 30 |
| H 62 | 45469 | 113810 | 1 | 4 | .55 | 6,400 | 4 | 26 | 150 | 1 | 200 | 15 | 50 | 5N | 20 |
| H 64 | 45311 | 114020 | 1 | 4 | .09 | 19 | 10 | 17 | 150 | 1N | 1,000 | 15 | 150 | 5N | 20 |
| H 67 | 45131 | 113865 | 1 | 1 | .07 | 99 | 13 | 31 | 1,000 | 1N | 5,000 | 10 | 150 | 5N | 30 |
| H 69 | 45862 | 113481 | 2 | 4 | .09 | 4,500 | 13 | 85 | 1,000 | 2 | 200 | 10 | 200 | 5N | 70 |
| H 72 | 45925 | 114010 | 2 | 4 | <.02 | 100 | 4 | 28 | 150 | 1N | 700 | 10 | 100 | 15 | 30 |
| H 74 | 45350 | 113576 | 2 | 4 | .03 | 190 | 9 | 21 | 200 | 1N | 200 | 30 | 700 | 5N | 100 |
| H 75 | 45543 | 113650 | 1 | 3 | .08 | 930 | 4 | 37 | 700 | 1N | 150 | 7 | 200 | 5N | 5 |
| H 77 | 45528 | 113868 | 1 | 4 | .28 | 3,800 | 18 | 45 | 700 | 1 | 200 | 7 | 200 | 5N | 10 |
| H 80 | 45407 | 113710 | 2 | 4 | .14 | 100 | 36 | 200 | 1,500 | 1N | 200 | 15 | 100 | 5N | 30 |
| H 82 | 45596 | 113722 | 1 | 4 | .10 | 840 | 27 | 350 | 1,500 | 1 | 200 | 10 | 70 | 5N | 20 |
| H 85 | 45648 | 113595 | 1 | 2 | .29 | 4,200 | 98 | 140 | 700 | 1 | 200 | 15 | 50 | 5N | 10 |
| H 87 | 45890 | 113621 | 2 | 4 | .17 | 670 | 6 | 33 | 200 | 1N | 150 | 15 | 70 | 7 | 20 |
| H 94 | 45748 | 113642 | 1 | 4 | .44 | 4,900 | 4 | 31 | 300 | 1 | 150 | 10 | 30 | 5N | 15 |
| H 99 | 45807 | 113825 | 1 | 2 | .18 | 2,200 | 4 | 27 | 300 | 1 | 150 | 10 | 30 | 5N | 10 |
| H 100 | 45990 | 113757 | 1 | 2 | .00 | 650 | 10 | 320 | 1,500 | 1 | 200 | 10 | 30 | 5N | 15 |
| H 105 | 45977 | 113872 | 1 | 2 | .00 | 150 | 6 | 31 | 50 | 1N | 200 | 15 | 50 | 50 | 15 |
| H 117 | 45967 | 113530 | 1 | 4 | .08 | 140 | 76 | 27 | 1,500 | 1 | 500 | 10 | 30 | 5N | 10 |
| H 120 | 45777 | 113436 | 2 | 4 | .06 | 2,900 | 36 | 80 | 200 | 1N | 1,500 | 10 | 50 | 5N | 30 |
| H 127 | 45500 | 113925 | 1 | 4 | .02 | 1,500 | 87 | 200 | 1,000 | 2 | 500 | 10 | 30 | 5 | 30 |
| H 148 | 45150 | 113445 | 1 | 4 | .09 | 1,100 | 12 | 56 | 700 | 1N | 300 | 10 | 50 | 5N | 15 |
| H 150 | 45355 | 113360 | 2 | 3 | <.02 | 160 | 12 | 26 | 500 | 1N | 300 | 15 | 300 | 5N | 100 |

Helecho were also omitted from the statistical analysis because of unpredictable variations in the data due to weathering and secondary copper enrichment.

R-mode factor analysis of the data reduced the variables to four factors of geologic significance: Factor 1, positively loaded on Ag, Mn, Pb, and Zn; factor 2, on Ba, K, and Tl; factor 3 on Ag, Au, and Cu; and factor 5, on Co, Cr, S, and Se. Mo and Te had more than 30 percent of the values qualified (below lower limit of detectablity) and thus could not be treated statistically; the distribution of these elements was considered qualitatively, and only tentative conclusions were drawn.

### COPPER-GOLD-SILVER

Figure 30 maps the distribution of samples in the Tanamá deposit and their scores on factor 3. Samples with high positive scores in this factor expectedly fall within the 0.4-weight-percent-Cu limits shown on figure 11. Samples within the barren core score negatively on factor 3 at 430-m elevation; a similar correspondence is shown by factor 3 scores for Helecho drill-core samples. East of the main Helecho ore body, high Cu-Au values are associated with small porphyry dikes cropping out in the Río Coabey.

No correlation between Cu-Au-Ag values and type of alteration was found at either Tanamá or Helecho. Although median gold values are higher in samples containing magnetite than in pyrite-rich samples, a plot of medians and associated confidence limits suggests that this difference may not be significant. A plot of gold versus total sulfur shows no correlation between these factors. There is no evidence for outward migration of gold to form peripheral vein deposits in these data or in the soil geochemical data collected by R. E. Learned (written commun., 1976).

### SULFUR-SELENIUM-CHROMIUM-COBALT

At Tanamá, factor 5 is strongly positive in samples of altered basalt surrounding the mineralized porphyry stocks (fig. 31). Factor 5 thus indicates the pyrite halo of the Tanamá deposit. The positive loading of Cr and Co in this factor derives from the initial high content of Cr and Co in basalt. Factor 5 is strongly negative in the porphyry stock affected by feldspar-stable alteration. Figure 32, which maps the S content of bedrock samples collected from the Río Coabey, suggests the presence of a strong pyrite halo surrounding the Helecho deposit.

### MOLYBDENUM

Molybdenum is sparse at Tanamá and Helecho; the highest value measured was 100 ppm (0.01 weight percent), and more than 30 percent of the values were less than 5 ppm (limit of detectability). Figure 33 maps the distribution of Mo at Tanamá. Low Mo concentrations were measured in samples from the barren core zone, and higher concentrations occur erratically in the ore zone and in metabasalt 100 m outward from the boundary of the ore body. At Helecho (fig. 32), low Mo concentrations were measured in most samples from the ore zone; higher concentrations occur in a discontinuous zone 200 to 300 m outward from the ore-body boundary. The highest concentrations (100 ppm Mo) were measured in the small outlier of ore-grade porphyry sampled on the Río Coabey east of the main Helecho ore body.

### LEAD-ZINC-MANGANESE-SILVER

Factor 1 scores for Tanamá samples (fig. 34) reveal a strong negative correlation between Pb-Zn-Mn and pervasive feldspar-destructive alteration. Positive scores occur erratically in the northern ore body in the same samples that score high on factor 3 (Cu-Au-Ag). In the southern ore body, especially at the 430-m elevation (fig. 34*A*), large negative scores on factor 1 occur within the zone of feldspar-destructive alteration.

The strong depletion of Pb, Zn, Mn, and Ag in the zone of pervasive sericite-clay-carbonate alteration seems to conflict with the observation that sphalerite occurs in type F veins (samples T124-2, T128-2, table 12) with sericite-clay-carbonate alteration envelopes. I conclude that the feldspar-destructive alteration was a complex process with an early deep-seated sphalerite-stable stage and a later stage in which sphalerite and, presumably, Pb and Mn minerals were leached.

The site of deposition of the remobilized Pb, Zn, Mn, and Ag is a peripheral zone or halo 200 to 500 m outward from the margin of the copper ore body. This halo has been recognized in soils in the Río Vivi district (Learned and others, 1973) and in bedrock at the Sapo Alegre prospect (Cox and others, 1975). At Tanamá, the Pb-Zn-Mn halo lies beyond the outermost drill holes and has been recognized in soil geochemistry studies (R. E. Learned, written commun., 1976). Remobilization of zinc apparently continued into the postmineral intrusive stage, as evidenced by the high Zn content of sample T108-2 (table 12).

At Helecho, factor 1 (Pb-Zn-Mn-Ag) scores are strongly negative in and near the ore body and strongly positive in stream-outcrop samples northeast and southwest of the ore body (fig. 35). These positive scores suggest the presence of a Pb- Zn-Mn-Ag halo 100 to 600 m outward from the ore body and approximately coextensive with the pyrite halo.

TABLE 14. —*Analytical data for selected elements in outcrop samples from the Helecho deposit*

[$K_2O$, $Na_2O$, and S values in weight percent; all others in parts per million. N, not detected at indicated limit. See figure 32 for sample localities. Locations in meters in Puerto Rico coordinate system. Rock types: 1, tonalite porphyry; 2, metavolcanic rock; 3, postmineral dike. Alteration zones: 1, amphibole-dominant feldspar-stable; 2, chlorite-dominant feldspar-stable; 3, biotite-dominant feldspar-stable; 4, feldspar-destructive; 5, unaltered]

| Sample | Location | | Rock type | Alteration zone | Au | Cu | Pb | Zn | $Na_2O$ | $K_2O$ | S | Mn | Ag | Ba | Co | Cr | Mo | Ni |
|---|---|---|---|---|---|---|---|---|---|---|---|---|---|---|---|---|---|---|
| | N. | E. | | | | | | | | | | | | | | | | |
| 9 | 45565 | 114075 | 2 | 4 | <0.02 | 3,800 | 13 | 110 | 1.5 | 1.1 | 0.01 | 1,000 | 5 | 500 | 20 | 700 | 5 | 70 |
| 10 | 45513 | 114044 | 2 | 4 | .00 | 810 | 13 | 100 | 3.8 | 1.3 | 1.05 | 500 | 1 | 300 | 15 | 50 | 10 | 70 |
| 11 | 45515 | 114007 | 2 | 4 | .09 | 510 | 23 | 150 | .3 | 1.6 | .11 | 700 | 1 | 300 | 15 | 20 | 20 | 100 |
| 12 | 45550 | 113985 | 2 | 4 | .38 | 1,100 | 55 | 55 | .3 | 1.6 | .04 | 1,500 | 7 | 700 | 10 | 500 | 7 | 15 |
| 13 | 45571 | 113953 | 1 | 4 | .40 | 8,200 | 8 | 42 | .3 | 2.1 | 1.10 | 1,500 | 7 | 700 | 15 | 70 | 30 | 15 |
| 14 | 45582 | 113950 | 3 | 5 | <.02 | 1,100 | 9 | 180 | 2.8 | 4.4 | .02 | 3,000 | 1 | 500 | 20 | 500 | 5N | 70 |
| 15 | 45610 | 113975 | 2 | 4 | <.02 | 2,500 | 6 | 45 | 1.1 | 2.2 | .78 | 700 | 3 | 500 | 15 | 50 | 10 | 10 |
| 16 | 45627 | 113990 | 2 | 4 | .06 | 2,600 | 8 | 52 | .9 | 1.1 | 1.12 | 1,000 | 7 | 300 | 20 | 70 | 20 | 10 |
| 17 | 45695 | 113982 | 2 | 4 | .10 | 130 | 14 | 24 | .2 | 1.5 | .03 | 300 | 1N | 700 | 5 | 150 | 5 | 10 |
| 19 | 45646 | 113896 | 1 | 1 | .08 | 910 | 9 | 53 | 3.4 | .6 | -- | 1,500 | 1 | 300 | 20 | 70 | 5N | 20 |
| 20 | 45627 | 113869 | 1 | 3 | <.02 | 1,700 | 8 | 74 | 3.7 | .7 | .12 | 1,500 | 1 | 200 | 15 | 70 | 5N | 15 |
| 21 | 45602 | 113856 | 1 | 2 | .26 | 1,900 | 30 | 130 | 3.7 | .2 | .62 | 1,500 | 7 | 300 | 15 | 50 | 5N | 15 |
| 23 | 45590 | 113810 | 1 | 2 | .11 | 2,600 | 26 | 24 | 3.0 | .3 | 1.55 | 300 | 7 | 300 | 10 | 30 | 20 | 10 |
| 24 | 45602 | 113808 | 1 | 2 | .07 | 3,400 | 9 | 100 | .7 | 2.2 | .57 | 500 | 1 | 200 | 20 | 30 | 5N | 15 |
| 25 | 45608 | 113808 | 1 | 2 | .06 | 1,900 | 7 | 47 | .6 | 2.0 | .67 | 300 | 1 | 300 | 20 | 30 | 5N | 15 |
| 26 | 45625 | 113820 | 1 | 4 | .03 | 2,400 | 97 | 130 | 2.7 | .5 | 1.00 | 3,000 | 3 | 700 | 15 | 30 | 5 | 15 |
| 27 | 45627 | 113820 | 1 | 2 | .16 | 2,550 | 9 | 39 | .6 | 2.3 | .59 | 500 | 1 | 300 | 15 | 30 | 5N | 10 |
| 29 | 45660 | 113841 | 1 | 4 | .29 | 2,300 | 19 | 130 | .6 | 1.0 | .00 | 2,000 | 1 | 200 | 20 | 50 | 5N | 20 |
| 30 | 45670 | 113775 | 1 | 2 | .06 | 2,150 | 9 | 100 | .6 | 1.9 | .25 | 1,500 | 1 | 300 | 15 | 30 | 5N | 15 |
| 31 | 45667 | 113770 | 1 | 2 | .18 | 3,250 | 9 | 70 | .1 | 1.7 | .65 | 1,500 | 1 | 700 | 15 | 50 | 5N | 15 |
| 33 | 45665 | 113762 | 1 | 4 | .22 | 5,900 | 24 | 72 | 1.0 | .1 | 1.60 | 2,000 | 5 | 700 | 15 | 30 | 5N | 15 |
| 34 | 45668 | 113752 | 1 | 2 | .19 | 4,800 | 9 | 64 | 2.2 | .8 | .60 | 300 | 1 | 200 | 15 | 30 | 5N | 15 |
| 35 | 45680 | 113744 | 1 | 2 | .40 | 7,800 | 9 | 73 | 6.3 | 1.6 | .73 | 700 | 5 | 200 | 15 | 30 | 5N | 15 |
| 36 | 45704 | 113732 | 1 | 2 | .23 | 2,400 | 8 | 40 | 2.1 | 1.7 | .89 | 700 | 1 | 300 | 15 | 30 | 5N | 20 |
| 37 | 45695 | 113688 | 1 | 2 | <.02 | 8,200 | 9 | 48 | 1.0 | 1.2 | 1.83 | 500 | 1N | 200 | 10 | 30 | 5N | 10 |
| 38 | 45682 | 113691 | 1 | 4 | <.02 | 600 | 7 | 36 | 2.5 | 2.2 | .00 | 300 | 1N | 200 | 10 | 30 | 5 | 10 |
| 39 | 45678 | 113690 | 1 | 4 | <.02 | 2,300 | 5 | 28 | 5.0 | 2.0 | 1.45 | 200 | 1 | 200 | 10 | 30 | 5N | 10 |
| 40 | 45636 | 113689 | 1 | 4 | .07 | 5,800 | 49 | 40 | 2.3 | .4 | -- | 300 | 3 | 300 | 15 | 20 | 5N | 10 |
| 41 | 45626 | 113683 | 1 | 4 | .04 | 6,100 | 17 | 40 | 2.2 | .3 | -- | 1,000 | 1 | 500 | 20 | 30 | 5N | 15 |
| 42 | 45620 | 113676 | 1 | 4 | .09 | 2,600 | 15 | 110 | 2.5 | .5 | 1.06 | 3,000 | 1 | 500 | 15 | 50 | 5N | 15 |
| 43 | 45619 | 113660 | 1 | 2 | .04 | 1,700 | 8 | 47 | .4 | .7 | .74 | 300 | 1 | 300 | 15 | 70 | 5N | 20 |
| 44 | 45620 | 113634 | 1 | 4 | .18 | 5,300 | 19 | 80 | .3 | .4 | 1.20 | 300 | 7 | 300 | 20 | 30 | 30 | 15 |
| 45 | 45620 | 113635 | 1 | 4 | .32 | 4,900 | 23 | 35 | .2 | 2.2 | -- | 300 | 10 | 300 | 10 | 30 | 20 | 15 |
| 46 | 45625 | 113606 | 1 | 4 | .35 | 1,300 | 9 | 60 | .5 | 2.0 | -- | 500 | 7 | 300 | 10 | 30 | 5N | 15 |
| 48 | 45550 | 114120 | 2 | 4 | <.02 | 1,300 | 12 | 82 | .8 | 2.5 | 1.31 | 1,000 | 7 | 1,500 | 10 | 20 | 7 | 15 |
| 49 | 45681 | 114170 | 1 | 4 | <.02 | 700 | 130 | 140 | .3 | 2.5 | 3.00 | 700 | 5 | 700 | 10 | 30 | 5N | 30 |
| 50 | 45637 | 114140 | 2 | 4 | <.02 | 1,100 | 17 | 40 | 1.0 | 1.1 | 4.80 | 300 | 1 | 300 | 15 | 70 | 50 | 50 |
| 51 | 45645 | 114080 | 2 | 4 | <.02 | 1,400 | 10 | 44 | .9 | 1.8 | 2.60 | 700 | 3 | 500 | 20 | 100 | 20 | 50 |
| 52 | 45656 | 114055 | 1 | 4 | .21 | 4,300 | 9 | 58 | 1.4 | .8 | .62 | 500 | 3 | 200 | 15 | 150 | 5 | 70 |
| 53 | 45670 | 114050 | 2 | 4 | .31 | 4,800 | 9 | 110 | 2.0 | 1.9 | .62 | 1,500 | 3 | 300 | 15 | 300 | 5N | 70 |

| | | | | | | | | | | | | | | | | | |
|---|---|---|---|---|---|---|---|---|---|---|---|---|---|---|---|---|---|
| 54 | 45690 | 114052 | 1 | 4 | .20 | 13,000 | 11 | 35 | 1.1 | 1.8 | 1.59 | 700 | 7 | 700 | 15 | 150 | 15 | 100 |
| 55 | 45710 | 114069 | 2 | 2 | <.02 | 3,700 | 10 | 74 | 1.6 | .5 | 1.15 | 3,000 | 7 | 200 | 15 | 1,500 | 5N | 100 |
| 56 | 45712 | 114070 | 2 | 3 | <.02 | 3,400 | 10 | 90 | 1.4 | .2 | .43 | 3,000 | 7 | 300 | 10 | 1,500 | 5N | 70 |
| 57 | 45723 | 114082 | 2 | 1 | .10 | 5,200 | 9 | 120 | 1.9 | .5 | .23 | 1,500 | 1 | 300 | 20 | 5,000 | 5N | 70 |
| 58 | 45790 | 114181 | 2 | 4 | <.02 | 250 | 7 | 69 | .9 | 1.1 | 3.30 | 70 | 5 | 700 | 10 | 700 | 5 | 10 |
| 59 | 45840 | 114086 | 2 | 4 | .05 | 5,000 | 16 | 76 | .5 | .8 | .90 | 1,500 | 3 | 200 | 15 | 7,000 | 5N | 70 |
| 60 | 45860 | 114085 | 2 | 1 | .08 | 2,500 | 18 | 110 | 1.6 | .5 | .93 | 1,500 | 3 | 200 | 15 | 3,000 | 5N | 70 |
| 61 | 45860 | 114085 | 2 | 4 | .08 | 3,600 | 7 | 46 | .7 | 1.3 | 2.30 | 300 | 1 | 200 | 15 | 5,000 | 20 | 30 |
| 62 | 45906 | 114075 | 2 | 4 | <.02 | 350 | 82 | 130 | .3 | 2.0 | 2.80 | 1,500 | 1 | 300 | 15 | 1,000 | 5N | 70 |
| 63 | 45920 | 114086 | 2 | 4 | <.02 | 460 | 52 | 55 | .3 | 1.9 | 3.00 | 1,000 | 7 | 500 | 15 | 1,000 | <5 | 70 |
| 64 | 45983 | 114120 | 2 | 4 | <.02 | 520 | 9 | 23 | .3 | 1.7 | 4.20 | 200 | 7 | 500 | 15 | 1,000 | 7 | 70 |
| 65 | 45990 | 114122 | 2 | 4 | <.02 | 71 | 2 | 8 | 4.0 | 2.7 | .15 | 70 | 1 | 700 | 5 | 50 | 20 | 20 |
| 66 | 46070 | 114151 | 2 | 1 | <.02 | 700 | 13 | 160 | 1.1 | .7 | .75 | 1,500 | 1 | 300 | 20 | 1,500 | 5N | 150 |
| 67 | 46067 | 114169 | 2 | 4 | <.02 | 290 | 17 | 45 | .4 | 2.2 | 2.70 | 500 | 1 | 700 | 10 | 1,000 | <5 | 20 |
| 68 | 46052 | 114171 | 2 | 4 | <.02 | 650 | 14 | 76 | .3 | 1.7 | 5.50 | 3,000 | 1 | 500 | 30 | 1,000 | <5 | 70 |
| 69 | 46027 | 114158 | 2 | 2 | <.02 | 710 | 15 | 180 | .3 | 1.1 | 5.10 | 1,000 | 1 | 200 | 20 | 1,500 | <5 | 70 |
| 70 | 46012 | 114166 | 2 | 4 | <.02 | 280 | 10 | 32 | .6 | 1.8 | 5.80 | 200 | 1N | 700 | 10 | 700 | 5N | 50 |
| 71 | 46005 | 114191 | 2 | 4 | <.02 | 290 | 18 | 67 | .6 | 2.7 | 8.10 | 1,500 | 1 | 1,000 | 15 | 700 | 5N | 50 |
| 72 | 45995 | 114206 | 2 | 4 | <.02 | 200 | 15 | 90 | 1.1 | 1.1 | 4.90 | 1,500 | 1N | 700 | 20 | 700 | 5N | 150 |
| 73 | 46015 | 114217 | 2 | 4 | <.02 | 160 | 10 | 42 | 1.5 | 2.5 | 5.30 | 300 | 1N | 3,000 | 15 | 700 | 5N | 20 |
| 74 | 46010 | 114209 | 3 | 5 | <.02 | 68 | 14 | 100 | 2.0 | 4.3 | .18 | 1,500 | 1N | 200 | 15 | 150 | 5N | 70 |
| 75 | 46041 | 114217 | 2 | 4 | <.02 | 530 | 9 | 53 | .3 | 1.7 | 5.00 | 150 | 1N | 500 | 15 | 1,500 | 5N | 70 |
| 76 | 46067 | 114223 | 2 | 4 | <.02 | 29 | 8 | 53 | .5 | .6 | 4.50 | 200 | 1N | 700 | 15 | 200 | 10 | 15 |
| 77 | 46085 | 114232 | 2 | 4 | <.02 | 62 | 15 | 62 | .3 | 3.6 | 4.50 | 300 | 1 | 1,500 | 20 | 20 | 5N | 10 |
| 78 | 46135 | 114227 | 2 | 4 | <.02 | 80 | 37 | 80 | .3 | 1.9 | 6.10 | 1,000 | 1 | 1,000 | 30 | 150 | 5N | 70 |
| 79 | 46156 | 114199 | 2 | 4 | <.02 | 92 | 16 | 92 | .3 | 1.5 | 3.80 | 500 | 1 | 500 | 20 | 700 | 5N | 70 |
| 80 | 46145 | 114184 | 2 | 1 | .03 | 180 | 11 | 180 | .8 | .5 | 1.57 | 1,500 | 1N | 300 | 20 | 700 | 5N | 150 |
| 81 | 46155 | 114170 | 2 | 1 | <.02 | 100 | 8 | 100 | .7 | 1.1 | 2.40 | 1,500 | 1N | 700 | 15 | 700 | 5N | 70 |
| 83 | 45600 | 113585 | 1 | 2 | .33 | 8,300 | 10 | 58 | 2.3 | .3 | .40 | 300 | 5 | 200 | 15 | 50 | 5N | 15 |
| 84 | 45565 | 113563 | 1 | 2 | .26 | 5,000 | 10 | 54 | 2.5 | .2 | .70 | 500 | 1 | 150 | 10 | 20 | 5N | 15 |
| 85 | 45522 | 113559 | 1 | 2 | .37 | 3,900 | 10 | 90 | 2.4 | .6 | .50 | 300 | 2 | 200 | 15 | 100 | 5N | 20 |
| 86 | 45487 | 113532 | 1 | 3 | .18 | 6,700 | 7 | 36 | 2.3 | 1.0 | .92 | 300 | 2 | 150 | 15 | 70 | 5N | 30 |
| 87 | 45460 | 113580 | 1 | 2 | .09 | 3,300 | 9 | 180 | 2.5 | 2.8 | .05 | 700 | 1 | 300 | 15 | 50 | 5N | 20 |
| 88 | 45405 | 113556 | 2 | 4 | <.02 | 3,900 | 29 | 380 | .5 | .4 | 1.03 | 5,000 | 1 | 500 | 15 | 1,000 | 5N | 70 |
| 89 | 45397 | 113520 | 2 | 4 | <.02 | 2,400 | 9 | 35 | .8 | 1.6 | .79 | 300 | 1 | 300 | 15 | 30 | 5N | 30 |
| 90 | 45400 | 113462 | 2 | 4 | <.02 | 130 | 49 | 280 | .1 | 2.2 | 9.30 | 300 | 2 | 200 | 15 | 500 | 7 | 70 |
| 91 | 45382 | 113467 | 1 | 4 | <.02 | 250 | 14 | 28 | .1 | .8 | 11.40 | 70 | 1N | 100 | 15 | 150 | 5N | 50 |
| 92 | 45345 | 113544 | 2 | 4 | <.02 | 100 | 6 | 9 | .6 | .9 | 2.50 | 70 | 1N | 300 | 10 | 50 | <5 | 10 |
| 93 | 45345 | 113508 | 2 | 4 | .03 | 260 | 12 | 220 | .1 | .2 | 2.75 | 700 | 1N | 100 | 50 | 1,500 | 5N | 1,500 |
| 94 | 45263 | 113536 | 1 | 4 | .31 | 96 | 9 | 25 | .5 | 2.0 | 3.55 | 150 | 1N | 700 | 15 | 100 | 5 | 20 |
| 95 | 45319 | 113607 | 2 | 4 | .15 | 290 | 15 | 70 | .1 | .3 | 3.30 | 700 | 1N | 200 | 70 | 1,500 | 5 | 1,500 |
| 96 | 45300 | 113720 | 2 | 1 | .21 | 250 | 13 | 40 | .1 | 1.0 | 4.20 | 500 | 1N | 150 | 30 | 1,500 | 5N | 300 |
| 98 | 45535 | 113516 | 1 | 1 | .54 | 4,000 | 10 | 64 | 2.2 | .2 | .17 | 300 | 1 | 150 | 10 | 30 | 5N | 20 |
| 100 | 45525 | 113495 | 1 | 2 | .04 | 5,800 | 7 | 58 | 2.2 | .3 | .46 | 300 | 1 | 200 | 15 | 20 | 5N | 20 |
| 101 | 45463 | 113427 | 2 | 4 | .30 | 2,300 | 8 | 40 | .5 | 2.3 | 1.49 | 500 | 1 | 500 | 15 | 30 | 5 | 15 |
| 102 | 45525 | 113408 | 2 | 4 | <.02 | 2,300 | 18 | 200 | .5 | .2 | 13.80 | 300 | 5 | 100 | 700 | 2,000 | 5 | 2,000 |
| 103 | 45480 | 113385 | 2 | 4 | <.02 | 240 | 10 | 200 | .8 | .7 | .51 | 1,000 | 1 | 200 | 20 | 1,500 | 5N | 200 |
| 104 | 45495 | 113325 | 2 | 1 | <.02 | 30 | 7 | 5 | .2 | 2.5 | 6.00 | 30 | 1 | 300 | 10 | 30 | 5 | 10 |

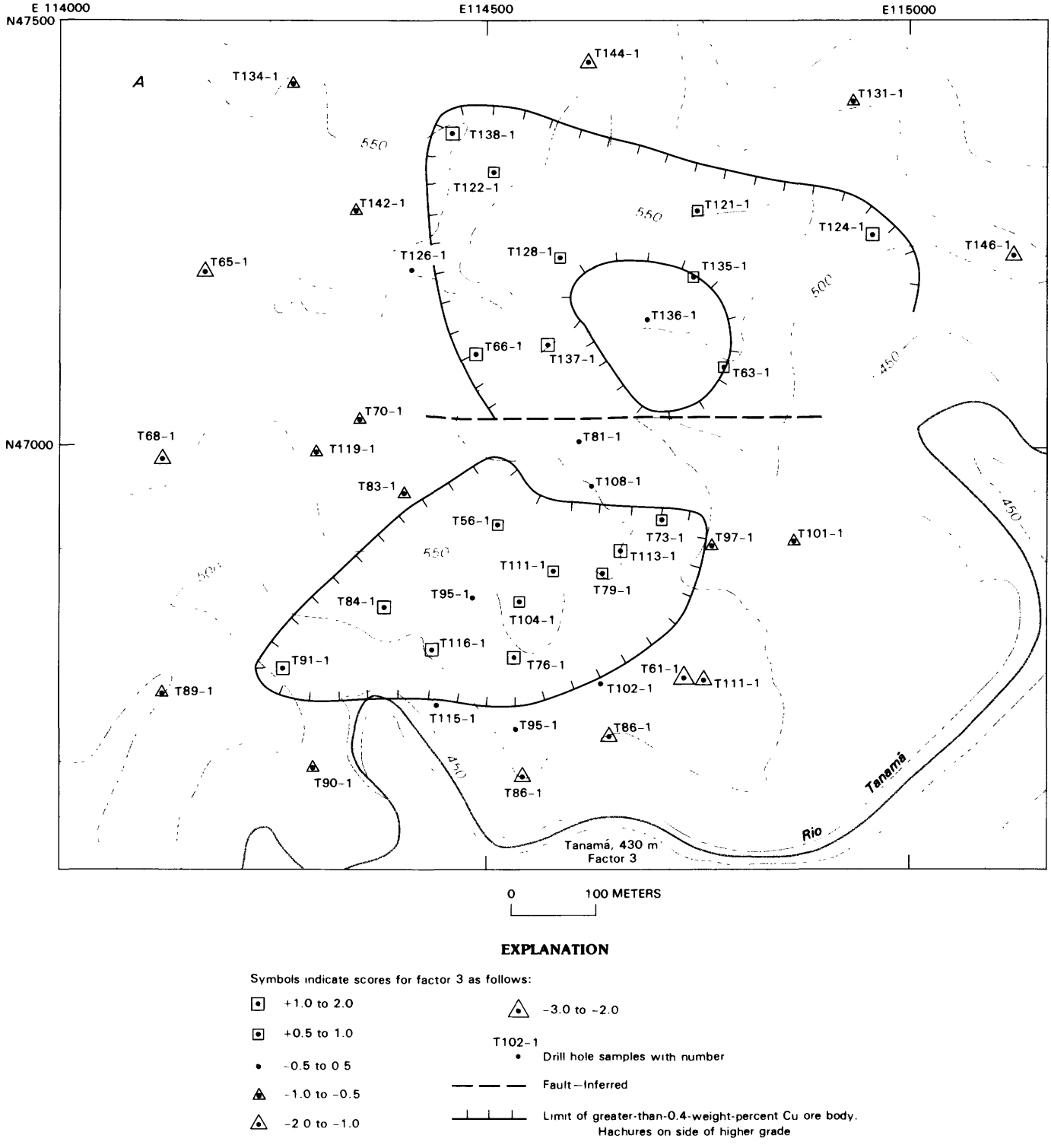


FIGURE 30.—Outline of greater-than-0.4-weight-percent-Cu ore body in comparison with scores on factor 3 for Cu-Au-Ag, Tanamá deposit. *A*, 430-m elevation. *B*, 300-m elevation. Coordinates in meters, Puerto Rico coordinate system.

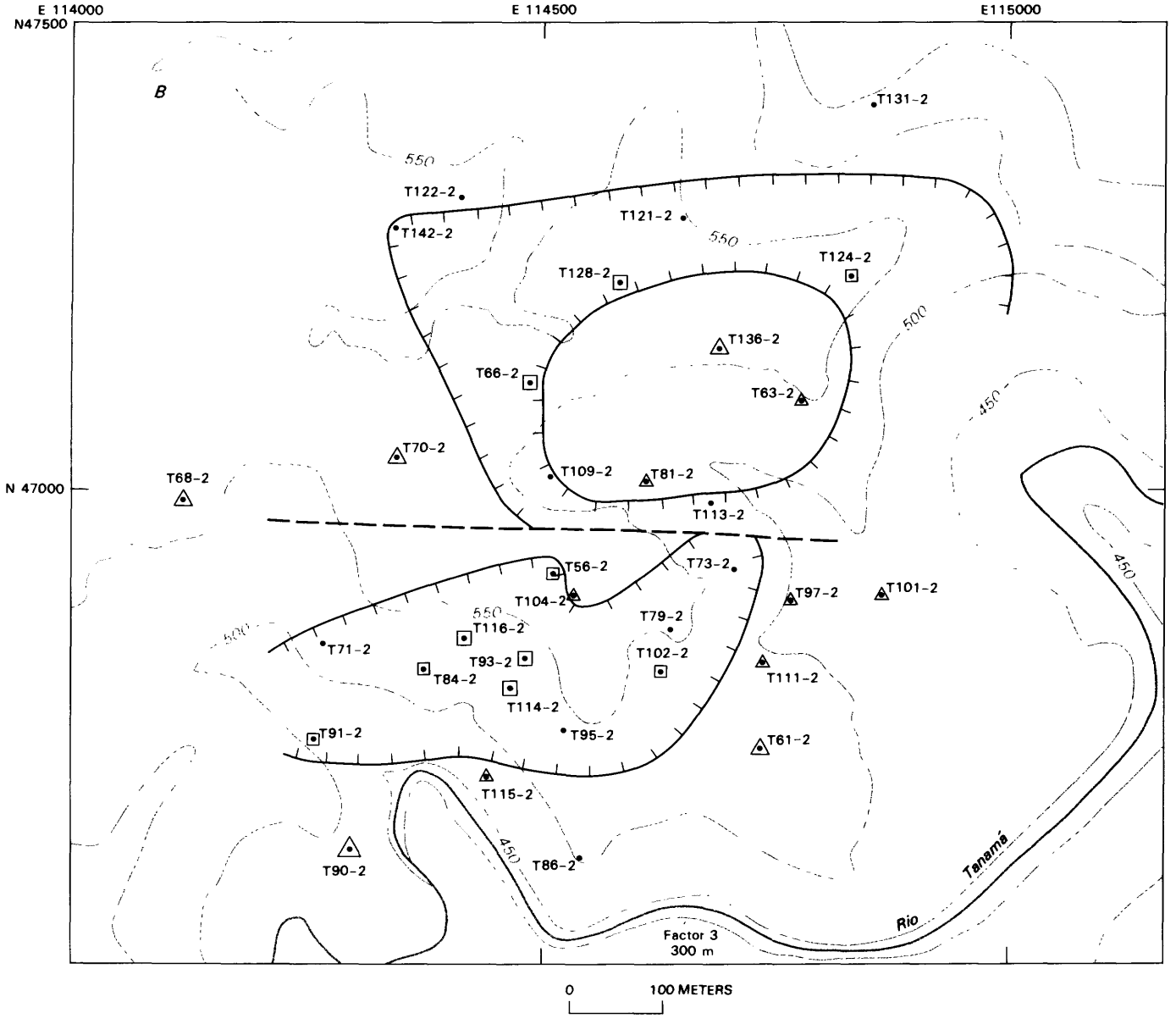


**EXPLANATION**

Symbols indicate scores for factor 3 as follows:

- +1.0 to 2.0
- +0.5 to 1.0
- -0.5 to 0.5
- -1.0 to -0.5
- -2.0 to -1.0
- -3.0 to -2.0
- T102-2 Drill hole samples with number
- Fault—Inferred
- Limit of greater-than-0.4-weight-percent Cu ore body. Hachures on side of higher grade

FIGURE 30.—Continued.

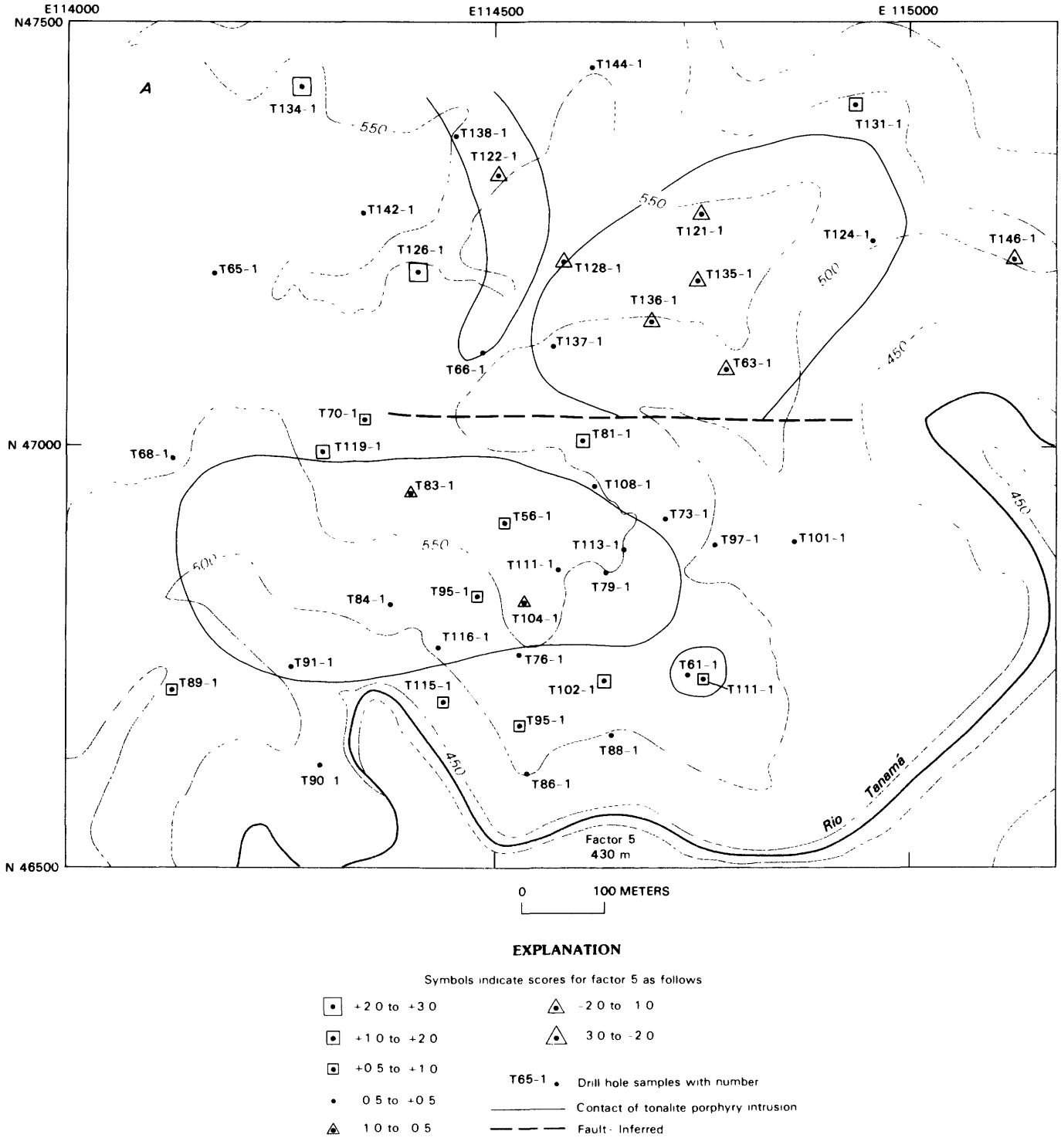


FIGURE 31.—Contact of tonalite porphyry in comparison with scores on factor 5 for S-Se-Cr-Co, Tanamá deposit. *A*, 430-m elevation. *B*, 300-m elevation. Coordinates in meters, Puerto Rico coordinate system.

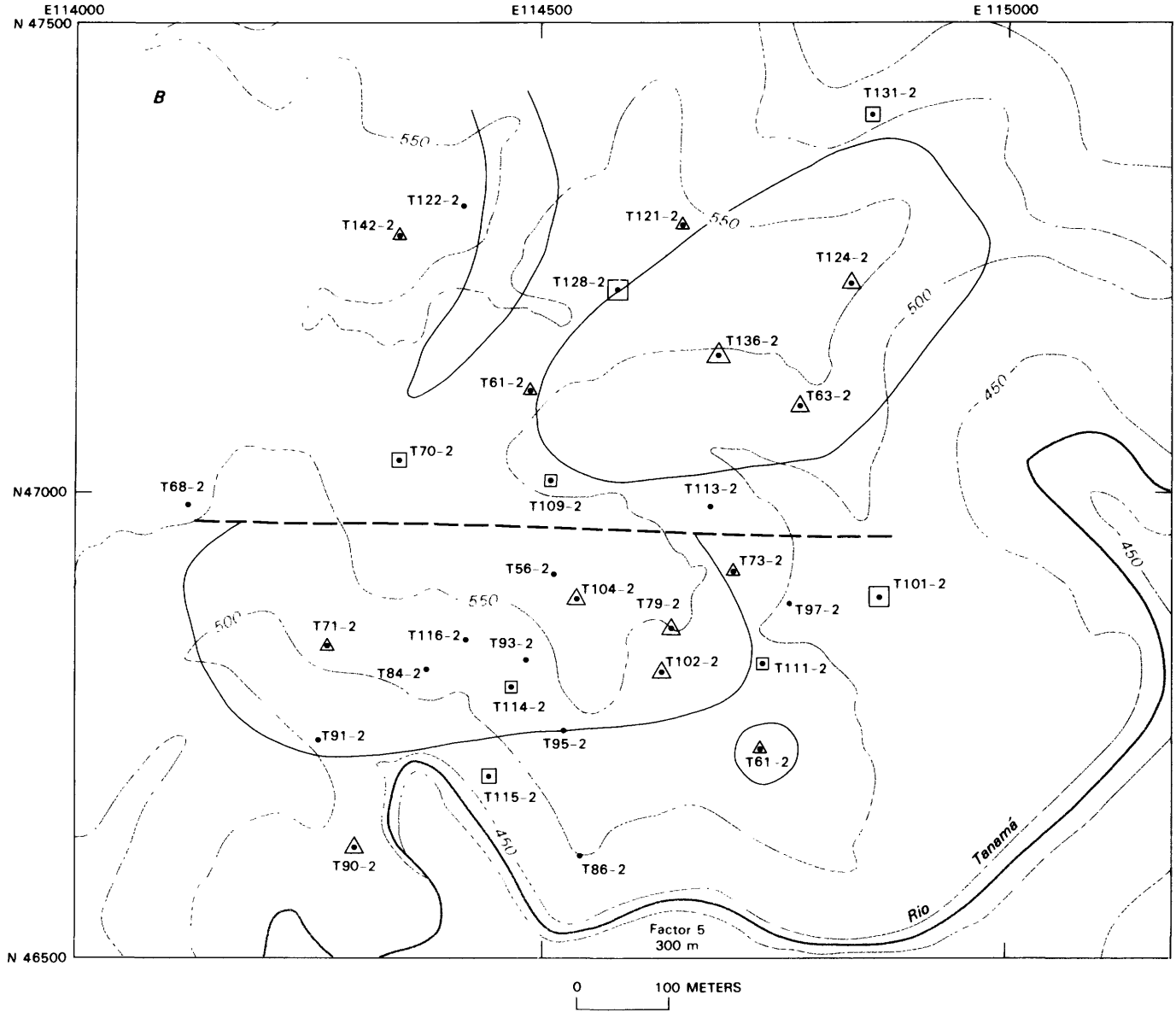


**EXPLANATION**

Symbols indicate scores for factor 5 as follows

| | |
|---|---|
| +2.0 to +3.0 | 2.0 to -1.0 |
| +1.0 to +2.0 | -3.0 to 2.0 |
| +0.5 to +1.0 | T65-2 • Drill hole samples with number |
| 0.5 to +0.5 | Contact of tonalite porphyry intrusion |
| -1.0 to -0.5 | Fault - Inferred |

Figure 31.—Continued.

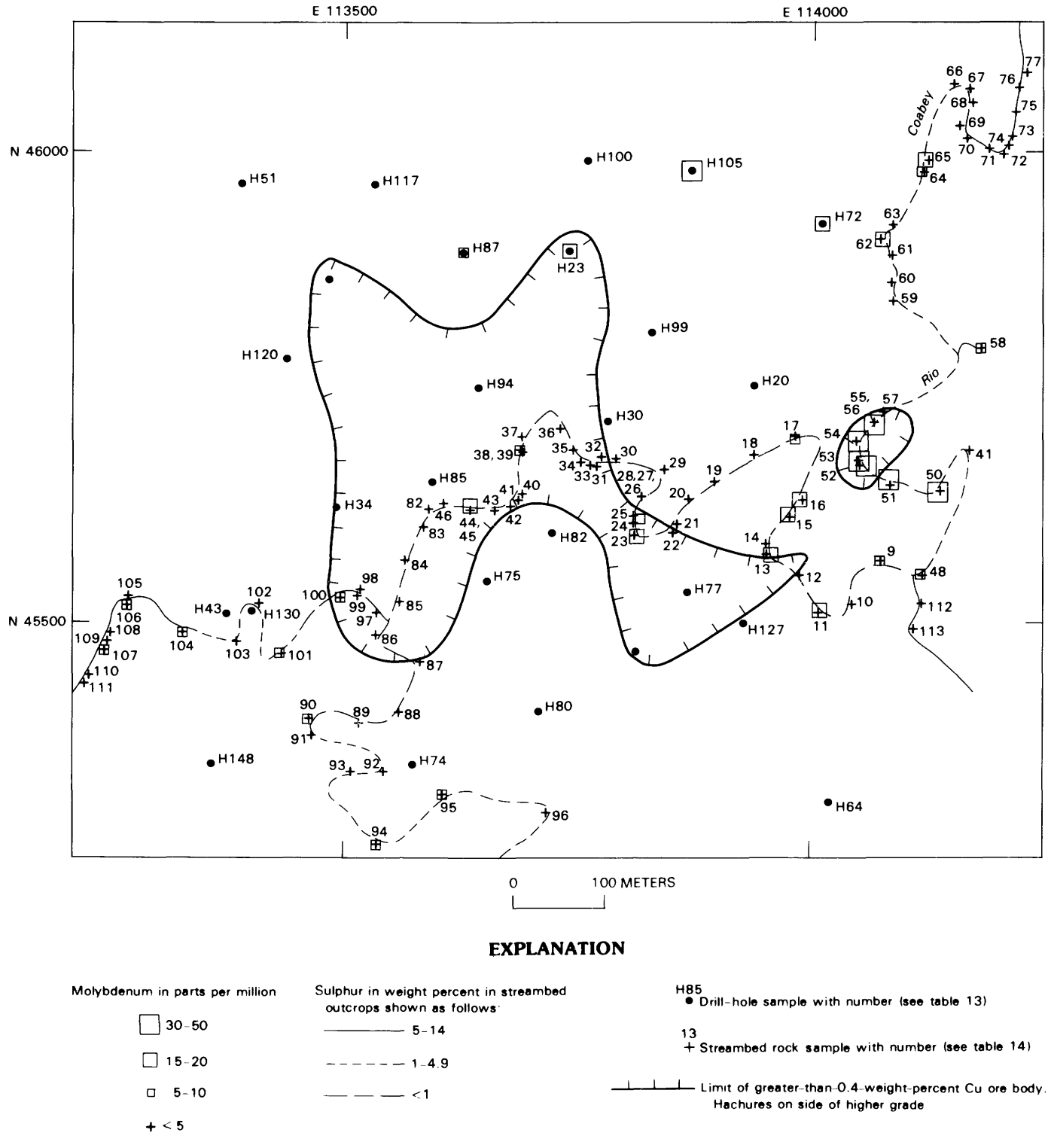


FIGURE 32.—Outline of greater-than-0.4-weight-percent-Cu ore body in comparison with S values in streambed outcrops and Mo values in drill holes and outcrops, Helecho deposit. Coordinates in meters, Puerto Rico coordinate system.

### OTHER ELEMENTS

Factor 2, positively loaded for K, Ba, and Tl and negatively loaded for Na, characterizes feldspar-destructive alteration in the porphyry stock at Tanamá. The mineralogic residence of thallium is not known. Barite was noted in a type F vein in one sample (T91-2) from the southern ore body (fig. 11*C*). Te values were too highly censored for statistical analysis, and a map plot of Te values did not suggest a control by any known geologic features.

## CONCLUSIONS

From the data presented here for the Tanamá and Helecho deposits and their geologic environment, the following principal points may be extracted:

1. Tonalite porphyry intrusions and dacitic flows and breccia formed as a terminal igneous event during a long period of subduction-related volcanism and plutonism.
2. At Tanamá and Helecho, columnar-shaped tonalite porphyry intrusions in a transverse alignment of stocks contain copper mineralization
3. The mineralized porphyry intrusions are mostly altered to propylitic mineral assemblages and contain closely spaced veinlets of quartz, magnetite, chlorite, amphibole, chalcopyrite, and other minerals. At Tanamá, throughout the lower part of the column, the $K_2O$ content is low, but traces of biotite and potassium feldspar are locally present. Biotite forms unreplaced cores in chlorite in the Tanamá and Helecho deposits.
4. Metabasaltic country rocks, with low initial $K_2O$ contents, locally are altered to biotite hornfels near the porphyry contact, presumably by introduction of potassium-bearing fluids. Quartz veinlets are rare in the country rock in comparison with the porphyry intrusions. Chalcopyrite is only locally abundant in the country rock, near the porphyry contacts.
5. Sericite-clay-pyrite blankets cover the tops of the porphyry columns and extend locally downward into the porphyry and outward over the metabasalt. The blanket at Tanamá contains about 4 times the $K_2O$ content of unaltered tonalite porphyry and has about 4 times the sulfide-S content in comparison with the lower parts of the ore body.
6. At Tanamá, a shell of copper ore shaped like an inverted tumbler is localized along the contact zones of the porphyry in the lower part of the column and, in the upper part, occurs throughout the porphyry column without regard to alteration type. In both deposits, the copper ore contains gold and silver and less than 100 ppm Mo; at Helecho, however, the highest Mo concentrations occur outside the copper ore body. Copper and gold distribution is unrelated to silicate-alteration zones, but lead, zinc, and manganese are depleted in the sericite-clay-pyrite blankets and appear to have moved outward to form peripheral anomalies.
7. Quartz and magnetite in early-stage veinlets have isotopic-equilibrium temperatures of 680 to 685 °C
8. Fluids trapped as inclusions in veinlets contain abundant chlorides of Na, Fe, and K, as well as unknown amounts of Ca, Mg, and traces of Cu. They were trapped, under boiling conditions, at temperatures mainly above 350 °C. Other, more dilute fluids are abundant in inclusions throughout the deposit; these fluids were trapped mainly at temperatures between 150 and 350 °C.
9. Water in amphibole, chlorite, and sericite in the Tanamá ore body has isotopic ratios typical of meteoric or marine water.

The distribution of silicate minerals, sulfur, copper, and other metals can be explained by assuming upward flow of fluids through a magma column at a depth of about 3 km. As the column cooled from magmatic temperatures of about 800 °C, and in response to sharp decreases in confining pressure related to volcanic activity at the top of the column, crystallization took place. Crystallization was followed, at temperatures below 700 °C, by fracturing in response to tectonic activity and high fluid pressures in the rapidly crystallizing rocks. Fracturing allowed a gradually increasing inflow of meteoric or marine water that effectively removed all evidence of the presumed magmatic stage by isotopic exchange. Cooling of the system took place from the top downward.

Within this framework, the relation between alteration silicates, chlorite, biotite, amphiboles, and white mica can be discussed. Hemley and others (1980) stressed the importance of seawater and seawater-meteoric water mixtures in alteration. Fixation of $Mg^{2+}$ from these fluids occurs strongly with increasing temperature, so that chlorite and magnesian amphiboles are produced and basic cations, alkalis, and $H^+$ released, as illustrated by the reaction

$$\underline{\text{pargasitic amphibole}}$$
$$2NaCa_2Mg_4Al_3Si_6O_{22}(OH)_2 + 12H_2O + 7Mg^{2+} =$$
$$\underline{\text{chlorite}}$$
$$3Mg_5Al_2Si_3O_{10}(OH)_8 + 2Na^+ + 4Ca^{2+} + 3SiO_2 + 4H^+ \quad (1)$$

The resulting $H^+$ contributes to destruction of feldspars higher in the system. At Tanamá, the low $K_2O$ content of amphiboles in intrusive and country rocks makes it unlikely that this reaction could have provided the potassium now present in the upper, feldspar-destructive-alteration part of the deposit. The existence of a

deep-seated source of potassium would explain the $K_2O$-rich upper zone, the widespread traces of biotite in the lower, feldspar-stable-alteration part of the porphyry, and the biotite hornfels formed from basaltic rocks near the porphyry contact. Cores of unreplaced biotite in chlorite grains indicate that some of the chlorite was formed at the expense of biotite, as in the reaction

$$\underset{\text{biotite}}{2KMg_3AlSi_3O_{10}(OH)_2} + 4H^+ = \underset{\text{chlorite}}{Mg_5Al_2Si_3O_{10}(OH)_8} + 2K^+ + Mg^{2+} + 3SiO_2 \qquad (2)$$

Therefore, I propose that at Tanamá and, probably, also at Helecho and Laundry Creek, extensive biotite

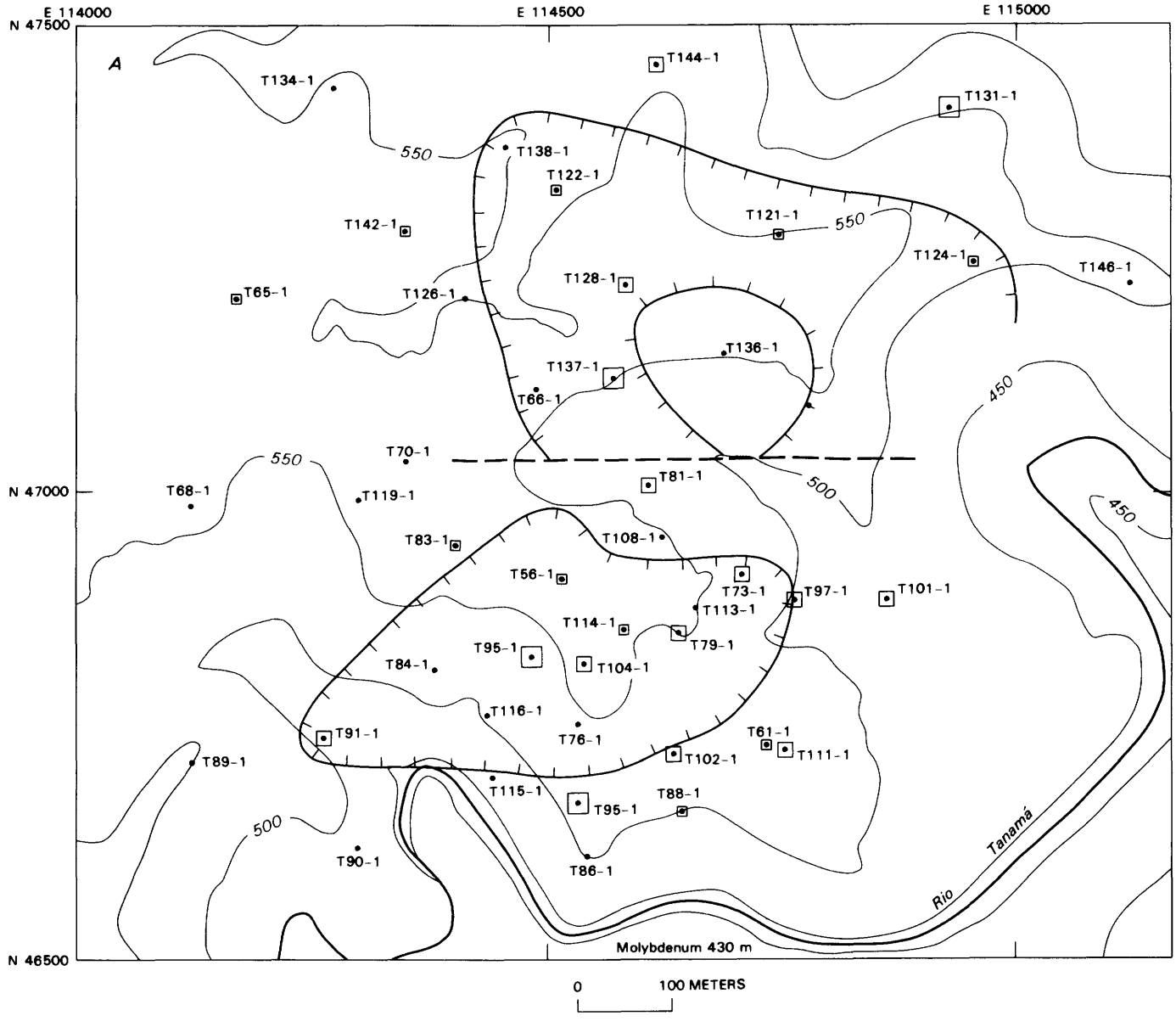


FIGURE 33.—Outline of greater-than-0.4-weight-percent-Cu ore body in comparison with Mo values in drill cores, Tanamá deposit. *A*, 430-m elevation. *B*, 300-m elevation. Coordinates in meters, Puerto Rico coordinate system.

alteration typical of the potassic-alteration zone took place at temperatures between 300 and 600 °C. This zone of potassic alteration surrounded the internal amphibole-dominant assemblage at Tanamá and was probably coextensive with the copper-gold ore body, as shown in figures 36*A* and 36*C*. Inflow of meteoric water and (or) seawater at temperatures between 200 and 300 °C produced a propylitic overprinting on the potassic-alteration zone and on part of the amphibole assemblage and released $H^+$ and $K^+$, as proposed by

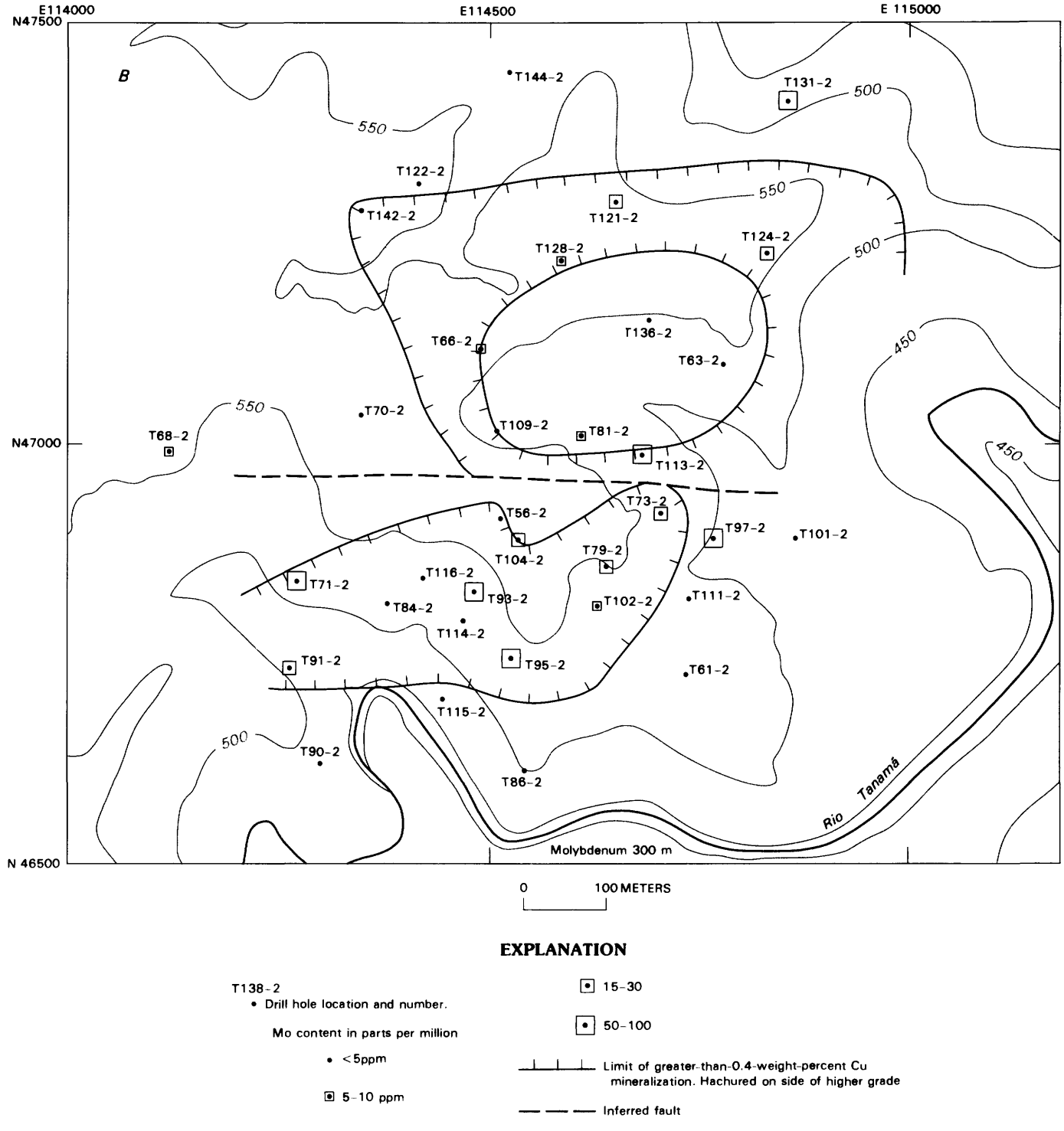


FIGURE 33.—Continued.

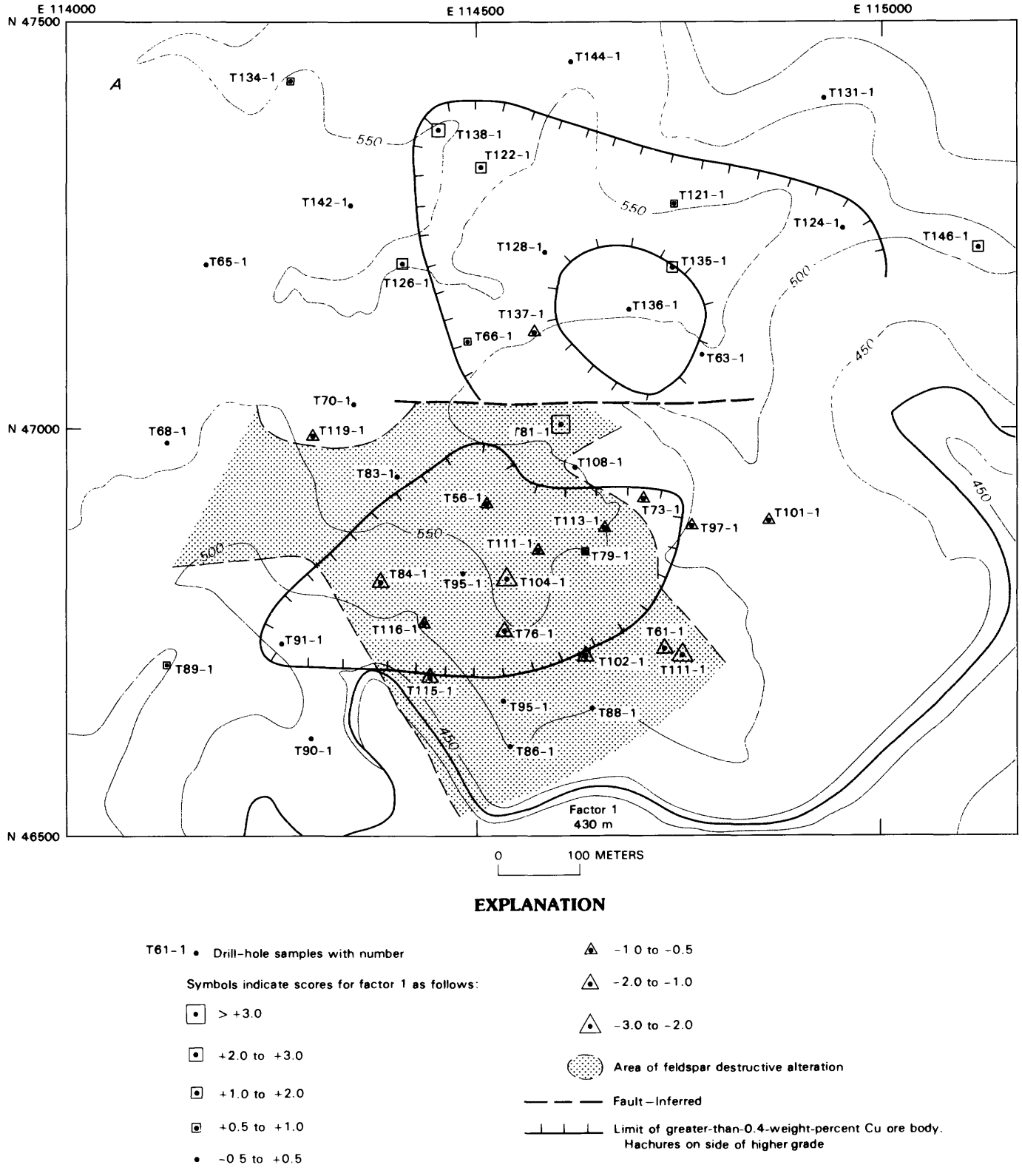


## EXPLANATION

T61-1 • Drill-hole samples with number

Symbols indicate scores for factor 1 as follows:

- ⊡ > +3.0
- ⊡ +2.0 to +3.0
- ⊡ +1.0 to +2.0
- ⊡ +0.5 to +1.0
- • -0.5 to +0.5
- △ -1.0 to -0.5
- △ -2.0 to -1.0
- △ -3.0 to -2.0
- Area of feldspar destructive alteration
- — — — Fault—Inferred
- Limit of greater-than-0.4-weight-percent Cu ore body. Hachures on side of higher grade

FIGURE 34.—Limits of pervasive feldspar-destructive alteration and outline of greater-than-0.4-weight-percent-Cu ore body in comparison with scores on factor 1 for Pb-Zn-Mn-Ag, Tanamá deposit. *A*, 430-m elevation. *B*, 300-m elevation. Coordinates in meters, Puerto Rico coordinate system.

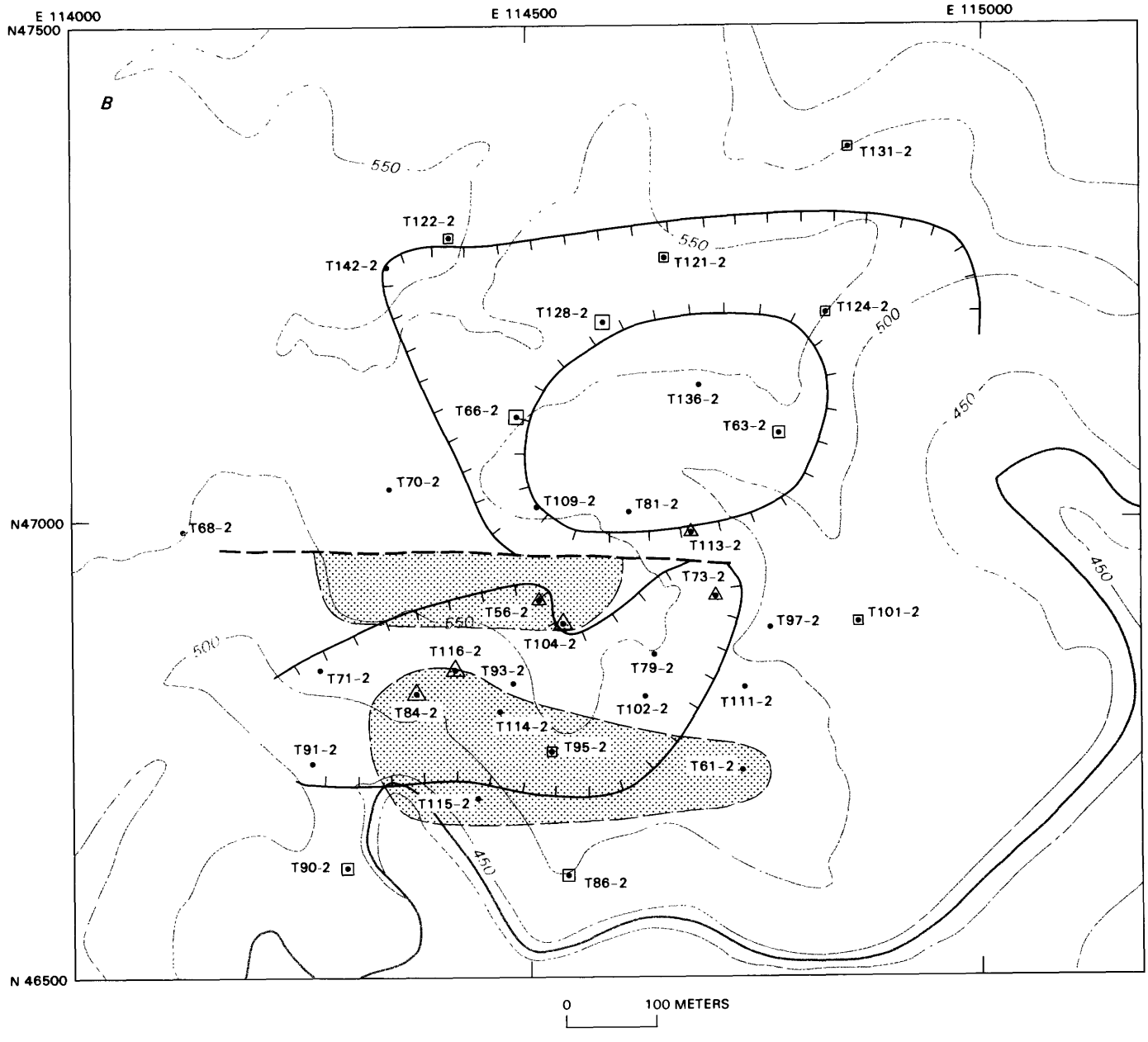


**EXPLANATION**

T61-2 • Drill-hole samples with number

Symbols indicate scores for factor 1 as follows:

- > +3.0
- +2.0 to +3.0
- +1.0 to +2.0
- +0.5 to +1.0
- -0.5 to +0.5
- -1.0 to -0.5
- -2.0 to -1.0
- -3.0 to -2.0
- Area of feldspar destructive alteration
- Fault—Inferred
- Limit of greater-than-0.4-weight-percent Cu ore body. Hachures on side of higher grade

FIGURE 34.—Continued.

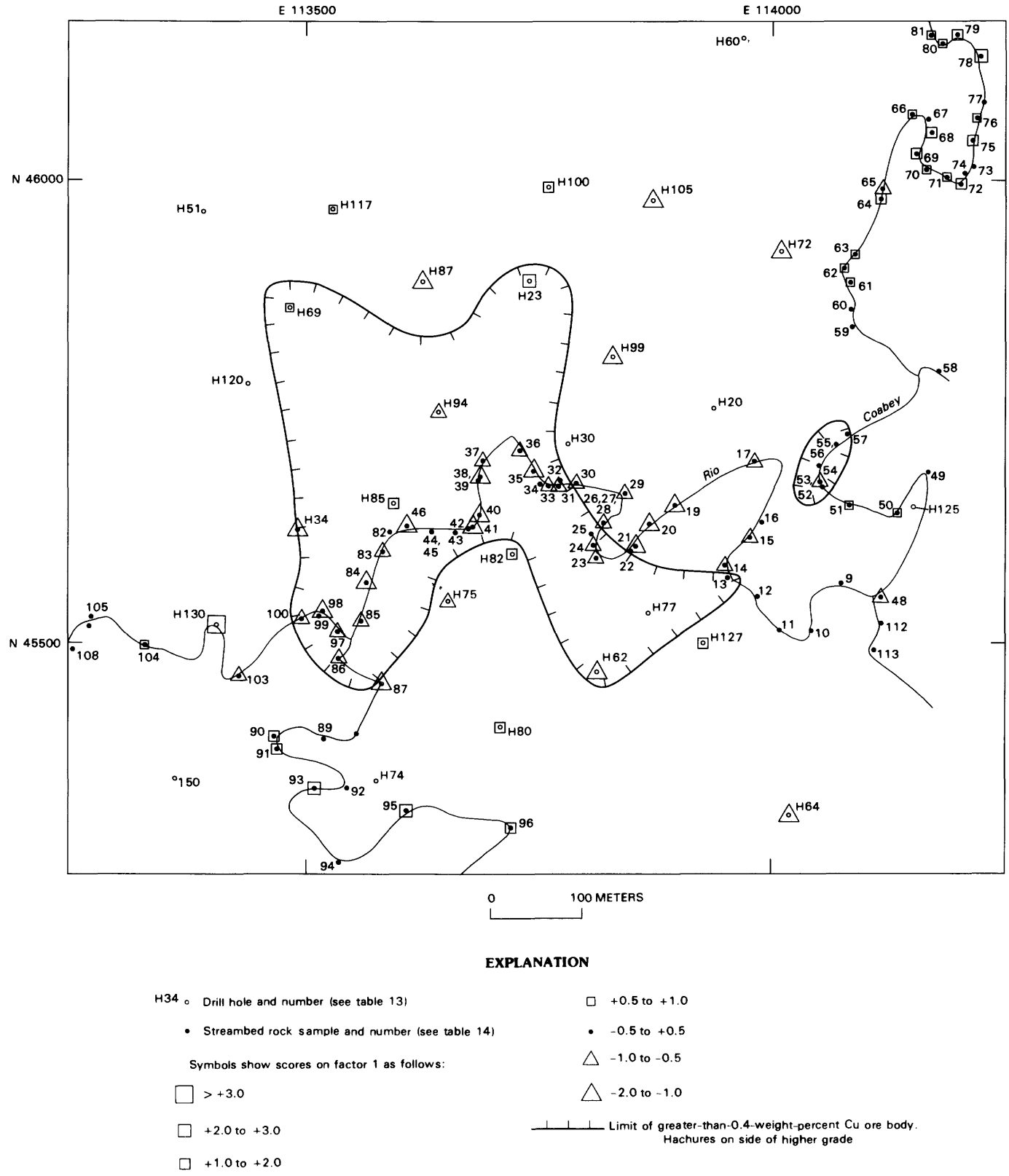


Figure 35.—Outline of greater-than-0.4-weight-percent-Cu ore body in comparison with scores for factor 1 for Pb-Zn-Mn-Ag, Helecho deposit. Factor scores are not precisely comparable between stream-outcrop and drill-core samples because the two data sets were tested separately. Coordinates in meters, Puerto Rico coordinate system.

Hemley and others (1980) (fig. 36*B*). The upward flow of $H^+$ and $K^+$ resulted in alteration of plagioclase in the overlying feldspar-destructive-alteration cap, as in the reaction

$$\underset{\text{anorthite}}{3CaAl_2Si_2O_8} + 4H^+ + 2K^+ = \underset{\text{muscovite}}{2KAl_3Si_3O_{10}(OH)_2} + 3Ca^{2+} \quad (3)$$

The calcium released in reactions 1 and 3 was then fixed as calcite in the feldspar-destructive-alteration assemblage. Because both reactions 1 and 2 have $SiO_2$ as a product, any fractures would tend to be sealed by quartz deposition. Tectonic fracturing and continued reopening of the system must have occurred to permit the pervasive chloritization and feldspar-destructive alteration observed in these deposits.

The relation between magnetite, pyrite, chalcopyrite, and gold depends on oxygen and sulfur activities in the cooling porphyry system. Sulfur activity presumably was controlled by the flow of $H_2S$ through the porphyry column from a deep-seated source and remained high throughout the lifetime of the system. Oxygen activity ($a_{O_2}$) was internally controlled by reactions between mafic silicates and $H_2O$ and by dissociation of $H_2O$ to $H_2$ and $O_2$ in the hot interior of the intrusion. The greater upward diffusion of $H_2$ relative to $O_2$ would cause a higher ($a_{O_2}$)deep in the system and a steadily decreasing ($a_{O_2}$)in the upper part. As the system cooled and the ($a_{O_2}$) activity fell, pyrite stability was attained, and the reaction

$$\underset{\text{magnetite}}{Fe_3O_4} + 6H_2S = \underset{\text{pyrite}}{3FeS_2} + 4H_2O + 2H_2 \quad (4)$$

occurred along an irregular descending front coextensive with feldspar destruction and growth of sericite (fig. 36*B*).

The absence of correspondence between copper-gold grade and alteration type is evidence that chalcopyrite and gold were deposited early, during the postulated biotite-alteration stage. Subsequent chloritization, feldspar-destructive alteration, and sulfidation did not result in redistribution of the copper and gold. Copper and gold were introduced as chloride complexes, as indicated by the high chloride content of fluids trapped in quartz veinlets. Crerar and Barnes (1976) showed that the solubility of copper in chloride solutions decreases rapidly between 350 and 250 °C, and Henley (1973) showed a rapid decrease in the solubility of gold as a chloride complex with decreasing temperature from 500 to 400 °C. Falling ($a_{O_2}$) and dilution of chloride solutions would also cause precipitation of chalcopyrite, according to Crerar and Barnes. Formation of gold thiocomplexes was not favored owing to the high ($a_{O_2}$) (Henley, 1973) that prevailed during the period of chalcopyrite-magnetite stability and ore-body formation. By the time pyrite stability was attained, gold may have been armored by inclusion in chalcopyrite, so that its remobilization and outward migration as gold bisulfide ion could not take place.

There is clear evidence at Tanamá and Helecho for depletion of Pb, Zn, and Mn in the zone of feldspar-destructive alteration and pyritization relative to the feldspar-stable-alteration zones of the ore body (fig.

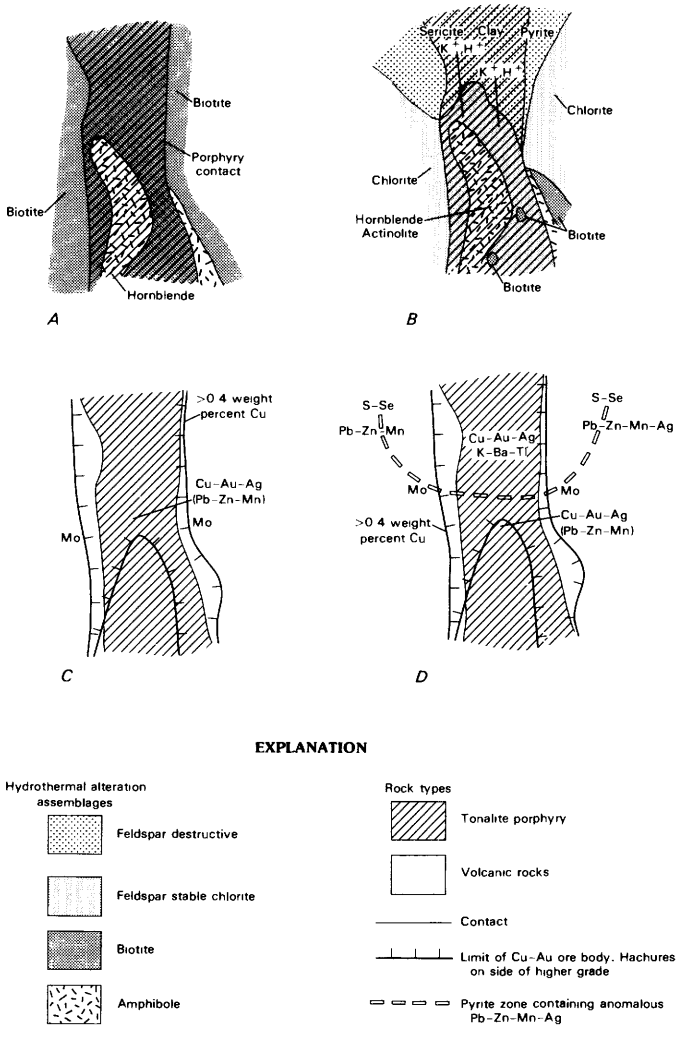


FIGURE 36.—Schematic cross sections showing deposition and redistribution of silicates (*A*, *B*) and metals (*C*, *D*) in a Tanamá-type porphyry Cu-Au deposit. Sections *A* and *C* illustrate the early hydrothermal deposition stage; *B* and *D* the late hydrothermal redistribution stage.

36*D*). This depletion and outward dispersal were apparently facilitated by low-pH fluids and high sulfide activity. Evidence is less clear for outward migration of molybdenum from the ore body at Helecho.

The Tanamá and Helecho deposits provide two important observations that must be included in a general porphyry-copper-deposit model. First, the presence of propylitic mineral assemblages and the absence of hydrothermal biotite should not necessarily be considered negative attributes of a prospect or cause for assignment of the prospect to a peripheral propylitic zone. If abundant quartz veining, abundant mineral-rich fluid inclusions, or copper and gold anomalies are present, the prospect is probably in a potassic-alteration zone, overprinted by late propylitic alteration. Second, the Pb-Zn-Mn peripheral halo that is typical of most porphyry deposits is, at Tanamá, the product of dispersal from a feldspar-destructive-alteration/pyrite-rich zone. Where such a zone is absent owing to erosion or faulting, this peripheral halo may also be absent, and the Pb, Zn, and Mn concentrations may occur within the copper ore body.

## REFERENCES CITED


Barabas, A. H., 1971, K-Ar dating of igneous events and porphyry copper mineralization in west central Puerto Rico [abs.]: Economic Geology, v. 66, no. 6, p. 977.

———1977, Petrologic and geochemical investigations of porphyry copper mineralization in west central Puerto Rico: New Haven, Conn., Yale University, Ph. D. thesis, 466 p.

———1982, Potassium-argon dating of magmatic events and hydrothermal activity associated with porphyry copper mineralization in west central Puerto Rico: Economic Geology, v. 77, no. 1, p. 109-126.

Barabas, A. H., and Quinn, E. J., 1980, Alteration, mineralization, and fluid inclusions in the Helecho porphyry copper prospect, west central Puerto Rico [abs.]: Caribbean Geologic Conference, 9th, Santo Domingo, Dominican Republic, 1980, Transactions, p. 2-3.

Bergey, W. R., 1966, Geochemical prospecting for copper in Puerto Rico, *in* Annual Caribbean Geological Conference, 3d, Kingston, Jamaica, 1966, Transactions: Jamaica Geological Survey Department Publication 95, p. 113-119.

Bottinga, Yan, and Javoy, Marc, 1973, Comments on oxygen isotope geothermometry: Earth and Planetary Science Letters, v. 20, no. 2, p. 250-265.

Chen, Ju-Chin, 1969, Petrological and chemical studies of the Utuado Pluton, Puerto Rico: Acta Geologica Taiwanica, no. 13, p. 21-41.

Cox, D. P., Larsen, R. R., and Tripp, R. B., 1973, Hydrothermal alteration in Puerto Rican porphyry copper deposits: Economic Geology, v. 68, no. 8, p. 1329-1334.

Cox, D. P., Marvin, R. F., M'Gonigle, J. W., McIntyre, D. H., and Rogers, C. L., 1977, Potassium-argon geochronology of some metamorphic and plutonic hydrothermal events in Puerto Rico and the Virgin Islands: U.S. Geological Survey Journal of Research, v. 5, no. 6, p. 689-703.

Cox, D. P., Pérez González, Ileana, and Nash, J. T., 1975, Geology, geochemistry and fluid-inclusion petrography of the Sapo Alegre porphyry copper prospect and its metavolcanic wallrocks, west-central Puerto Rico: U.S. Geological Survey Journal of Research, v. 3, no. 3, p. 313-327.

Crerar, D. A., and Barnes, H. L., 1976, Ore solution chemistry V. Solubilities of chalcopyrite and chalcocite assemblages in hydrothermal solution at 200° to 350°C: Economic Geology, v. 71, no. 4, p. 772-794.

Grimes, D. J., and Marranzino, A. P., 1968, Direct-current arc and alternating-current spark emission spectrographic field methods for the semiquantitative analysis of geologic materials: U.S. Geological Survey Circular 591, 6 p.

Hemley, J. J., Montoya, J. W., Marinenko, J. W., and Luce, R. W., 1980, Equilibria in the system $Al_2O_3$-$SiO_2$-$H_2O$ and some general implications for alteration/mineralization processes: Economic Geology, v. 75, no. 2, p. 210-228.

Henley, R. W., 1973, Solubility of gold in hydrothermal chloride solutions: Chemical Geology, v. 11, no. 2, p. 73-87.

Huebner, J. S., Lipin, B. R., and Wiggins, L. B., 1976, Partitioning of chromium between silicate crystals and melts: Lunar Science Conference, 7th, Houston, Texas, 1976, Proceedings, v. 2, p. 1195-1220.

Krushensky, R. D., 1978, Unconformity between Cretaceous and Eocene rocks in central-western Puerto Rico: A concept rejected: Geologie en Mijnbouw, v. 57, no. 2, p. 227-232.

Leake, B. E., 1978, Nomenclature of the amphiboles: American Mineralogist, v. 63, no. 11-12, p. 1023-1052.

Learned, R. E., and Boissen, Rafael, 1973, Gold—a useful pathfinder element in the search for porphyry copper deposits in Puerto Rico, *in* Jopnes, M. J., ed., Geochemical exploration, 1972: International Geochemical Exploration Symposium, 4th, London, U. K., 1972, Proceedings, p. 93-103.

Mattson, P. H., 1958, Geology of the Mayagüez area, Puerto Rico: Dissertation Abstracts, v. 18, no. 1, p. 197.

———, 1960, Geology of the Mayagüez area, Puerto Rico: Geological Society of America Bulletin, v. 71, no. 3, p. 319- 361.

———, 1968, Geologic map of the Adjuntas quadrangle, Puerto Rico: U.S. Geological Survey Miscellaneous Investigations Map I-519, scale 1:20,000.

McIntyre, D. H., Aaron, J. M., and Tobisch, O. T., 1970, Cretaceous and lower Tertiary stratigraphy in northwestern Puerto Rico: U.S. Geological Survey Bulletin 1294-D, p. D1- D16.

Nash, J. T., 1976, Fluid-inclusion petrology—data from porphyry copper deposits and applications to exploration: U.S. Geological Survey Professional Paper 907-D, p. D1-D16.

Nelson, A. E., and Tobisch, O. T., 1967, The Matilde and Milagros Formations of early Tertiary age in northwest Puerto Rico, *in* Cohee, G. V., West, W. S., and Wilkie, L. C., eds., Changes in stratigraphic nomenclature by the U.S. Geological Survey, 1966: U.S. Geological Survey Bulletin 1254-A, p. A19-A23.

———1968, Geologic map of the Bayaney quadrangle, Puerto Rico: U.S. Geological Survey Miscellaneous Geologic Investigations Map I-525, scale 1:20,000.

Papike, J. J., Cameron, K. L., and Baldwin, K., 1974, Amphiboles and pyroxenes: Characterization of *other* than quadrilateral components and estimates of ferric iron from microprobe data [abs.]: Geological Society of America Abstracts with Programs, v. 6, no. 7, p. 1053.

Pease, M. H., Jr., and Briggs, R. P., 1960, Geology of the Comerío quadrangle, Puerto Rico: U.S. Geological Survey Miscellaneous Geologic Investigations Map I-320, scale 1:20,000.

Potter, R. W., II, and Clynne, M. A., 1978, Prossure correction for fluid-inclusion homogenization temperatures [abs.]: International Association on the Genesis of Ore Deposits, Symposium, 5th, Alta, Utah, 1978, Programs and Abstracts, p. 146.

Roedder, Edwin, 1962, Studies of fluid inclusions I: Low temperature application of a dual-purpose freezing and heating stage: Economic Geology, v. 57, no. 7, p. 1045-1061.

———1967, Fluid inclusions as samples of ore fluids, *in* Barnes, H. L., ed., Geochemistry of hydrothermal ore deposits: New York, Holt, Rinehart and Winston, p. 515-574.

———1971, Fluid inclusion studies on the porphyry-type ore deposits at Bingham, Utah, Butte, Montana, and Climax, Colorado: Economic Geology, v. 66, no. 1, p. 98-120.

Shapiro, Leonard, 1967, Rapid analysis of rocks and minerals by a single solution method, *in* Geological Survey research 1967: U.S. Geological Survey Professional Paper 575-B, p. B187-B191.

———1975, Rapid analysis of silicate, carbonate, and phosphate rocks—revised edition: U.S. Geological Survey Bulletin 1401, 76 p.

Sheppard, S. M. F., and Gustafson, L. B., 1976, Oxygen and hydrogen isotopes in the porphyry copper deposit at El Salvador, Chile: Economic Geology, v. 71, no. 8, p. 1549- 1559.

Sheppard, S. M. F., Nielsen, R. L., and Taylor, H. P., Jr., 1969, Oxygen and hydrogen isotopic ratios of clay minerals from porphyry copper deposits: Economic Geology, v. 64, no. 7, p. 755-777.

———1971, Hydrogen and oxygen isotope ratios in minerals from porphyry copper deposits: Economic Geology, v. 66, no. 4, p. 515-542

Sheppard, S. M. F., and Taylor, H. P., Jr., 1974, Hydrogen and oxygen isotope evidence for the origins of water in the Boulder batholith and the Butte ore deposits, Montana: Economic Geology, v. 69, no. 6, p. 926-946.

Streckeisen, Albert, chairman, 1974, Classification and nomenclature of plutonic rocks: Recommendations of the IUGS Subcommission on the Systematics of Igneous Rocks: Geologische Rundschau, v. 63, no. 2, p. 773-786.

Suzuoki, Tetsuro, and Epstein, Samuel, 1976, Hydrogen isotope fractionation between hydroxyl-bearing minerals and water: Geochimica et Cosmochimica Acta, v. 40, no. 10, p. 1229-1240.

Taylor, H. P., Jr., 1979, Oxygen and hydrogen isotope relationships in hydrothermal mineral deposits, *in* Barnes, H. L., ed., Geochemistry of hydrothermal ore deposits, (2d ed.): New York, John Wiley and Sons, p. 236-277.

Thompson, C. E., Nakagawa, H. M., and VanSickle, G. H., 1968, Rapid analysis for gold in geologic materials, *in* Geological Survey research 1968: U.S. Geological Survey Professional Paper 600-B, p. B130-B132.

Tobisch, O. T., and Turner, M. D., 1971, Geologic map of the San Sebastián quadrangle, Puerto Rico: U.S. Geological Survey Miscellaneous Geologic Investigations Map I-661, scale 1:20,000.

Ward, F. N., Nakagawa, H. M., Harms, T. F., and VanSickle, G. H., 1969, Atomic-absorption methods of analysis useful in geochemical exploration: U.S. Geological Survey Bulletin 1289, 45 p.

Weaver, J. D., 1958, The Utuado Pluton, Puerto Rico: Geological Society of America Bulletin, v. 69, no. 9, p. 1125-1141.